

NOTE TO USERS

This reproduction is the best copy available.

UMI

**Precision Mass Measurements of Some Isotopes of Tungsten and Mercury
for an Adjustment to the Mass Table in the Region
A=184 to A=204.**

by

Domenico K. Barillari

**A Thesis
Submitted to the Faculty of Graduate Studies
in Partial Fulfillment of the Requirements
for the Degree of**

Doctor of Philosophy

**Department of Physics and Astronomy
University of Manitoba
Winnipeg, Manitoba**

© September, 1999



National Library
of Canada

Bibliothèque nationale
du Canada

Acquisitions and
Bibliographic Services

Acquisitions et
services bibliographiques

395 Wellington Street
Ottawa ON K1A 0N4
Canada

395, rue Wellington
Ottawa ON K1A 0N4
Canada

Your file *Votre référence*

Our file *Notre référence*

The author has granted a non-exclusive licence allowing the National Library of Canada to reproduce, loan, distribute or sell copies of this thesis in microform, paper or electronic formats.

L'auteur a accordé une licence non exclusive permettant à la Bibliothèque nationale du Canada de reproduire, prêter, distribuer ou vendre des copies de cette thèse sous la forme de microfiche/film, de reproduction sur papier ou sur format électronique.

The author retains ownership of the copyright in this thesis. Neither the thesis nor substantial extracts from it may be printed or otherwise reproduced without the author's permission.

L'auteur conserve la propriété du droit d'auteur qui protège cette thèse. Ni la thèse ni des extraits substantiels de celle-ci ne doivent être imprimés ou autrement reproduits sans son autorisation.

0-612-45134-8

Canada

**THE UNIVERSITY OF MANITOBA
FACULTY OF GRADUATE STUDIES

COPYRIGHT PERMISSION PAGE**

**Precision Mass Measurements of Some Isotopes of Tungsten and Mercury for an
Adjustment to the Mass Table in the Region A=184 to A=204**

BY

Domenico K. Barillari

**A Thesis/Practicum submitted to the Faculty of Graduate Studies of The University
of Manitoba in partial fulfillment of the requirements of the degree**

of

Doctor of Philosophy

DOMENICO K. BARILLARI©1999

Permission has been granted to the Library of The University of Manitoba to lend or sell copies of this thesis/practicum, to the National Library of Canada to microfilm this thesis and to lend or sell copies of the film, and to Dissertations Abstracts International to publish an abstract of this thesis/practicum.

The author reserves other publication rights, and neither this thesis/practicum nor extensive extracts from it may be printed or otherwise reproduced without the author's written permission.

Scope and Contents:

Four mass spectroscopic doublets involving a comparison between ^{201}Hg , ^{199}Hg and ^{183}W (and using a chlorocarbon reference) are reported from measurements made with the upgraded Manitoba II deflection instrument. The measurements address the problem of a mass table misadjustment in the region of the valley of β -stability between the tungsten group and the noble metals. The results, forming a well-closed loop of mass differences, support the earlier results of Kozier [Ko(1977)] regarding the (stable) mercury isotope masses and confirm an approximate 20 μu discrepancy in the mass adjustment of Audi *et al.* [Au(1993)]. A local least-square re-adjustment conducted using these and existing mass table data suggests that the error originates with mass differences pertaining to one or more other nuclide pairs, perhaps ^{193}Ir - ^{192}Ir .

The work on upgrading the precision voltage supply and potentiometry system of the Manitoba II instrument is also reported, as is a new assessment on the data processing method.

Reflectiri noli, ad ubi terminum perveneris. Publius Syrius
Reflect not and to the same place return.

fortuna audentes juvat (common in Cicero's time, author unknown)
chance favours the bold

Preface

There is virtually no corner of physics that does not benefit from high-precision-measurement: indeed as the following list clearly indicates, tiny effects on the limits of measurement ability often spell a revolution in this business:

- Kusch [Ku(1948a,b)] makes one of the first precision measurements of the μ of the electron to show that it is NOT an integral multiple of $e\hbar/2mc$.
- Michelson and Morley discover that the H α line is a doublet
- Lamb and Retherford [La(1947,1950a,b,1952)] find that $2^2P_{1,2} - 2^2P_{3,2} = 0.033 \text{ cm}^{-1}$ or $\sim 1 \text{ GHz}$ (a test of nascent QED, in predictions of radiative corrections)
- Cronin and Fitch [Ch(1964)] find a small but convincing signal that about 1 in 10^3 decays in the $K^0\bar{K}^0$ system violate CP parity
- precision Z^0 decay-width gives maximal lepton family size for $m_\nu < \sim M_{Z^0}$
- 1940's - precision mass table and reaction data, showing deviations from the Bethe-Weizsäcker empirical mass formula, give strong support to the idea of shell closure in nuclei

....

making foolish the comment uttered at the end of the last century (1898!) about the tedium of "adding the next decimal place to [well understood physics]": the reader will doubtless think of other experiments in this category.

This thesis concerns the precise re-measurement of mass values in the region of the mercury isotopes, such that important discrepancies in the high-mass end of the mass table could be resolved. In the area of nuclear physics, the sobering fact is that much of our knowledge of the systematics of nuclear binding energies comes from precision mass measurements, or rather, mass comparisons. The present theory of the microscopic many-body states that is the nucleus is in many ways circumscribed and tested against binding energies and Q-values experimentally available. It is therefore important that the masses of the stable species that make up the backbone of the table of nuclides are known to high precision and that, as accepted, the values are consistent when checked by various Δm or $\Delta E/c^2$ connections. Clearly such efforts as those to understand nuclei far-from-stability, as a major field of nuclear studies, require such a reference set. Elsewhere, precise Q-values are essential to particle physics models and experiments that are sensitive to small variations in reaction energies. A well known case of this is in the search for neutrino mass and the closely related issue of the nature of the neutrino (see, *e.g.*, Kayser [Ka(1989)]); the chain of implications ultimately taking us to concerns of cosmogeny and string/supersymmetric theories.

It is with these considerations in mind that the re-measurement of mercury masses, with mercury an important linchpin element in the connection between the stable "metals" and the actinides, was undertaken.

Acknowledgements:

The author wishes to express his deepest gratitude to a supervisor who was not only highly knowledgeable and professional, but on a personal level was also patient, gracious and firmly practical in his attitude to his graduate students. His indulgence of my occasional tinkering in the lab only increased my respect for someone who appreciated the scientific mind: he is very much, in this author's humble opinion, such a high caliber scientist himself.

Special thanks are due to Mr. Joseph Vaz, (destined to be Dr. Vaz in the not too distant future) for his strenuous efforts in the lab in helping to produce the data presented here, and, of course, for his good humoured company. Similar kudos are due to Mr. Gilles Roy, our ever helpful, all-round finder of parts and instruments and shire-reeve of the Physics Department, for his direct help on many occasions.

The author also thanks the University of Manitoba for its Graduate Fellowship funding, which very much helped to see him (and his family) keep alive throughout this work.

Final thanks are to his wife Anne Gajerski-Cauley, who deserves a special award for probably having suffered the most through her husband's desire to academically better himself. The author hopes that she, and his boys Cedric, Everett and Matteo (born during this "campaign") will benefit from all of this.

July 23rd, 1999

Contents

<i>Scope and Contents</i>	<i>i</i>
<i>Preface</i>	<i>ii</i>
<i>Acknowledgements</i>	<i>iii</i>
<i>Contents</i>	<i>iv</i>
<i>I Introduction</i>	<i>1</i>
<i>II Nuclear Masses and Their Determination: Deflection Mass Spectrometry for Precision Mass Measurement</i>	<i>2</i>
1. Introductory Remarks-Nuclear Physics	2
2. The Mass Table and Mercury	7
3. Mass Measurement Technique	11
<i>III Ion Optics</i>	<i>14</i>
1. Direction Focusing in Magnetic and Electric Sector Fields	14
2. Double Focusing in Tandem Fields.....	18
3. Bleakney's Theorem	20
<i>IV The Manitoba II Instrument</i>	<i>24</i>
1. Optical Specifications.....	24
3. Visual versus Computer Matching	26
4. Matching Modes.....	31
<i>V New Electronics for the Manitoba II Instrument</i>	<i>33</i>
1. The ESA Cells.....	33
2. ESA Supplies and Measurement Circuit	36
3. Voltage Reference.....	39
4. ΔV Supplies and ΔV Switching System	39
5. Digital Chopper System	47
6. Source Ion-Optics Electronics System Changes	48
7. Source Electron Emission Control.....	48
8. Future Enhancements	49
<i>VI New Software for the Manitoba II Instrument</i>	<i>59</i>
1. Digital/Computer Peak Matching – AMDPRIME5	59
2. Magnet Control Software - BORIS	61
3. Computer Measurement Control Software.....	61

VII Peak Matching.....	62
1. Definitions and a Brief Review of Methods and Issues	63
2. Processing Stages: Some Details	71
VIII Results of Measurements on the Mercury-Tungsten System.....	84
1. Assessment of the Data Quality	84
2. The Results	85
3. Local Least-Squares Adjustment of the Results.....	89
4. Implications for the Mass Table	89
Appendix A: Functional Specification for AMDPRIME5	Ap. A-1
Appendix B: Some Data Analysis Studies	Ap. B-1
Appendix C: Circuit Schematics	Ap. C-1
Appendix D: Example Linkage Calculations	Ap. D-1
References.....	R-1

I Introduction

Historically, data from nuclear mass measurement have been our foremost probe of nuclear structure, giving the first hints that the trends in binding energy per nucleon could be the key to technological sources of energy from the nucleus and revealing an energetic stabilization of the nucleus as the number of its constituents pass the so-called "magic numbers" indicating shell closure.

Nuclear models can now provide sufficiently precise binding energy predictions that the corresponding nuclear data, in the form of masses and Q-values, must in some cases be of order few-10-keV precision to be relevant: see, *e.g.*, Nix and Möller [Ni(1995)] or Pearson *et al.* [Pe(1986)]. A strong interest, of course, lies in projecting these models out way beyond the valley of beta stability. That these models contain parameters that have been tuned by previous experiment is not surprising given the extremely complex nature of the *ab initio* problem of the nuclear state, and the reasonable desire to create models that possess any semblance of a physical picture, as opposed to only a mathematical statement. Given this, the data set on the stable nuclides that shape our fine-grained understanding now must be made consistent to better than the aforementioned order of magnitude.

Nuclear data such as Q-values are also essential in high energy physics where we continue the search for "new physics", that is, particles and phenomena beyond the standard model. This may be heralded by the discovery of neutrinoless double-beta decay, constraining or seeing the signature of neutrino mass, or the investigation of some other process not yet envisioned.

The relative masses of nuclei in the stable regions of the mass table below and above mercury have been determined to an astonishing precision by the standards of the rustic chemical methods by which such study began in the last century. Current precisions on many stable nuclides approach and often exceed 1 part in 10^8 . Some reference species such as H and Cl isotopes are known to a precision two orders of magnitude better (see Audi *et al.* [Au(1993)]). However, beginning perhaps with tungsten, there is an "inconsistency" of order possibly 20μ between the middle and upper end of the table. This was first noted in work by Kozier *et al.* ([Ko(1977),(1980)] on mercury, after examining results for samarium and uranium by the "Minnesota" group [KaJ(1975), Br(1973)]. Further mass adjustments in this vicinity have exacerbated the residuals in a number of mass/energy loops around stable nuclei here. This is not a tolerable situation given the needs mentioned above. As will be elaborated upon throughout this thesis, the Manitoba II deflection mass spectrometer, at the University of Manitoba, can achieve the precision required to help settle the issue. The importance of a re-measurement is reflected in the fact that this first investigation into the mercury system was carried out 20 years ago, and that the results, in the last few crucial decimal places, are still in dispute (see again [Au(1993)] and Wapstra and Audi [Wa(1985)]). The present moment is especially opportune given that the critical electrical components of the apparatus have been rebuilt on somewhat new lines and that some systematics may therefore be better understood.

This thesis therefore concerns the upgrade of an historically useful and productive high-precision mass-measurement system and, as its first new task, a new attack on "the mercury issue".

II Nuclear Masses and Their Determination: Deflection Mass Spectrometry for Precision Mass Measurement

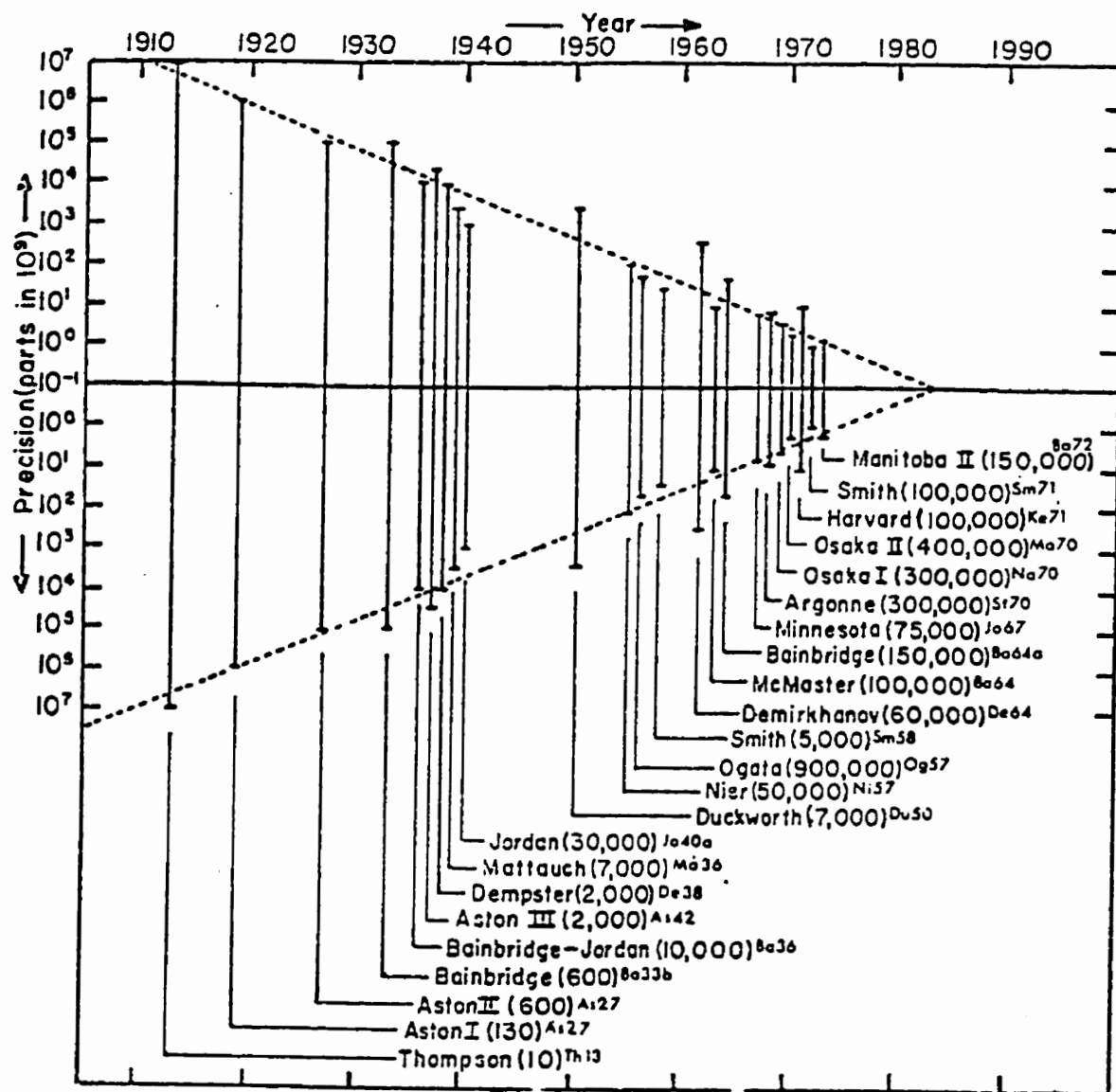
1. Introductory Remarks - Nuclear Physics

Deflection mass spectrometers have been used since the dawn of experimental nuclear physics as one of the most important tools in examining nuclear structure. They have steadily evolved in precision over the decades (Fig.2.1), and alongside other probes of nuclear structure, have been a steady source of information on stability and relative energies between stable and even some unstable nuclide ground-state energy levels. Early work concentrated on plotting the well known packing fraction curve, giving at a glance the trend in binding energies with mass for nuclei (see Aston [As(1942)] and Dempster [De(1938a,b)]), and clearly pointing out the energies available from fission and fusion processes. Systematic mass table data on nucleon separation energies, accumulated through mass spectrometry, established early on the location of major nuclear shell closures, as well as provided hints of residual interactions (see, for instance, [Ma(1948),(1949)] or [Fe(1949)]). Indeed, before M.G. Mayer and O. Haxel, J.H.D. Jensen and H.E. Scuss firmly established the "locations" of major shell closures around 1950, (partly by abundance arguments as well), Bethe and Bacher [BeB(1936)] were calling for a much higher levels of precision in mass measurements in 1936 to clarify whether shells should be constructed on the basis of independent nucleons or α -particle-like clusters.

There is ongoing intense interplay between theoretical work focussed on creating nuclear models suitable for generating predictions of such observables as masses/binding energies, energy levels, quadrupole moments, *etc.*, and experiments providing the next round of constraining data. Outside of this loop, there is important use for the data and predictions on nuclear energetics in such research as stellar nucleosynthesis processes, double-beta decay searches (Q-value constraints for candidate nuclides) and the search for exotic nuclei (*e.g.*, "halo nuclei").

The problem of computing such parameters from a literally elementary beginning, *i.e.*, valence quarks and QCD, is largely beyond our present calculational ability, even in terms of setting up a mathematical statement of the problem. Ironically, since quarks are essentially permanently confined by the colour field, there are no "constituent" masses to tally up in the sense of, say, an isolated atom! In the language of field theory, masses formally become like coupling strengths in the system Lagrangian, and thus subject to momentum rescaling.

The situation is somewhat more tractable at the level of nucleons and the effective force carriers: the pion and heavier mesons with suitable quantum numbers. Since the (dimensionless) coupling in the nuclear interaction is larger than 1, there is no immediate perturbational approach in the sense of a quantum field theory. Luckily the non-relativistic momentum scale of nucleon motion in the nucleus means that we can achieve many of our aims with the Schrödinger equation. This is NOT to say that a field-theoretic approach is not possible: indeed a rich theoretical framework with intimate ties to other fermi and bose condensed-matter systems exists (see, *e.g.*, [Ma(1976)] or [Th(1972)]). Interestingly, relativistic mean-field theory actually seems to "explain" the size of spin-orbit coupling and the form of the nuclear potential! ([Gr(1996)], [Br(1978)]).



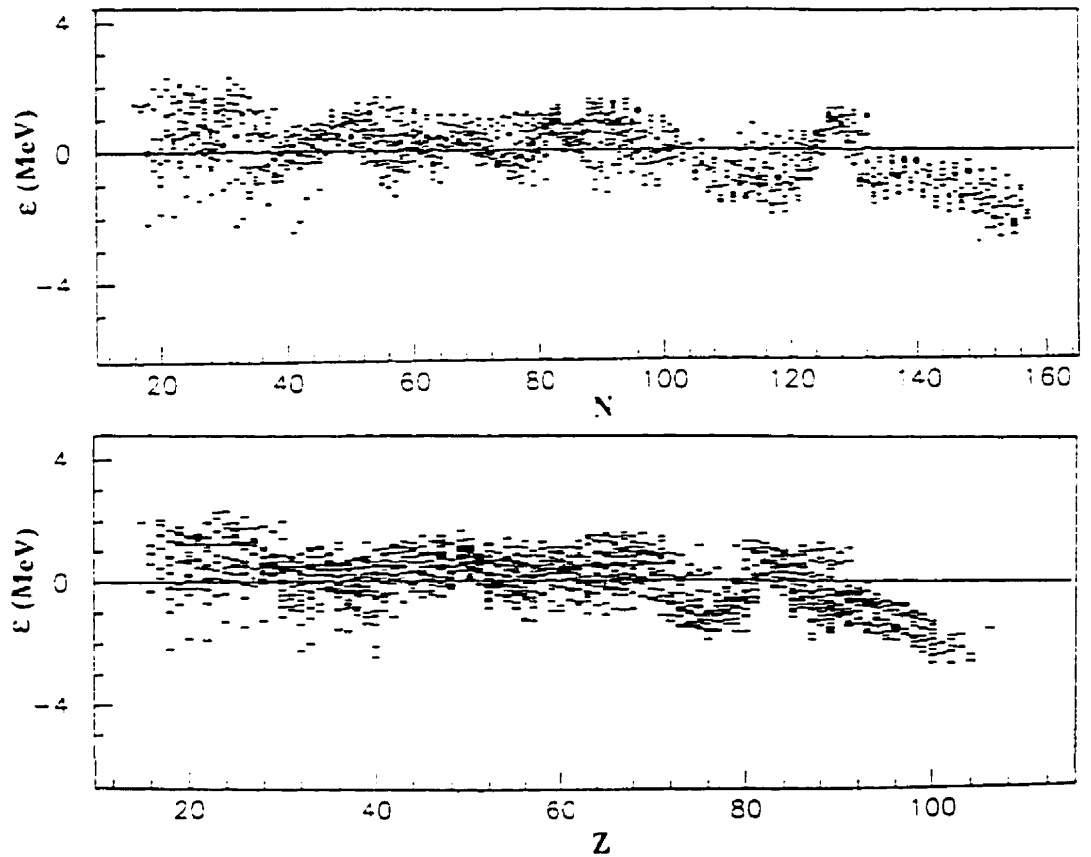
FOLLOWING WILLIAMS AND DUCKWORTH, [Wi(1972)]

Figure 2.1 The Development of Precision in Mass Spectrometry

Generally speaking, possessing a model with few or no empirical components that precisely predicts nuclear binding energies (and hence masses), nuclear densities, and other basic parameters, implies a "good" model, in the sense of approaching a fundamental description of the nature of the nucleus and in being a predictive tool. One of the first highly intuitive and accurate "macroscopic" descriptions was of course Bethe and Weizsäcker's Semi-Empirical Mass Formula, which is based on the Liquid Drop Model (LDM) and incorporates a good deal of phenomenology about the short-range nature of the effective nuclear force and the propensity for nucleon pairing. Many descendants of this model now exist, elaborating on such phenomenological factors as "surface stiffness", compressibility, *etc.*. Recognizing the critical importance of angular momentum and of the coupling of nucleon angular momenta, the shell model was a major achievement in terms of understanding nuclear phenomenology. It is, however, largely an "independent particle" description, *i.e.*, it assumes an effective central potential partly controlling outer "valence" nucleons. Notwithstanding, building upon the LDM, it qualitatively gives us a correct prediction of the variation of binding energies with N or Z, as well as the angular momenta and moments of ground state nuclei (see, *e.g.*, Strutinsky [St(1967)], Zeldes [Ze(1972)] or Bauer [Ba(1975)] on predictions of nuclear masses).

"Microscopic models" attempt to address the problem of constructing a description based on the degrees of freedom of nuclear constituents, and thereby at least appear more fundamental. One relatively fundamental approach to a mass formula, in the sense of addressing microscopic forces for instance, is the Extended Thomas-Fermi (ETF) approximation to the Hartree Fock (HF) method [Ki(1967)]. The HF method is a variational method that seeks to establish a consistent potential starting from a given trial configuration of particles experiencing mutual forces, taking fermion statistics into account (see, *e.g.*, Bethe and Jackiw, [BeJ(1968)]). Since the space of self-consistent potentials for mutually attracting particles is not unique, the nature of the interaction is still important; thus an *a priori* description of nuclear properties is not fundamentally possible through a self-consistent method - it merely provides a mathematical framework in which to extract predictions of certain global properties given presumably sensible assumptions about the underlying microscopic forces. These come closer in many cases to a quantitatively predictive picture, but with theory shaped *a posteriori*. Thus *a posteriori*, they can reproduce with high accuracy the properties of many stable nuclei, for example, binding energies to within <10 keV near closed-shell configurations. Given that modern mass-spectrometric measurements routinely achieve a precision of 1 keV (Audi *et al.* [Au(1993)]) when it comes to stables, as do the better nuclear reaction/spectrometry data, the implication is that a precise experimental mass data set will still serve as the calibration for nuclear models.

One area where mass formulae are most challenged are predictions for nuclei far from the valley of beta-stability and alpha/fission-stability. Precise measurement of mass of mass for the highly unstable nuclei, *i.e.*, those with very short half-lives, are technically difficult, requiring on-line production. An exciting new development in this area is "trap" mass spectrometry, capable of examining nuclei with lifetimes on the order of seconds to precisions ~ 1 in 10^8 or better (see [Bo(1998)] and [Sh(1995)]). Although older Hartree-Fock-based theoretical results such as those of Quentin and Flocard [Qu(1978)], Figure 2.2, show that typical "theoretical errors" for the mass of stables can be of order tens of MeV, more recent calculations, such as those of Pearson *et al.* [Pe(1991)], involving Skyrme effective forces, or better still, the Finite-Range Droplet Model [Ni(1995)], are becoming more precise. The latter show typical errors of below 1 MeV, making predictions about unstable nuclei more confident, and, in turn, requiring more precise experimental input for confirmation.



Error of fit ($\epsilon = M_{\text{exp}} - M_{\text{calc}}$) of force SkSC1 to mass data as functions of N and Z .

Figure 2.2 The state of microscopic/macroscopic mass predictions in 1991.

(Reprinted from Nuc. Phys. A528, Pearson *et al.*, Thomas-Fermi Approach to Nuclear Mass Formula (III). Force fitting and construction of the mass table., Copyright 1986, p. 32, with permission from Elsevier Science, ([Pe(1986)]))

An exciting point of contact between nuclear mass measurement and particle physics/cosmology is on the topic of neutrino mass. There has been intense interest in the subject of whether the neutrino, or rather, the three known neutrinos, are truly massless. Their apparent masslessness creates a problem in the context of Supersymmetric or other models that may prove successful in encompassing the Standard Model, $SU(3)_c \times SU(2)_l \times U(1)_{em}$ [Ka(1986)]. The question revolves around why in the apparently natural flavour multiplets that we assume in these models, (at currently accessible energies), described by:

$$2.1 \quad 3 \otimes \begin{bmatrix} u \\ d \\ e \\ \nu \end{bmatrix}$$

the neutrino should "arbitrarily" have zero mass, *i.e.*, why should it be the only fully relativistic member? There is a glaring un-naturalness to this, and such sentiments about the aesthetics of fundamental laws often presage important conceptual breakthroughs. On the cosmic scale, should any of the neutrinos have mass of order ~ 1 eV, they could contribute enough gravitating mass to the mass/energy of the universe to slow and possibly reverse the expansion of space-time that began at the Big Bang [Gr(1990)].

The mass of the neutrino may be the controlling factor in the rate, that is to say, the dynamics, of special rare decays of nuclei two Z units away from stability, *i.e.*, double-beta decay. The extreme low rate of such processes (typical $\tau \sim 10^{22}$ years) is largely due to the fact that decay to the nucleus one Z unit away is energetically forbidden and hence a (unfavourable) virtual process is involved. That such decays occur, and that they occur accompanied by double-neutrino emission as predicted by the Standard Model, has been demonstrated by detection and kinematic measurements of the decay betas in ^{82}Se decay [El(1987)]. The excitement in this case is whether one can detect double-beta emission in the absence of neutrino emission, that is neutrinoless double-beta decay or $\beta\beta_{0\nu}$, wherein the betas carry away the full energy represented by the Q -value of the decay process. Such events are largely forbidden by the Standard Model, whether the neutrino has a Dirac or Majorana character, unless it has mass ([Ka(1989)]). The signature for such a process would be a "spike" at the high extreme of the spectrum of the sum of the beta energies. Since such "endpoint" measurements would be exceedingly difficult to make with rare events, highly accurate mass values for the nuclei involved would be helpful in narrowing the kinematic phase space to search [Si(1981)].

Measurements have been made on the Manitoba II instrument in order to help narrow the phase-space to search for the possible $\beta\beta_{0\nu}$ decay of ^{76}Ge to ^{76}Se , first by Ellis *et al.*, [El(1985)], and later by Hykawy [Hy(1991)]. When the Q -value obtained was used in examining data from counting experiments on ^{76}Ge , the lifetime extracted suggested a Majorana mass no greater than about $1 \text{ eV}/c^2$ for the electron neutrino; this figure is calculated by the following relationship with the lifetime $T_{1/2}^{0\nu}$ given in the standard model by:

$$2.2 \quad \langle m_{\nu_e} \rangle \leq \left[\frac{m_e^2}{T_{1/2}^{0\nu} \cdot C_{mm}^{(0\nu)}} \right]^{1/2} \text{ eV}$$

Even as far as the less-exotic $\beta\beta_{2\nu}$ processes are concerned, accurate Q-values combined with actual decay-rate measurements help to improve the nuclear transition-matrix calculations and thereby provide a better theoretical grounding for calculation of $\beta\beta_{0\nu}$ rates (see, e.g., [Civitaresc *et al.* [Ci(1987)], Doi *et al.* [Do(1985)]). The decay amplitude is a product of a relatively straightforward double-weak vertex component and a complex nuclear vertex (also involving weak processes) that introduces a fair degree of theoretical uncertainty. Thus, more examples of nuclei undergoing such decays need to be found. A recent tabulation shows that the number of such experimental candidates with accessible estimated lifetimes is in the dozens (Ha[1984]).

2. The Mass Table and Mercury

The acceptance of new data for the mass table, whether a first measurement of a nuclide or a re-measurement contributing to an existing data set, is almost entirely based on the links between members of the table. All precise atomic mass measurements are actually mass difference or, equivalently, energy difference measurements. The consistency of the data is thus reflected in the comparison between the relevant experimental doublet ΔM and/or reaction Q-values, as obtained by various investigators. Generally the data form a highly overdetermined set of numerical relationships between the nuclides, though clearly such a system will in practice demonstrate some inconsistency due at least to statistical variation. This is the classic problem faced by that mathematical genius, Carl Friedrich Gauss, at the dawn of modern scientific measurement, early in the 19th century. The necessity of reconciling astrometric data obtained by his students, which stubbornly insisted on showing an irreducible statistical variation (!) even when the master himself was driven to take measurements at the telescope, required the invention of the least-squares method. The method is used to this day in all the sciences for statistically rationalizing data sets from different groups (for the present context, see, e.g., [Wa(1960)], [Kö(1960)], [Co(1960)] and [Au(1986)] .

The mass tabulation generally used as a standard reference is based on the least-squares analysis and compilation of Audi *et al.* ([Au(1993)]). A persistent problem with the consistency of the existing mass tabulation revolves around the determination of the absolute masses of the mercury isotopes. At present, most of the data for elements in the valley of β -stability are consistent both below and above the region of $A \approx 200$ to within a few microunits or better. Connections to the actinides as well as to the lighter elements via reaction bridges and mass-doublet measurements can be made through mercury ("mercury" here meaning the set of relevant mercury isotopes). Wapstra *et al.* [Wa(1985)], [Au(1993)] report that their last two major adjustments of the mass table indicate an approximate $20 \text{ keV}/c^2$ mass deficiency with the mass spectrometric data of [Ko(1977)], *i.e.*, the latter are approximately $20 \mu\text{u}$ too heavy for the Hg isotopes in question. Construction of a number of closed-loops in the vicinity of the precious metals group reveals some suspicious residuals. More specifically, one of the worst cases of those seen in a general survey is illustrated in Fig. 2.3 below as loop "Γ". Here, a residual of $60.77 \pm 19.7 \mu\text{u}$ appears based on a sum of original reaction data given in Audi *et al.* [Au(1993)] (the calculation is shown in Appendix D). In this case, a worse than estimated error on the $^{188}\text{Ir}(\epsilon)^{188}\text{Pt}$ K-capture energy would be a prime suspect, given the difficulty of this category of Q-measurement.

There are a number of other less spectacular examples, all lending weight to the notion that one or more reaction data, at the least, have been mismeasured this region. Of direct relevance to the mercury issue are the loops given in Figure 2.4 as "Δ" and "9". These loops

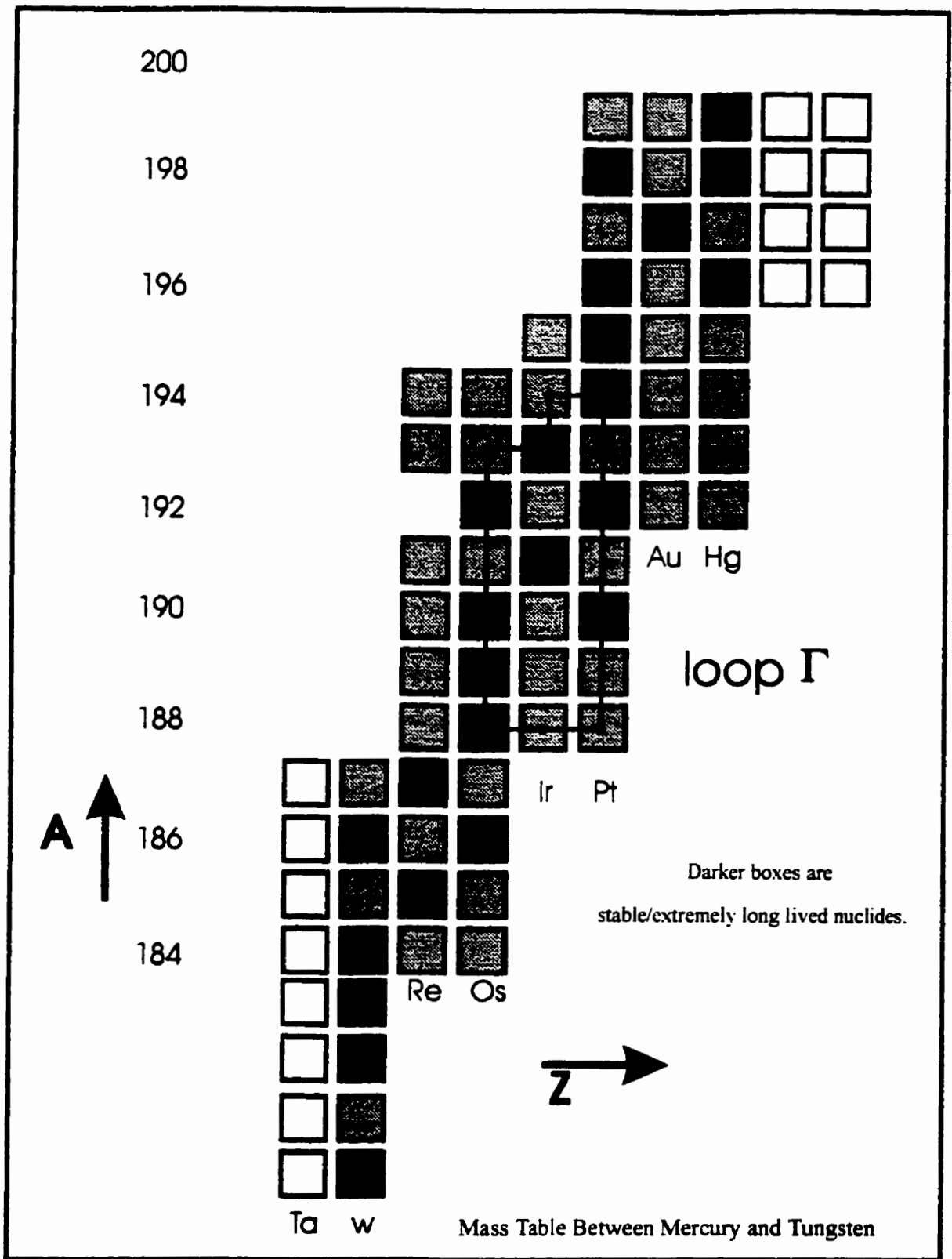


Figure 2.3 An example of a mass(/energy) differences loop with very poor closure.

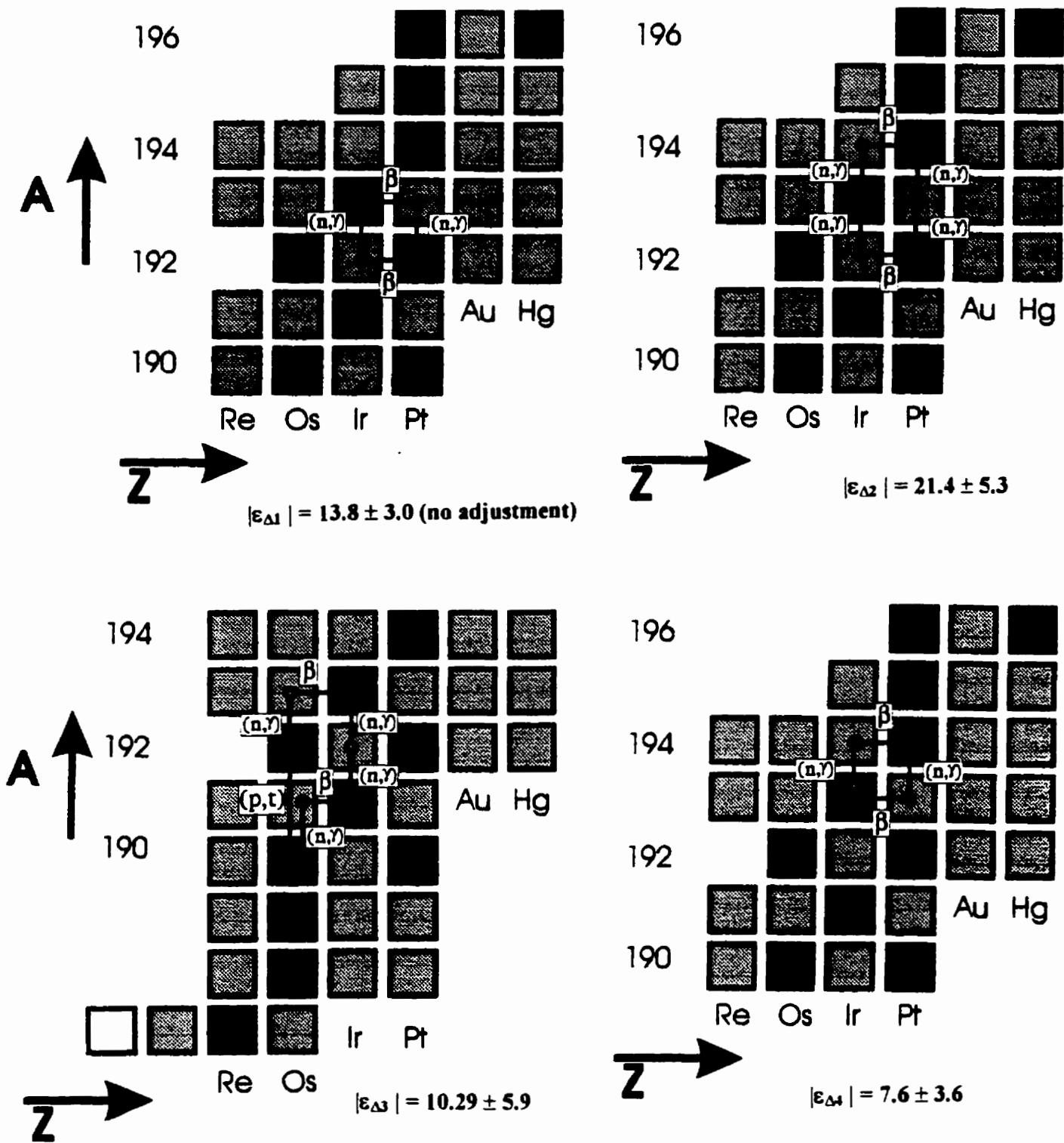


Figure 2.4a

Study Δ : Loops in the mass table network that suggest a poor linkages $^{192}\text{Ir} - ^{193}\text{Ir}$ and $^{193}\text{Ir} - ^{194}\text{Ir}$.

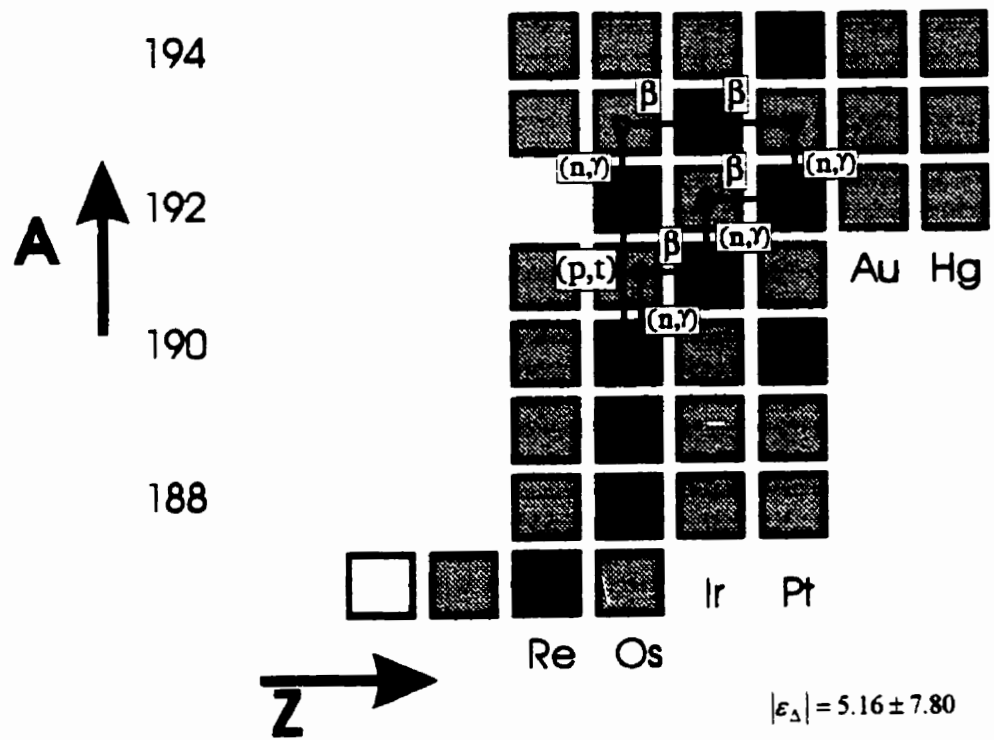


Figure 2.4b Study 9: A loop in the same region as 2.4a that closes by avoiding the linkages $^{192}\text{Ir} - ^{193}\text{Ir}$ and $^{193}\text{Ir} - ^{194}\text{Ir}$.

contain Q-value and Δm links that would form part of any overdetermined set of data connecting the mercury and tungsten isotopes along the valley of beta-stability. It is found that the inclusion of the ^{192}Ir - ^{193}Ir and ^{193}Ir - ^{194}Ir linkages in particular leads to loop residuals in excess of what would be expected from the reported uncertainties (Δ in the Figures of 2.4a). The encompassing loop which avoids these links (§ in Figure 2.4b), shows better closure, even though it is somewhat longer. Herein may lie the resolution to the mercury issue.

3. Mass Measurement Technique

As mentioned above, deflection mass spectrometry has been the technique of choice for mass/energy measurements, at least for stables, since the dawn of nuclear science. Its importance is strongly implied in the diagram above (Fig. 2.1), indicating its evolution throughout this century, in terms of precision (compare with, say, the evolution of particle accelerator energies, computer cycle times, *etc.*).

Traditionally, some of the most effective techniques for establishing mass differences have involved nuclear reaction energy measurements and doublet comparison via deflection mass spectrometry. A brief enumeration includes:

- "natural" decays:

α -decay energies for heavier elements, often using a semiconductor detector for precision α -particle energy measurements, but a magnetic-deflection spectrometer for some of the highest precision in calibrating sources (see, for instance, Rytz [Ry(1980)] and Rytz *et al.* [Ry(1972)].)

β^+/β^- -decay energies for neutron- or proton-rich lighter elements involving precision particle-energy measurement via some sort of magnetic analyser. β measurements are somewhat troublesome in that an undetected neutrino is of course also emitted in the decay to a three body final state: thus one must make an endpoint energy determination. This type of study is obviously related to neutrino mass searches, an area in which mass spectrometric data provides candidates in the form of Q-value inputs. See [Be(1972)] for a description of a precision β -energy spectrometer.

- (n, γ) reactions, especially valuable since they span single-mass-unit links between nuclides (isotopes) and are often easily brought about using neutron beams from nuclear reactors. Further, gamma ray energies in the 1 MeV range are commonly measured to sub-keV precision using, *e.g.*, Ge(Li) detectors. The highest accuracies are achieved with so-called Dumond-type diffractometers; see, for instance Schult *et al.*, [Sc(1972)] , which describes the study of (n, γ) lines in thermal neutron capture on high cross-section elements at the ANL CP-5 reactor.

- (d,p) reactions, made possible by accelerating deuterons instead of protons in, say, a cyclotron and/or linac. Proton energies are hence measured via a magnetic-deflection analyzer.

- relative Q-values: measurements of *differences* in Q-values in two (or more) reactions that connect the same initial and final states. An example is the use of the exchange reaction ($^3\text{He},t$) to determine accurate Q_{EC} values for a number of proton rich/neutron poor nuclides by Koslowsky *et al.* [Ko(1985)]. This group used the same ^3He beam to bombard a convenient stable target nuclide twice, reaching a well-characterized nuclide while connecting through the species of interest. (As mentioned in §.2 above, measurements of electron-capture energies are otherwise quite difficult to make).

A very important class of mass-ratio measurement techniques that can achieve very high precision is cyclotron-resonance mass spectrometry (see, *e.g.*, the high precision mass determinations of chlorine by the "mass synchronometer" design of Smith [Sm(1967)]). The principle is to measure the cyclotron frequency of a charged particle circulating in a highly stable and homogeneous magnetic field, as well as that of a second comparison species. Given that the cyclotron frequency varies inversely with mass-

$$2.3 \quad f = \frac{Be}{2\pi \cdot M}$$

one can in principle achieve arbitrarily high precision with a long enough frequency counting time or ion flight path. Ion spread and systematic errors due to residual gases, space-charge of the sample ions and field inhomogeneities, among other factors, will at some level, however, give rise to the practical limitations on precision.

A relatively recent form of cyclotron or frequency method of mass measurement, which promises to meet or exceed the precision attainable with "deflection" and reaction techniques on a regular basis, is "trap mass spectrometry", involving measurements of few-ion cyclotron frequencies in highly uniform magnetic fields. The principle is the same as the mass synchronometer, although an axially trapping, static electrical field must be used, often elaborated to a precisely set-up quadrupolar field. This means a somewhat complicated (epicyclical) type of motion of the ion species, reminiscent of the superimposed elementary motions which electrons execute in magnetrons and other microwave tubes. The advantage in this case is that the motion is precisely characterized in frequency components to high order, even in non-relativistic analysis. Though not entirely new (indeed, see Penning [Pe(1936)]) the method has attracted much interest since the work of Van Dyck *et al.* (*e.g.*, [VnD(1980)]), and that of other similar groups, in using such a Penning trap to measure fundamental quantities of great interest, such as the e^+/e^- mass ratio.

There has been a great resurgence in interest in the use of traps for precision measurements in the last two decades. From the technical viewpoint, this is because of the availability of:

- 1) high-stability, high-strength magnetic fields using commercially made systems that exploit a mature superconductor technology
- 2) precision machining methods for fabrication of cavities of exotic (low- μ) materials to high tolerances
- 3) high vacuum pumps and systems that can routinely reach $10^{-9} - 10^{-10}$ torr pressures, at which particles can circulate with very low probability of scatter.

Scientifically, part of the reason for the renewed interest is the possibility of examining nuclei with fairly short lifetimes. This generally entails on-line entrapment of short-lived nuclides produced in a suitably chosen target at a medium energy nuclear beam facility. Often an auxiliary, lower-precision trap, such as a Paul trap, is used to perform this latter function. The ISOLTRAP group of Kluge and Bollen at Mainz, for example, has reported resolving powers exceeding $m/\Delta m(\text{FWHM}) = 10^6$ and precisions ($\delta m/m$) of order 10^{-7} in studies on Rb, Sr, Cs, Ba, Fr and Ra isotopes ([Kl(1992),(1993)]). Further, measurements on H, O, Ne and Ar isotopes on

the MIT Penning trap by David Pritchard's group have been made to spectacular precisions of order 100ppt [Sc(1993)]. The interested reader is also referred to a recent proposal that the Manitoba group has participated in preparing [Ba(1994)], describing the new Canadian Penning Trap (CPT) now beginning operation on the ATLAS beam line at Argonne National Laboratory in Illinois. (A more recent progress article on the CPT is [Sh(1998)].)

Deflection mass spectrometry, as currently practiced, is the technique of determining atomic masses to high precision by comparing the deflection of two or more ionized species that have been sent through a set of magnetic and often one or more sets of electric fields. Clearly it is preferable if the system is insensitive to the other characteristics of the ions, such as initial velocity or source location. Roughly speaking, a system possessing some immunity to energy and finite source size is termed, in the first case, "energy focusing", and in the second, "direction focusing". These terms will be defined in a more precise manner later. It is very important that this degree of insensitivity also be similar, if not the same, for all species under comparison.

The technique of "doublet matching" involves determining quantitatively how far apart the peaks from species under comparison are in terms of mass units. This may involve determining to high precision what machine conditions are required to achieve a signal cancellation of the two peaks, or equivalently, their peak separation in channel numbers. As will be described in §III.3, the machine parameter of choice is the deflection voltage of the ElectroStatic Analyser or ESA. This may seem unusual at first given that homogenous electric fields do not analyse particle trajectories for momentum, but rather energy. Thus for a monoenergetic source a homogeneous ESA might seem useless, however, we shall see by closer scrutiny that this is not true for a general electromagnetic deflection system. Indeed, the idea that forms the basis of almost all deflection measurements is Bleakney's theorem, wherein a mass difference is directly related to an applied voltage difference.

III Ion Optics

Some words about ion optics as related to deflection mass spectrometry are in order. The purpose is to provide a basis for the description of the Manitoba II instrument, its characteristics, modes of operation and the performance achieved in this study. As this is a brief review, the reader is directed, for further background, to a number of classic works, recent reviews and especially some of the experimental physics monographs on focusing and transport of charged particles, mentioned throughout this section and in the References.

1. Direction Focusing In Magnetic and Electric Sector Fields

A sector magnet possessing, ideally, a uniform field will act as a lens for electrons/ions to at least first order, in the plane perpendicular to the field. More properly, since overall bending of the incoming "ray" bundle occurs, the system is like a lens-plus-prism arrangement in this analogy. A diagram illustrating such a situation is given in Figure 3.1 (see, e.g., Ewald and Hintenberger, [Ew(1952)]). Here, a sector magnet with plane boundaries accepts an incoming ion-beam bundle from the object point A', at an angle ϵ' to the entrance normal, and ultimately brings it to a (first-order) focus at A'', at an angle ϵ'' to the exit normal. Notice that there is a simple, highly informative geometric construction for deriving the image form for any given homogeneous sector lens, known as a Cartan construction [Ca(1937)] (or see Bainbridge [Ba(1953)]). This provides the equivalent focal information as the first-order equations mentioned below.

These focusing relationships, to first order and in well recognized geometric optics notation for thick lenses, turn out to be (see Fig. 3.2):

$$3.1 \text{ a) } (l' - g')(l'' - g'') = f' \cdot f''$$

$$3.1 \text{ b) } g' = a \frac{\cos \epsilon' \cdot \cos(\Phi - \epsilon'')}{\sin(\Phi - \epsilon' - \epsilon'')}$$

$$3.1 \text{ c) } g'' = a \frac{\cos \epsilon'' \cdot \cos(\Phi - \epsilon')}{\sin(\Phi - \epsilon' - \epsilon'')}$$

and

$$3.1 \text{ d) } f' = f'' = \frac{a \cdot \cos \epsilon' \cdot \cos \epsilon''}{\sin(\Phi - \epsilon' - \epsilon'')} \equiv f$$

with $f=f''=f$ - equivalent focal length
 g',g'' - respective distances from the field boundaries (or equivalently, the principal planes, if l' and l'' are so defined) to the principal foci (p.f. in Figure 3.2)

l',l'' - object and image distances to the magnet (field) boundaries, respectively

- $\varepsilon', \varepsilon''$ - entrance and exit angles of the beam axes with the respective field boundary normals
- Φ - actual bending angle undertaken by the beam in the magnetic field; clearly field dependent and therefore not necessarily equal to the magnet sector angle Ω .

The actual focusing qualities, as far as aberrations, and apart from inhomogeneities, depend on the shape of the field boundaries, the details of the fringe fields and the energy spread of the beam. Were one to eliminate somehow the fringe fields, it would be possible to fashion a perfectly focusing magnet for a monoenergetic beam by correct shaping of the field boundaries, *e.g.* see [Ke(1949)]. Fortunately, constructing an instrument with very good direction focusing properties does not require such elaborations: as we shall see, by incorporating an appropriate electrostatic lens, or electrostatic analyser (ESA), in the ion path, we can not only deal with dispersion due to energy spread, but with the aberrations of a simple, straight field boundary. The simplification of magnet fabrication is an important benefit as well.

The situation for the electrostatic field, though a "parallel" and not "curl" force, is strongly analogous in the case of a (coaxial) cylindrical condenser system. Such lenses are almost universally used as normal entrance and exit systems. For small bending angles Φ or Ω , one winds up with the same form as the magnetic sector equations except for a $\sqrt{2}$ scaling factor in angle and length; the relevant equations here are (normal incidence):

$$3.2 \text{ a) } (l'_e - g'_e)(l''_e - g''_e) = f'_e \cdot f''_e$$

$$3.2 \text{ b) } g'_e = g''_e = a_e \frac{\cot \sqrt{2} \Phi_e}{\sqrt{2}} \equiv g_e$$

and

$$3.2 \text{ c) } f'_e = f''_e = \frac{a_e}{\sqrt{2} \sin \sqrt{2} \Phi_e} \equiv f_e$$

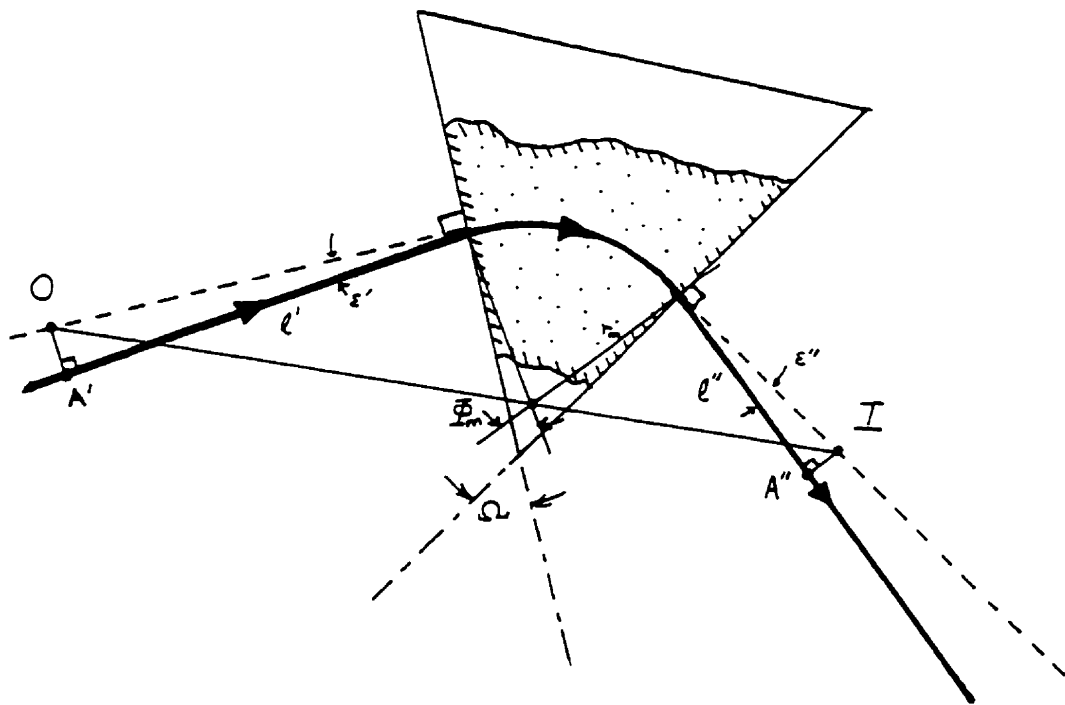
with $f'_e = f''_e = f_e$ - equivalent focal length

g'_e, g''_e - respective distances from the field boundaries (*i.e.*, for all intents, the principal planes) to the principal foci

l'_e, l''_e - object and image distances to the electric sector (field) boundaries, respectively

Φ_e - actual bending angle undertaken by the beam in the electrostatic field; clearly field dependent, however, almost universally the same as the sector angle Ω by design.

Again, a Cartan construction may be used to estimate the image position, as in the second part of Fig 3.1, having initially scaled the radius and sector angle by $1/\sqrt{2}$ and $\sqrt{2}$ respectively.



**Parameters of Homogeneous
Magnetic and Electric Sector Field Lenses
(with Cartan Construction of Image Points)**

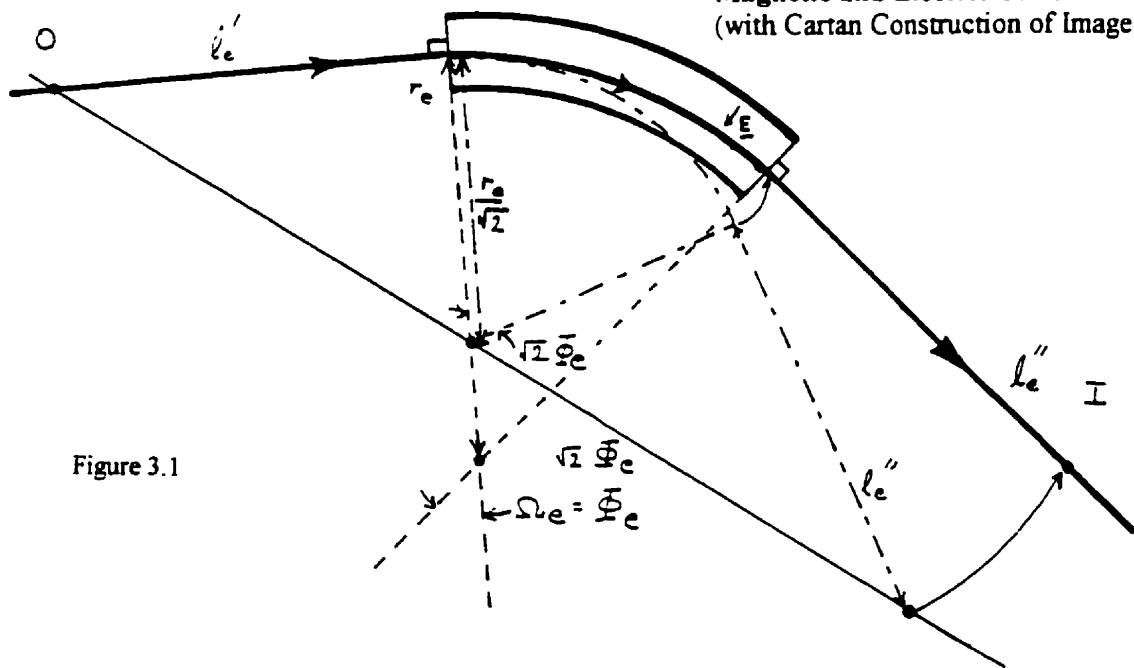


Figure 3.1

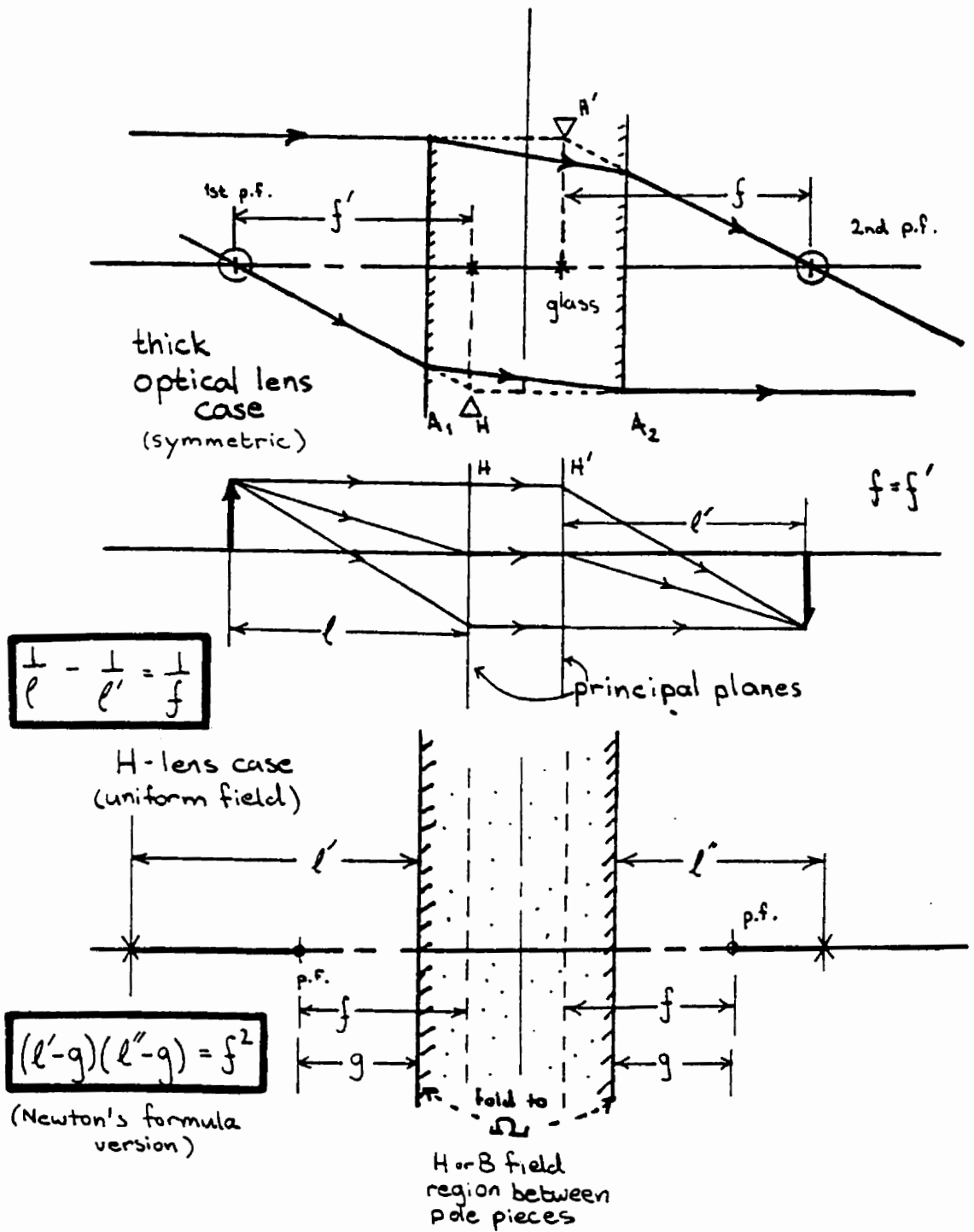


Figure 3.2 The Thick Optical Lens - Magnetic Lens Analogy

2. Double Focusing In Tandem Fields

The highest-performance mass spectrometers employ a combination of such lens systems to achieve good resolution. The principal issue is the finite spread in the initial energies and in the path angles of an ion beam provided by a source with (object) slit. Unless a deliberate design effort is made to correct for corresponding aberrations in a system intended to disperse by mass, bad images of the source slit, with what are analogous to optical chromatic and spherical aberrations, will likely result. In other words, the simplest sector fields guarantee only a first-order focus. It is ultimately because an electrostatic lens will disperse by energy, while a magnetic lens analyses for momentum, that they can be judiciously combined to cancel energy aberrations while providing direction focusing, at least to some order in δE and $\delta\alpha$, and at some point, if not some plane, in space.

A simple development for the 1st-order case follows Duckworth *et al.* [Du(1986)]. We have in addition to the axial focusing equations above, the following relations on lateral image size and displacement, due both to object location and change in beam parameters:

$$3.3 \quad b_e'' = r_e(\beta + \frac{1}{2}\gamma)[1 - \mu_e] + b_e\mu_e$$

$$3.4 \quad b_m'' = r_m(\beta + \gamma)[1 - \mu_m] + b_m\mu_m$$

where

b_e'' , b_e' -are the object and image displacements from the optic axis, respectively, for the electrostatic lens case; likewise for the magnetic lens case

β -is the variation in speed, *e.g.*, $v = v_0(1+\beta)$

γ -is the variation in mass, *e.g.*, $M = M_0(1+\gamma)$

$$3.5 \quad \text{and} \quad \mu_e \equiv \frac{-f_e}{l_e - g_e} \quad \text{-can be shown to be the lens magnification for the electrostatic lens, similarly for the magnetic field lens factor } \mu_m$$

Now, making the ESA's image the object for the magnetic lens,

$$3.6 \quad b_m'' = r_m(\beta + \gamma)(1 - \mu_m) + \mu_m[r_e(\beta + \frac{1}{2}\gamma)(1 - \mu_e) + b_e\mu_e]$$

We next demand that the system is velocity focused, *i.e.*, that the coefficient of β vanish - thus

$$3.7 \quad r_m[1 - \mu_m^{-1}] - r_e[1 - \mu_e] = 0$$

If we adopt an object width of S_0 , meaning in practice the ion-source slit width, and assume that a perfect image of the slit is formed at a normal angle on a photographic plate or image reticon, say, then two masses will be just resolved when the centres of the image lines are μS_0 apart, where μ is the total system magnification. If electronic detection is used in which a detection slit is used to actively scan the image plane, say also of width μS_0 in order to maintain sensitivity, this will be

degraded by a factor of 2. Notice, for instance, that for each ion species, one ideally observes a triangular peak of base width $2\mu S_o$, as the ion beam, of perfectly sharp image width, is swept across such an aperture. By this consideration, and using the imaging and constraint equations above, we arrive at,

$$3.8 \quad \frac{\Delta M}{M} = \gamma = \frac{2S_o}{r_e} \frac{-\mu_e}{1-\mu_e}, \text{ the resolution}$$

and

$$3.9 \quad d = \frac{r_m}{200} [1 - \mu_m] \text{ per 1\% mass difference, as the dispersion.}$$

Interestingly, resolution seems to depend only on the characteristics of the electrostatic analyser, as it were, how finely the image is drawn, whereas dispersion is a function only of the magnet, *i.e.*, how much the spectrum has been spread in space. In fact, the velocity focusing constraint implicitly ties the two together.

Although this is far from the end of the story on ion optics, one already can calculate these primary performance figures for the Manitoba II instrument using the primary optical dimensions presented below. Further, one must bear in mind that the development above, though extremely useful for conceptualizing and initial design, is a first-order theory.

The Manitoba II instrument is a high-resolution design, demanding attention to higher order aberrations not considered in the first order theory. For ions originating at the source and on the optic axis, the lateral displacement at the image plane can be expressed as:

$$3.10 \text{ a) } y_B = r_m \{ B_1 \alpha_e + B_2 \beta + B_{11} \alpha_e^2 + B_{12} \alpha_e \beta_e + B_{22} \beta^2 \}$$

again using the notation of Duckworth *et al.* [Du(1986)] where the radius of the magnet is the overall scale factor and:

3.10 b) $\alpha_e \equiv$ the angular displacement of the source ions at the system entrance (to the ESA in this case) from the axis or their angular spread if considered as a group

3.10 c) $\beta_e \equiv$ the deviation of a source ion velocity from the nominal, or the spread in ion group speeds

and

the subscripts to B are assigned a value of 1 or 2 to indicate a coefficient of direction or velocity deviation, respectively. Thus B_{12} , for instance, would be a second-order, mixed coefficient of direction and velocity.

The second-order coefficients are a complicated function of geometry, which can be summarized for our case as,

$$3.11 \quad B_{xy\dots} = B_{xy\dots}(\Phi_m, \Phi_e, \epsilon_m, \epsilon_e, d/r_m, r_e/r_m, l_e/r_m, l_m/r_m)$$

Here we see the eight "canonical" variables applicable to the Manitoba II system: the respective sector bending angles and ray entrance angles, as well as the instrument dispersion, electrostatic analyser radius and key element spacings, each of the latter normalized to the magnet bending radius.

For first-order direction and velocity focusing we require $B_1=B_2=0$, respectively, while for second order focusing B_{11} , B_{12} and B_{22} must also be zero; thus we need to solve for five equations simultaneously. Hintenberger and König[Hi(1959)] conducted an extensive numerical study of solutions to this problem, largely for cases involving straight field boundaries with the assumption of abrupt field boundaries. The result was an important compendium of possible designs for this category of mass spectrometer, one of which was chosen, mainly by virtue of its rather compact dimensions (with respect to the magnet radius) for what was to become the Manitoba II instrument.

Further developments in the design of high-order systems were brought about through the study of third-order trajectories for a number of useful cases by Matsuda and co-workers. Most notable were the cases of inhomogeneous B fields and toroidal electrical lenses, including the effects of fringe fields [Ma(1970a,b),(1972)]. This work was inspired by experience with the high dispersion Osaka II instrument built at Osaka University by Matsuda *et al.*[Ma (1966)]. It was indeed one of the high performance benchmarks in deflection instruments, often reaching peak resolutions of order 5×10^5 FWHM, a figure only exceeded on a regular basis by Kozier [Ko(1977)]. Nevertheless it suffered from design problems primarily related to fringe fields, as well as operational difficulties due to the mechanical and electrical noise pick-up in its long drift-spaces. This group was responsible for the development of the TRIO ion-optics analysis package [Ma(1976)]. This program has proved to be a highly useful tool for physicists in analysing ion optics designs, allowing for an arbitrary combination of electric and magnetic lenses of various field types (*e.g.*, homogeneous field, $1/r$ field, toroidal fields, *etc.*) as well as drift spaces and source profiles.

The TRIO system was used in this laboratory to show that the original calculations of Hintenberger and König, which did not take into account fringing fields, were imperfect in the sense that the second order terms were not quite zero. Subsequent investigation later showed (*see, e.g.*, Matsuda[Ma(1976)]) that fortuitously the operational implications as far as resolution were negligible.

3. Bleakney's Theorem

The basis of most measurements of mass, as mentioned in previous sections, is a mass *comparison between ion species*. In a mass spectrometer, where a number of electromagnetic fields are involved in directing charged particle motion, it is highly desirable that any comparison be made by changing only some single field value to achieve the matching condition in the instrument, *i.e.*, the same image peak location, for the two ions of interest. This change can then be related to their mass difference.

The reason for this approach is simple: whereas highly stable static fields are relatively easy to set up and maintain using commercially available equipment, at least for the length of time required for a measurement (of order 1 hour), absolute electric and magnetic field values are extremely difficult to measure to high levels of precision. Thus, one would make a mass

difference determination on the basis of a highly precise measurement in the change of one parameter. What is required is a relationship between such a field quantity and mass, and this turns out to be pleasingly simple: Bleakney's Theorem.

Bleakney [Bl(1936)] was one of the first to show that for ions traversing an arbitrary (static) electromagnetic system, the trajectory of an ion will be identical for one mass value with respect to another when all of the electric fields are varied in proportion to the mass difference between the two. Since electric field strengths are, in principle, in proportion to the voltage generator values used to produce them, this is commonly expressed as:

$$3.12 \quad m_1 V_1 = m_2 V_2$$

Mass spectroscopists often use the instructive form,

$$3.13 \quad \frac{\Delta m}{m} = \frac{\Delta V}{V}$$

(in which the algebraic sign coming from 3.12 has been dropped, but the appropriate "directions" of respective Δ s are carefully noted in use).

The proof is quite straightforward:

recall the Newton-Lorentz (N-L) equation

$$3.14 \quad m \bar{x}'' = q \{ \bar{E} + \bar{x}' \times \bar{B} \}, \text{ valid when } v_{\text{ion}} \ll c \quad (\bar{x}' \text{ is simply } \frac{d\bar{x}}{dt} \equiv \bar{v}, \text{ etc.})$$

and the Euclidean distance element,

$$3.15 \quad ds^2 = dx^2 + dy^2 + dz^2$$

(where we pick $ds \equiv +\sqrt{ds^2}$)

Then writing the left-hand side of 3.14 in terms of the distance parameter,

$$3.16a) \quad m \frac{d}{dt} \left(\frac{d\bar{x}}{dt} \right) = m \frac{ds}{dt} \frac{d}{ds} \left(\frac{d\bar{x}}{dt} \right)$$

$$3.16b) \quad = m \frac{ds}{dt} \frac{d\bar{v}}{ds}$$

but

$$3.17 \quad \frac{ds}{dt} = v$$

therefore, in terms of velocity and distance parameter s ,

$$3.18 \quad Mv(s) \cdot \frac{d\bar{v}(s)}{ds} = q\{\bar{E}(s) + \bar{v}(s) \times \bar{B}(s)\}$$

This differential equation will solve for a unique space path for two boundary conditions, say, initial distance $s=0$ and speed $v=0$ (see Fig 3.3).

Now, allow a variation in mass by δM , *i.e.*, let some $M'=(1+\delta)M$, and require that by varying the velocity and E-field, by γ and α respectively, one obtains the same path. This will be guaranteed provided we retain the same form as 3.18. $s(t)$ will naturally change with γ , but since t does not explicitly appear, it is irrelevant¹: the ion will simply arrive at its destination at another time. Thus, assuming no change to the B field for simplicity,

$$3.19 \quad (1 + \delta)M \cdot (1 + \gamma^2)v \frac{d\bar{v}}{ds} = q\{(1 + \alpha)\bar{E} + (1 + \gamma)\bar{v} \times \bar{B}\} \quad (\gamma \text{ here not to be confused with the } \gamma \text{ as conventionally used in eq. 3.3 for mass variance})$$

we have the global rescaling,

$$3.20 \quad (1 + \delta) \cdot (1 + \gamma^2) = (1 + \alpha) = (1 + \gamma)$$

that is

$$3.21 \quad (1 + \delta)(1 + \gamma) = 1 \quad \text{but then we have also}$$

$$3.22 \quad (1 + \delta)(1 + \alpha) = 1$$

Now, rewriting eq. 3.22 in terms of finite differences, and multiplying by $M (=m)$ and $E \equiv |\bar{E}|$,

$$3.23 \quad (M + \Delta M)(E + \Delta E) = ME$$

Finally, assuming that we can always talk about field strength in terms of the applied potentials that "create" E,

$$3.24 \quad (M + \Delta M)(V + \Delta V) = MV$$

which is equivalent to 3.12 and 3.13 (again, being mindful of implicit signs). *QED.*

Turning the point around, or stated as a Lemma, any mass comparisons to be made to high precision must respect the same-path-condition if 3.24 is to provide a meaningful result. That previous work with the Manitoba II instrument has provided mass values with absolute errors estimated in the parts-per-billion range, based very directly on this relation, is the result of a design feature where this can be rather directly checked. This feature is an accessible intermediate focus, situated between the ESA and magnetic analyser, and will be discussed further in the next section.

¹ if the rescaling exists, as we shall see here it does, this illustrates a type of *path-parameterization invariance* for the N-L equation.

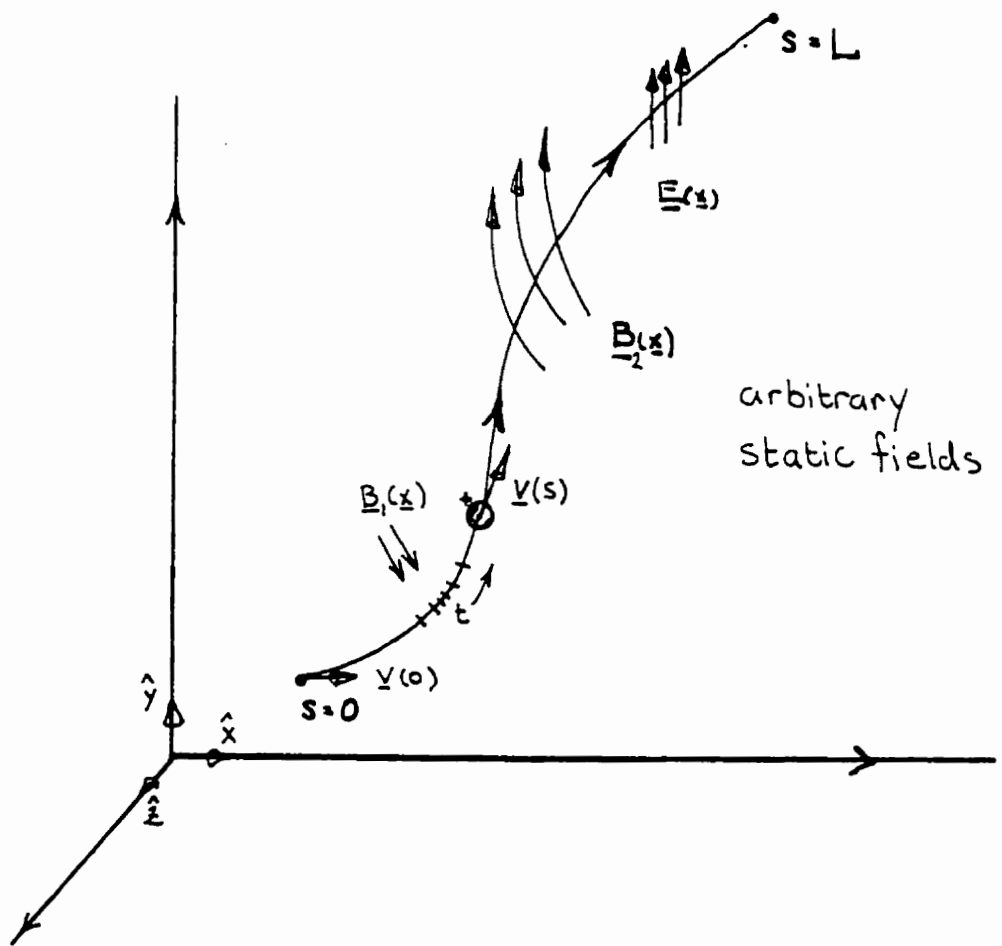


Figure 3.3 An arbitrary path through static electric and magnetic fields.

IV The Manitoba II Instrument

1. Optical Specifications

The Manitoba II mass spectrometer is a deflection-type instrument, composed of a tandem electrostatic analyser (ESA) and uniform-field magnet sector. The instrument possesses double focusing properties, to second order in direction and energy. This means that positive ions sent through the system from the source slit, having some variation in initial energy and direction, will be brought back to an image of this slit with an excellent focus. This in turn results in a respectably high resolution. The system is based on one of the ion-optical specifications calculated by Hintenberger and König (in [Hi(1959)]). The system actually exhibits rather small third-order coefficients in the plane, with some convergence in the vertical direction due to the magnet fringe fields. This is largely known through the work of Matsuda [Ma(1976)]. (The theory of the focusing of positive ions was very briefly reviewed in Section III above, as well see, *e.g.*, Barber *et al.* [Ba(1971)] and Ewald and Hintenberger [Ew(1952)]).

The instrument has been described in great detail elsewhere (see, *e.g.*, Bishop[Bi(1969)]). The main dimensional parameters of the ion path are given in Fig.4.1 (plan view), with the other main characteristics:

accelerating potential	$V_A = 19.7 \text{ kV}$
magnification	$\mu = -1/2$
practical resolution	$R \approx 300,000^{-1}$
(object/image) slit width	$\approx 2 \mu\text{m}$
M/c range	$\approx 350 \text{ u/c}$

One of the very desirable characteristics of this machine includes a relatively short beam path, both in its entirety and in field free regions. This makes the system far less prone to vibration and keeps the influence of unwanted EM fields (*e.g.*, 60-cycle mains) on the beam to a minimum. Further, this particular design achieves second-order properties using only straight magnet boundaries, as compared to some competing schemes which required specially machined, *i.e.*, curved magnet end shapes. Since any mass spectrometer magnet for a high dispersion instrument tends to be of respectable weight and size, this is no small consideration. Finally, as mentioned earlier in this work, an important feature of the optics is the intermediate direction focus between electric and magnetic analysers, at which an energy selector slit is located (S_B in the figure). This allows the operator to check for identical beam paths for the species under comparison using the live display. The operator increases the main acceleration voltage until a peak disappears, and notes whether its partner is also simultaneously occluded.

Manitoba II was completed in the late '60's, and has undergone very little mechanical change since. However, substantial electrical and electronic upgrades were done during the course of this study in order to restore and improve capabilities being lost to passing commercially available technologies. This will be described in detail in Section V.

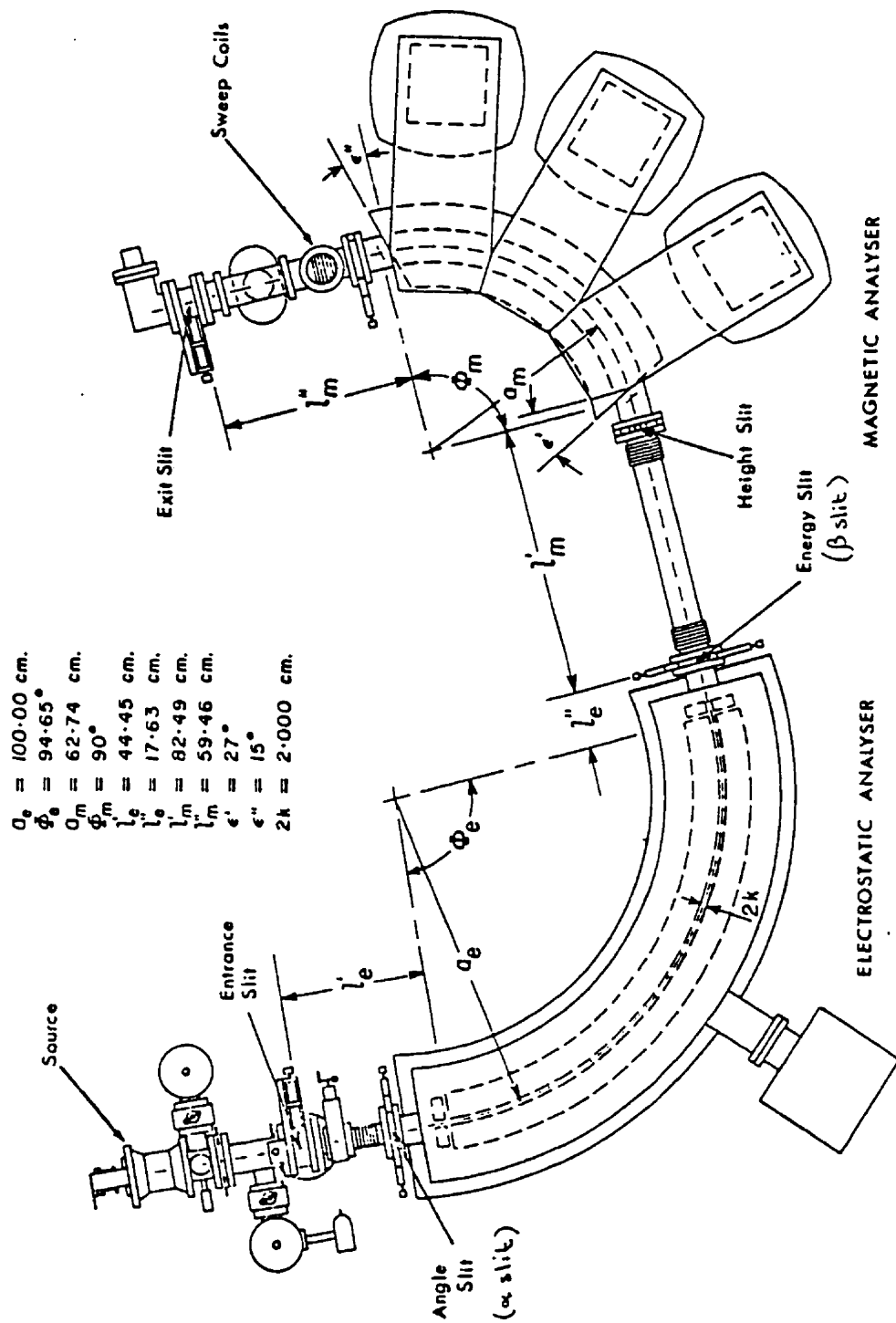


Figure 4.1 GEOMETRY OF THE MANITOBA II MASS SPECTROMETER

2. Electrical/Data Acquisition Characteristics of the Manitoba II

Presented in Figure 4.2 is a block diagram of the Manitoba II potentiometric mass measurement system as it appeared in 1993. The operation at this block diagram level is essentially unchanged. The system serves basically to provide repetitive changes in system voltages, in accord with the requirements of Bleakney's theorem (see III.3), synchronised to periods of data collection with the instrument at each voltage. The idea is to determine precisely what difference in potential would be required to match peaks originating from elements or compounds of similar mass. Bleakney's theorem can then be used to derive the mass difference of the species involved. Generally one is concerned with comparing species fairly close in mass, often much less than a mass unit apart. Figure 4.3 provides a case of a multiplet being matched through comparison of peaks stored in a multichannel analyser (MCA) instrument while the system was switched between two voltages. Indeed the peak-matching process revolves around the MCA, where peaks can be compared visually as in this example or, with some refinements, stored for off-line computer analysis.

Although described in depth elsewhere (see, *e.g.*, Southon [So(1973)]), the control system bears some scrutiny here. The differences in operation between visual and computer matching modes (see §IV.3) are not great at this level, and these differences will be ignored for the moment.

A mechanical chopper, typified by a Guildline Low Thermal (gold contact) type 9745-4, provided the master timing for the instrument. The chopper would both generate timing pulses and distribute the required ΔV sources to the electrostatic analyser plates. The latter were simply small batteries feeding high precision resistors near the ground point of the old main battery stack (this will be described later). The timing pulses were used to engage other ΔV sources in the system at the appropriate time using isolation techniques such as relays and opto-couplers. The ΔV for the 20 kV primary accelerating potential, for instance, was toggled on and off via neon light and photocell, or more recently, by a light emitting diode facing a phototransistor. The timing pulses would also be used to trigger the oscilloscope sweep and signal averager. A highly linear sweep signal was taken from the oscilloscope for use in generating the current used in the ("Helmholz") coils that would sweep the emerging ion beam across the image slit. Finally, as the raw ion detector signal could be routed through either one of two amplifier channels, the timing signals were also used to switch this analogue signal back and forth between the two at the appropriate times.

3. Visual versus Computer Matching

Two procedures have been employed in performing peak matches in this work. In "visual (null) matching", two conditions alternatively exist during a match: one in which an appropriate ΔV is added to the base voltage of the electrostatic elements, and one in which only the base voltage is applied. As always in this work "appropriate ΔV " is to be taken to mean a value determined for the particular electrode nominal V and the $\Delta M/M$ expected for the match, in accordance with Bleakney's Theorem. The phases are about 20 ms wide, thus approximately 50 sweeps of either phase will be presented and accumulated per second. The data accumulation occurs in a single memory block of a MultiChannel Analyser (to be described further later) with subtraction on alternate sweeps. The effect is to produce a flat cancellation signal upon matching peak positions and intensities. This is illustrated for the ideal case in Figure 4.3. The operator

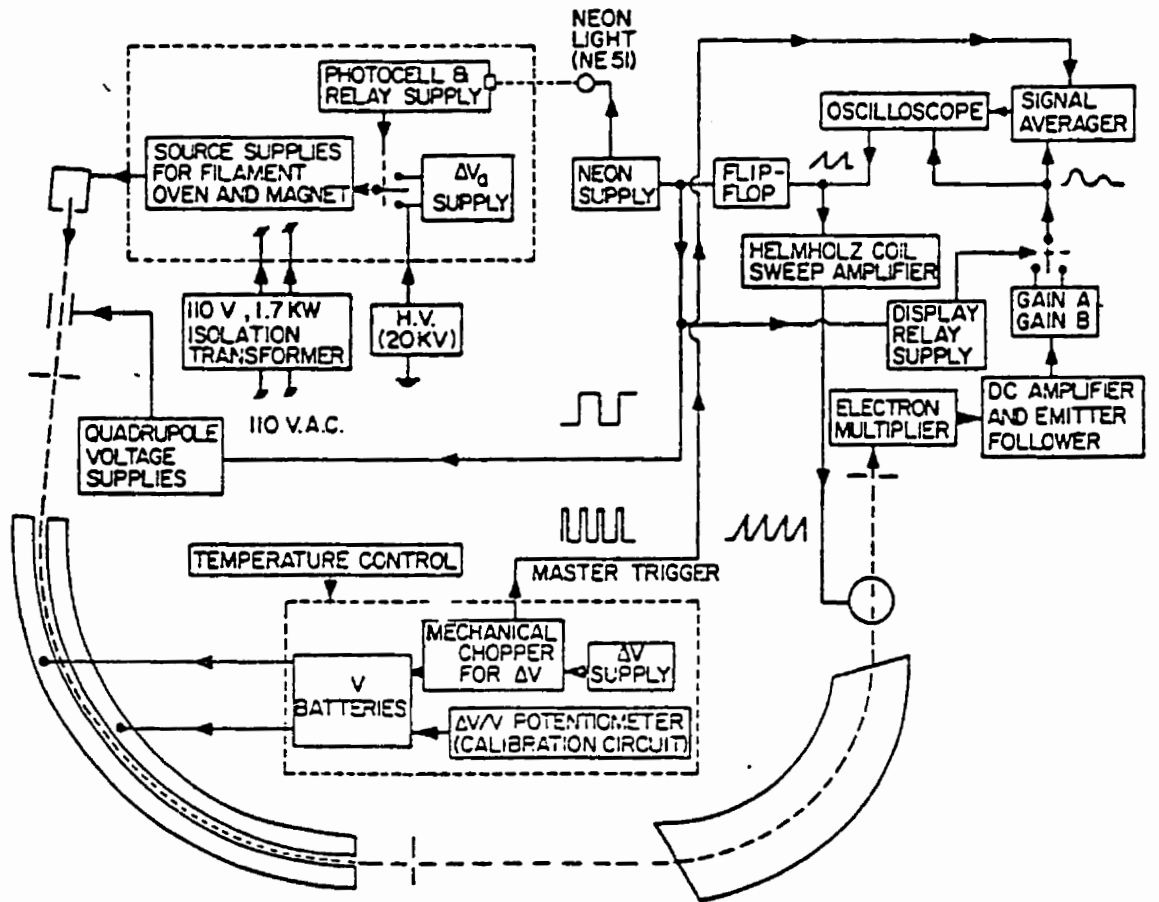


Figure 4.2 OVERALL CONTROL SYSTEM

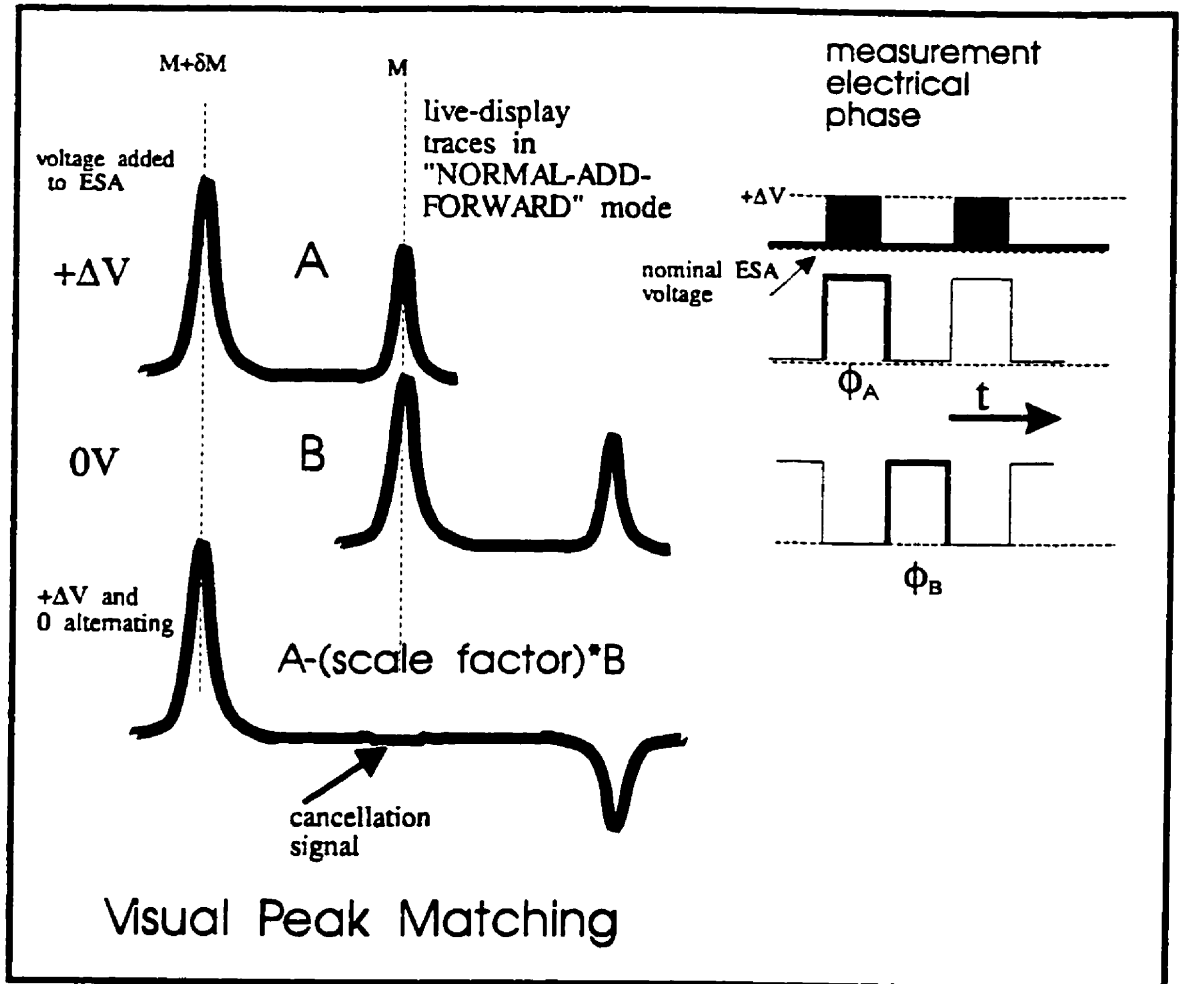


Figure 4.3 Appearance of the live display at match in a visual run: potentials associated with each comparison phase.

adjusts the source of the ΔV applied to the ESA plates until satisfied with the match. The operator then "merely" measures this ΔV using the precision potentiometer system. Experience has shown that match conditions to within nearly $f=1/1000$ of a peak width can be reliably achieved by the human eye using this technique.

In "computer matching", there are four phases: one in which a " ΔV " estimated to give a good match is presented, one in which a smaller "+ δV " is applied, another in which no added voltage is applied and one in which a "- δV " is applied. The symbol " ΔV " is often used both to refer to any voltage change or to the largest of the voltage changes, *i.e.*, that occurring during nominal Φ_0 . The context should make clear which meaning is intended. The timing of the application of the various ΔV values is illustrated in the right-hand side of Figure 4.4. The purpose of the δV values, referred to as the "splits voltages" for reasons which will become clear, is to provide a channel number versus ΔV calibration. The corresponding effect on the peaks is illustrated for an idealized MCA display drawn in the left-hand side of Figure 4.4, mentioned previously. Here, the operator performs no adjustment other than an initial setup during the run. The operator must, however, still measure all of the ΔV values, both the larger ΔV and smaller δV s, upon completion of the data accumulation in the MCA. The data taken are analysed by computer after transfer from the MCA, hence the name computer match. As will be described later in greater detail, a program finds the centroids of all relevant peaks and effectively performs a mathematical match using the given measurement voltages.

Since the δV values applied to the ESA plates are very small, the system has been kept simpler than would seem to be strictly required by arranging for no change to the other system potentials when these ΔV s are applied. The corresponding values elsewhere, say, the source-focusing quadrupole, would be as small as any local variation in supply voltages. These, in turn, are not a concern due to the second-order energy-focusing properties of the system.

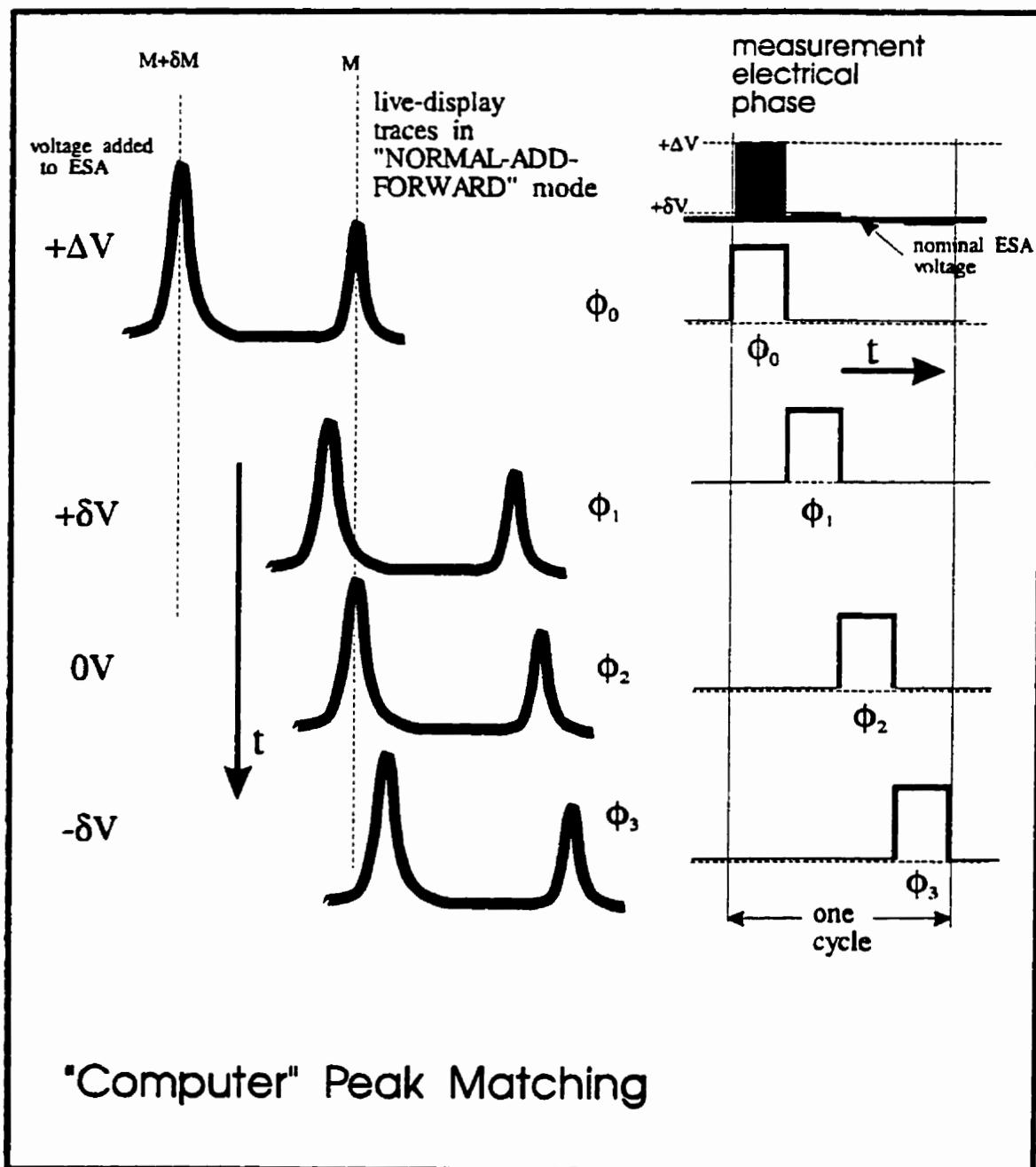


Figure 4.4 Appearance of the live display at match in a computer run: potentials associated with each comparison phase.

4. Matching Modes

Peak matching, whether executed visually or by mathematical analysis, involves comparison of peaks purposely obtained under the somewhat different ion-beam sweep conditions of the two or four cycles in a match. Therefore, without some scrutiny, there could be ample opportunity for erroneous systematic contributions to the peak separation measured, especially considering the high ultimate precision we demand of the system. One of the best methods for finding such factors, once any obvious problems have been eliminated, is to take all match sets under a combination of diagnostic modes. These include, for visual matching, all of the permutations of:

N vs. B: "normal" versus "backwards" routing of the ion signal through the respective amplifier channels. This checks for front-to-back human as well as signal handling biases. Part of the former concern is with how the operator trims peak magnitudes in order to achieve the best visual signal cancellation on the MCA. This obviously is not relevant in the case of a computer match; in this case, a similar type of check is affected by reversing the phase of the application of the small δV s.

A vs. S: adding versus subtracting the ΔV , *i.e.*, applying a $-\Delta V$ in the latter case, since either is possible by Bleakney's theorem. This checks for a number of problems, including failure of the ΔV relays throughout the system, and front-to-back differences in the potentiometric measurement system. In the case of the 4-phase computer match cycle, the δV order is also reversed (including any extra reversal in a "B" type match, *i.e.*, a "BS" match mode would give the nominal δV order).

F vs. R: forward versus reverse sweep sense of the magnetic scanning field at the final image point. This is a diagnostic for systematic offsets in the start and/or magnitude of the sweeps that are front-to-back sensitive.

In summary, in the 8 match modes, the relevant parameters are set as shown in table 4.1.

mode	visual	computer
NAF	normal routing; add ΔV ; forward sweep	nominal splits order; add all ΔV s; forward sweep
BAF	backwards signal routing; add ΔV ; forward sweep	backward splits order; add all ΔV s; forward sweep
BAR	backwards signal routing; add ΔV ; reverse sweep	backward splits order; add all ΔV s; reverse sweep
NAR	normal routing; add ΔV ; reverse sweep	nominal splits order; add all ΔV s; reverse sweep
NSF	normal routing; subtract ΔV ; forward sweep	nominal splits order; subtract all ΔV s; forward sweep
BSF	backwards routing; subtract ΔV ; forward sweep	backward splits order; subtract all ΔV s; forward sweep
BSR	backwards routing; subtract ΔV ; reverse sweep	backward splits order; subtract all ΔV s; reverse sweep
NSR	normal routing; subtract ΔV ; reverse sweep	nominal splits order; subtract all ΔV s; reverse sweep

Table 4.1 Summary of matching parameters for each mode.

V New Electronics for the Manitoba II Instrument

Within a year of when the studies described in this thesis were begun, (in 1993), it was clearly established that the performance of the Manitoba II had deteriorated as a result of several emerging problems associated with aging electronics. It was realized that the introduction of modern devices and techniques would offer improved performance.

The most severe problem was the unavailability of true reference mercury cells for the Electrostatic Analyser (ESA) high-stability electro-voltaic stack. Other problems included the originally impressive, but now troublesome, low thermal emf chopper used for delta-V switching in digital runs, as well as an aging MultiChannel Analyser (MCA) and dated computer processing technique.

Although we intended to address all of these problems, and develop designs for the refurbishment of the instrument, only the most essential items are covered in this study. These include:

- new ESA voltage supply and measurement system
- new primary reference voltage source
- new linear ΔV voltage generator
- new hardwired digital chopper with solid state (CMOS) ΔV summing relays
- upgrade to ion-optics switching circuits, simplifying "subtracts"-type doublet comparisons
- a source filament emission stabilization system to relieve some burden on the operator

- new data download and analysis software
- new magnet control software

as these were crucial to operating the mass spectrometer.

Items which will be pursued in the future to improve the operation of the instrument include:

- a superior ΔV generator with fast switching capability
- an automated system for measuring V and ΔV
- a computer directed digital chopper system
- a newer MCA system, made up of embedded personal computer hardware and software

The former items are described below.

1. The ESA Cells

Referring to Fig. 5.1, one can see how the original stable V and ΔV supplies were configured in the design of Barber and Bishop ([Bi(1969),(1970)]). The design centred around a stack of electrovoltaic cells, specifically, Union Carbide 97.3 V mercury reference batteries, themselves composed of series packaged cells. This grouping was somewhat arbitrary, based on availability and on a convenient subdivision of an approximately 1000 V stack for measurement

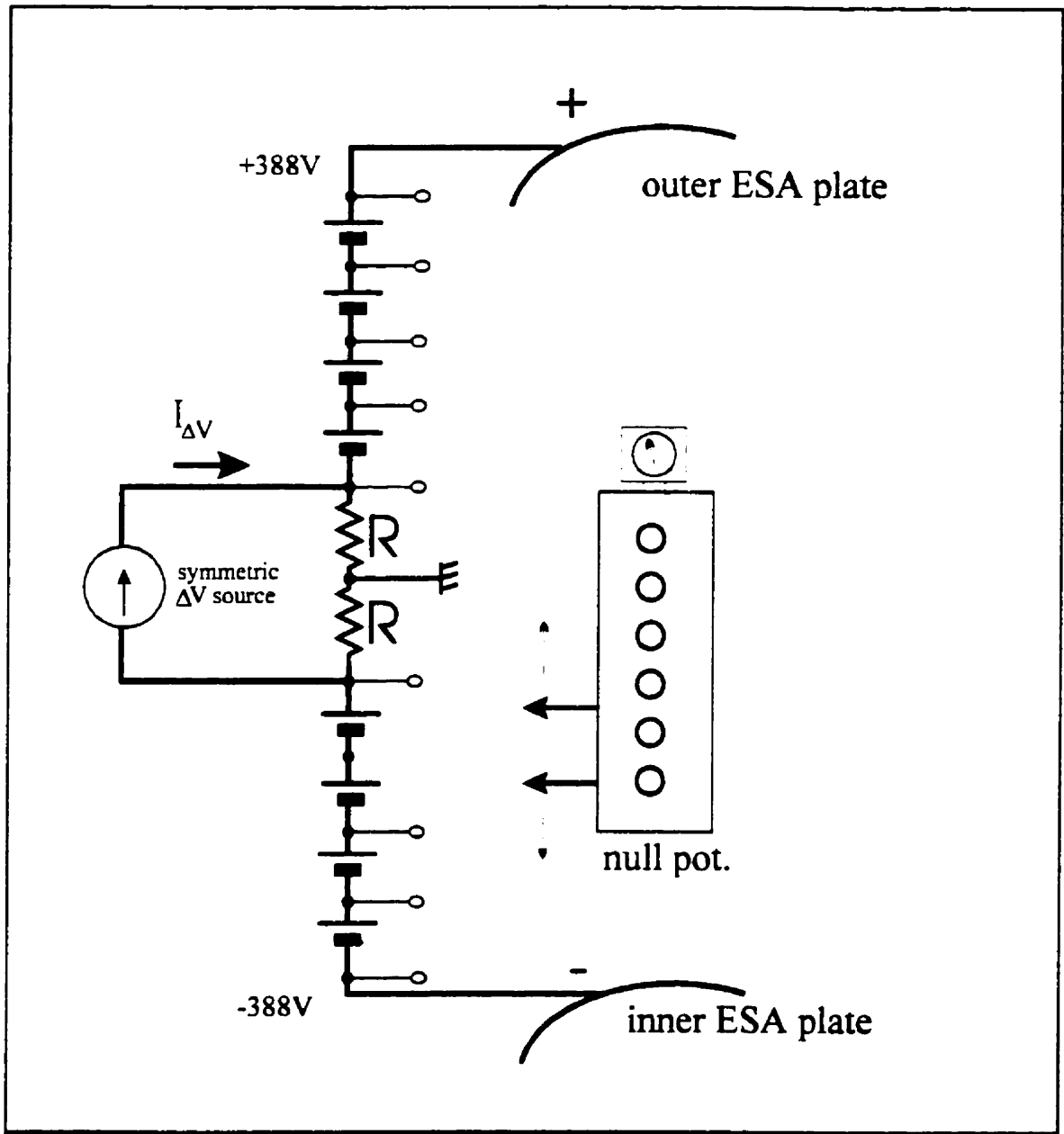


Figure 5.1 The voltage supply and potentiometry system before modification.

purposes. The original stability of these reference batteries, relative to each other, was a few parts in 10^9 . These cells were later repackaged by the manufacturer as the TR-13xR series of mercury reference batteries, variously offered in 8.08 V (TR-136R) and later in 4.04 V (TR-133R) per unit values at room temperature. The stability figures for the TR-13xR units, both long and short term, were still impressive and they became the standard component of the ESA stack. These batteries were combined in modules comprising 24 such units, giving a nominal 97.3 V per battery as specified in the original design. Again this value was rather arbitrary, being chosen to conserve the existing circuitry.

The fact that a stack of batteries could be arbitrarily floated above ground allowed for a simple method of introducing the ΔV , as a current supply feeding a matched pair of precision resistors between each stack and ground. Further, a similar module served as the voltage reference for the system, that is, the "power source" of the potentiometer.

This system demonstrated and possessed some highly desirable traits. First of all, as mentioned, the cells were remarkably stable both in the short term, that is to say, for the course of a run, and in the longer term as far as longevity near a useful operating point. The former property can be attributed to both an intrinsically high electrochemical stability and to the statistical cancellation of fluctuations in voltage when summed in a large stack. Secondly, as nearly ideal voltage sources, the batteries possess high electromagnetic interference (EMI) immunity; the entire stack appearing as perhaps a 1 k Ω resistor to earth ground (*i.e.*, Thévenin series resistance). Finally, they were relatively cheap and required only nominal thermostatic regulation in a "warm-box" to assure a stable output.

Unfortunately, the TR-133R cell design, then the most current offering of this type of cell in the cell voltage range desired, had undergone a change by the maker(s) to a H133R grade. A number of cells with this nominal number specification were ordered from several apparently primary sources for test, all demonstrating a very disappointing stability. On any given day, tests of the ESA stack against the reference battery showed an alarming drift (as bad as 1000 μ V per run for each 97.3 V stack battery pack). It was difficult even assembling a trustworthy reference battery. No brand that was available seemed to be any better than the other. Further, no manufacturer would assure us of the original performance of this cell type. Indeed, the information verbally provided indicated that the Mn content of the cell electrolyte mixture had likely been increased in order to improve the ampere-hour performance of the design, very likely for medical instrument application.

The replacement of the battery stack by an equivalent device had become unavoidable, and would pose a severe design challenge due to the simultaneous requirement for stability and noise immunity, and further still, a rapidly switchable V value. (The efforts to accomplish this are described further below.²)

² As an aside, Julius Caesar is infamous in philological circles for inflating the size and fierceness of his military opponents in his writings, (*e.g.*, see [Ca(1917)]) in order to make his ultimate victories seem all the more impressive to his audience. The author feels only a slight association: the work here speaks for itself.

2. ESA Supplies and Measurement Circuit

The requirements of the basic ESA voltage supplies and their attendant measurement circuitry were determined by analysing the propagation of errors in the nominal voltage in Bleakney's Theorem, (see eq. 3.13). One examines the maximum allowable contribution of any statistical variation in the V value as delivered by the ESA supplies, assuming a largest allowed error on ΔM , *i.e.*, $\delta(\Delta M)$:

$$5.1 \quad (\delta(\Delta M))^2 \approx \left(\frac{\Delta V}{V^2} M\right)^2 (\delta V)^2$$

Clearly at larger mass numbers and for larger doublet separations our constraint on voltage variation will be tighter. This work involves such "wide doublets" and an M of about 200u (*i.e.*, the region around A=200 in the mass table). If one accepts, over a large set of measurements, a statistical contribution to a mass doublet measurement of 0.3 μ u, which is commensurate with the historical performance of the machine, and a typical wide-doublet ΔV of about 0.1V (\equiv about 0.1u at mass 200), then,

$$0.3 \cdot 10^{-6} u = \frac{0.1V}{(800V)^2} \cdot 200u \cdot \delta V$$

or $\delta V \leq 0.0096V$ on 800V.

and if split between two supplies, $9.6mV/\sqrt{2} = 6.8mV$ on each 400V unit. This limit on the variation would have to be respected for about one hour, the course of a run.

Of the very few commercial offerings available with such a specification, Drs. Barber and Sharma had previously identified the Fluke series model 5440 precision voltage calibrators. These seemed quite suited to providing a quiet, highly stable potential of about 400V each into a nominally very high impedance (but see below) of the ESA plates. These units are based on a highly stabilized switching-transistor output-stage, ultimately referenced to an internal "ovenized" zener diode. The zener technology used will be briefly discussed below in connection with the potentiometer supply. The specification for stability was $\pm(0.3ppm$ of output + 200 μ V) over ten minutes, and only a little worse over 24 hours. We were assured in communication with the Fluke engineers that the ten-minute constraint was rather pessimistic and that, therefore, we could consider this a several-hour constraint. The resulting nominal $\pm 320 \mu$ V figure easily met our specification in any case.

Despite the above, the supplies were found to have a substantial level of "hash" at their outputs. This was of order several millivolts, at frequencies ranging from the known 5440 switcher frequencies up to the RF range. The solution turned out to be simple - a low-pass LC filter consisting of a large-value choke and electrolytic capacitor was added to each supply leg. It was feared that adding even these passive components would spoil the existing DC regulation; however, care in choosing a good-quality capacitor and in thermally regulating both averted any problem. The latter were tested for low leakage loss, but more importantly, for "spiking". It was noticed that certain capacitors, although of rated breakdown voltage and respected brand name, experienced what seemed to be "mini"-breakdown, seen as spiking in oscilloscope traces taken (via AC coupling) of the ESA plates when at high voltage. There was actually no hint of what would turn out to be a "good" capacitor before testing.

The ESA potential during a run must be precisely known with respect to the system reference (see sec. 2. above). Retaining much of the existing circuit layout (see Fig 5.1), this potential was measured by applying the supply voltages across a resistor chain so that the smaller potentials available at intermediate taps could be measured against our floating, null potentiometer (see Fig 5.2). The latter is based on a large Kelvin-Varley-type potentiometer in either a direct or a series divider connection to our reference pseudo-battery (see Bishop [Bi(1969)]). There are four resistors per supply, with the two supplies in "totem-pole" connection, earth grounded at the centre. The resistors are 300.00 k Ω , high-stability, high-precision, wirewound types, supplied by Julie Research as "NB" grade³. This value is somewhat arbitrary, though it is based on a trade off between noise-immunity considerations, which call for lower impedances, and the need to avoid excessive ohmic heating of resistors having low values, which would raise their temperatures too far above room temperature and their optimal $\partial R/\partial T$ point.

Presently, switching between the taps is handled manually via large, Guildeline, all-copper, low-thermal rotary switches. The measurement of the $\Delta V/2$ taps is handled similarly, and further described below.

³ that is, directly traceable to NIST via MIL-STD45662A.

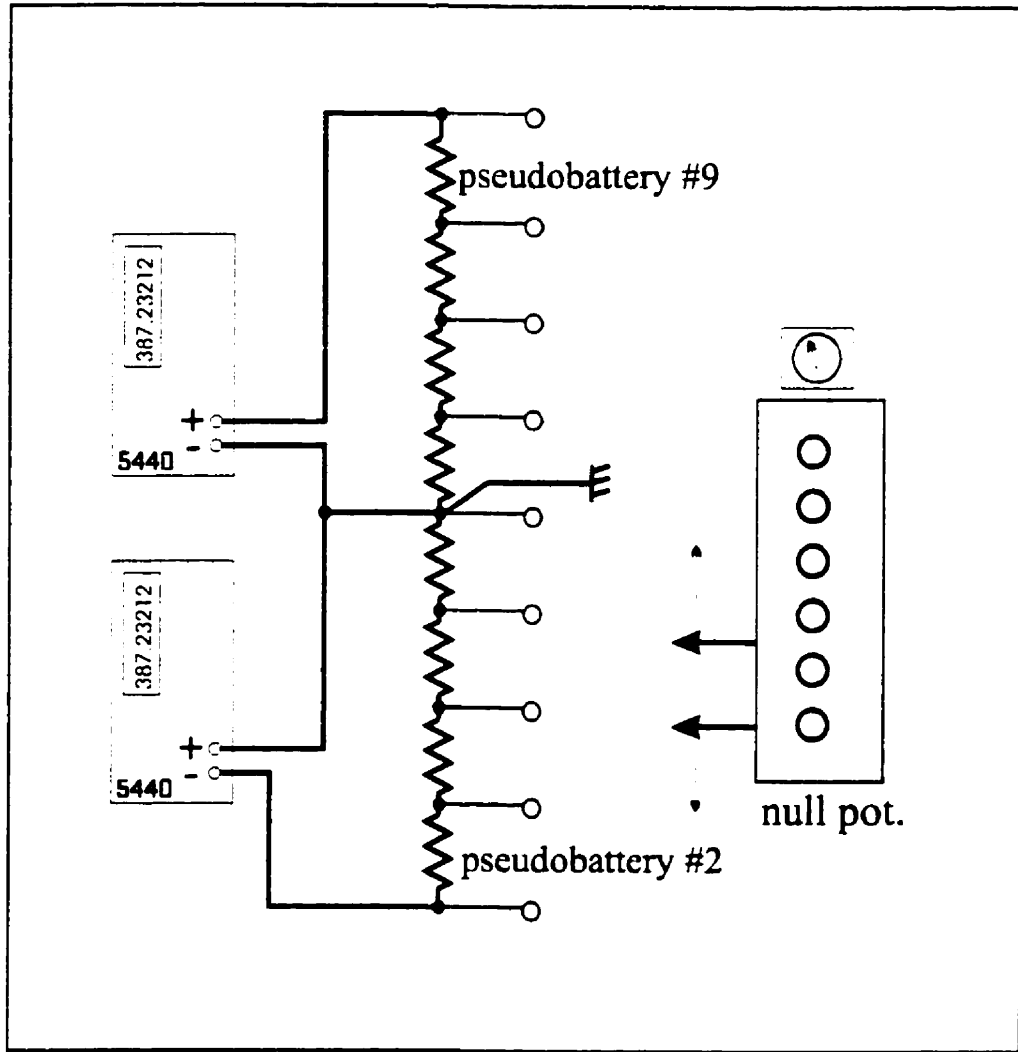


Fig 5.2 The new ESA basic voltage supply and associated potentiometer connections.

3. Voltage Reference

Low Temperature Coefficient/Stabilized Zener Reference

A decision had to be made as to how to acquire or construct a voltage reference to replace the one constituted of mercury cells, one capable of at least the same long- and short-term drift performance. The choice was made to try a solid-state design based on a special zener diode reference. The technology in such accurate/stable zener junctions has advanced to the point where ppm-level precision in low voltage supply design is now relatively straightforward using commercial offerings.

One such device, a ZR-512 module marketed by Julie Research, provides a nominal 12.xxx xxx V output when loaded at exactly 1 mA. Its voltage stability specifications seemed adequate, and it was adopted for the first and only design that the author had to try. The result was the pseudo-battery whose reference is shown configured in the schematic of Fig. [Appx. C-1995-001], (from here on, plan figures will be designated as, *e.g.*, in this case, "Fig. C-95-1"). The so-called "Julie-Cube" is provided with all necessary supplies, the output taken at the recommended current draw, and hence buffered, filtered and multiplied, by the multiplier shown in Fig. C-96-51, to the desired 97.3 V level. Due in part to the use of high-performance op-amps and high-precision resistors, the multiplication seemed not to have increased any small fluctuation or drift that may have been present at the reference module outputs such that we could measure it. In practice this meant that we never observed fluctuations on any ΔV measurement that in normal operation could be attributed to the potentiometer.

4. ΔV Supplies and ΔV Switching System

The Fluke ESA supplies cannot be floated above earth ground to any significant extent, especially when operated in the "stacked" or "totem-pole" configuration, (*e.g.*, as the chemical batteries are in Fig. 5.1). There exists an internal protection circuitry that senses any significant ground current from the nominally negative "black" terminal, in addition to the overcurrent protection provided on the "red". For a single calibrator unit, we noticed that this system allowed up to 30V with respect to earth on the black terminal. However, with the "totem-pole", a current path is established between the units, through the central resistors or current-supplies (chemical batteries), that would in practice force one or the other to shut down.

Disabling the protection circuitry and/or floating the unit metal cases was NOT considered a viable option. Stability, and certainly noise immunity, might have been lost and lethal voltages would have been presented to the operator without taking mitigating rack-mount re-design measures. Therefore, we needed to re-arrange the circuit to place the ΔV source(s) at the extremes of the stack, (Fig. 5.3). This involved some complications, leading to the development of special supplies that would sit at about 400 V with respect to earth ground and provide a switchable, small $\pm\Delta V/2$. Recognizing that it would prove tiresome to configure up to four separate ΔV supplies during a run, (two for close doublet values and two for calibration), the ΔV supplies should provide their separate + and - ΔV voltages based on some common, easy to set input.

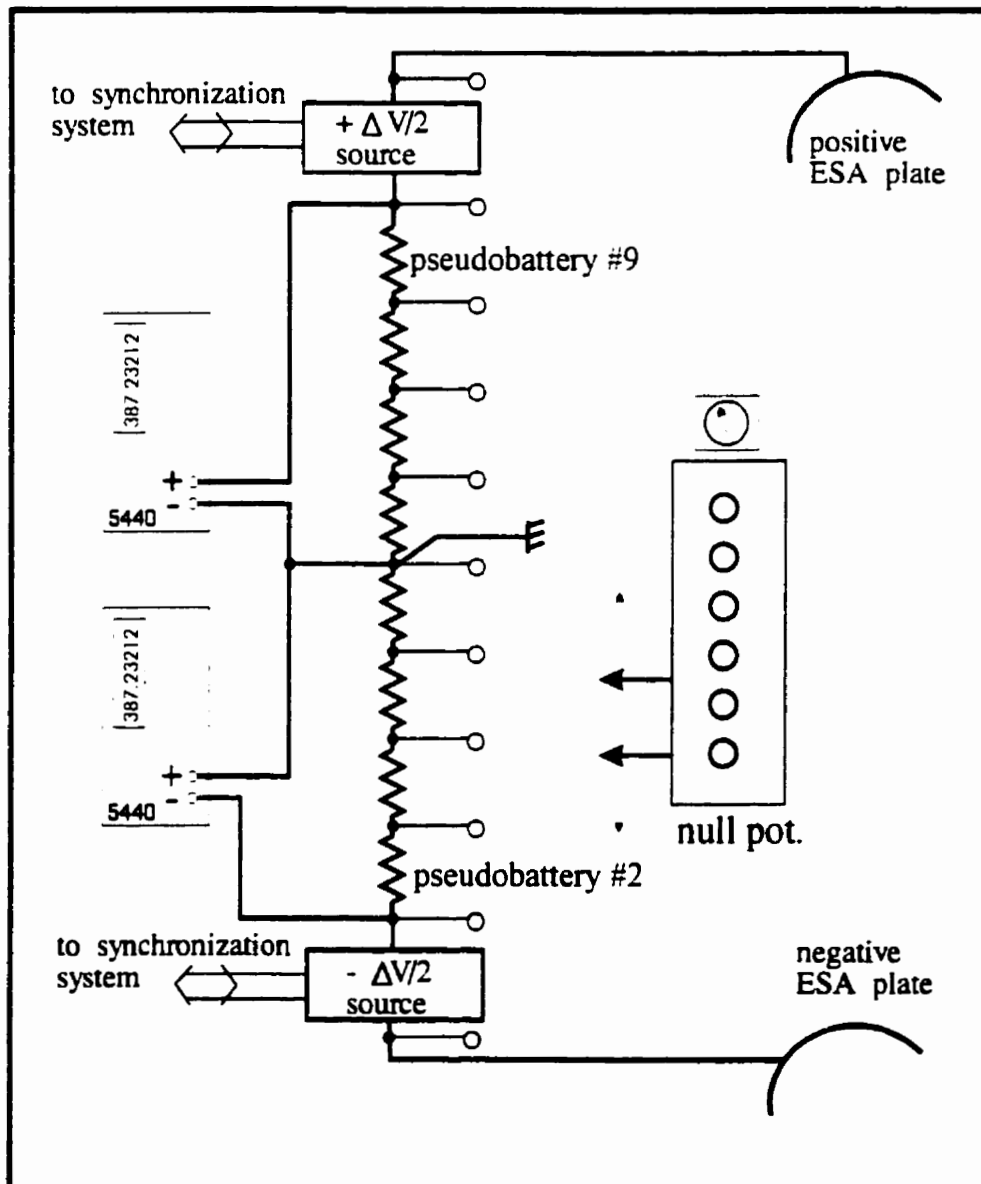


Figure 5.3 New method of applying ΔV 's to the basic ESA voltage.

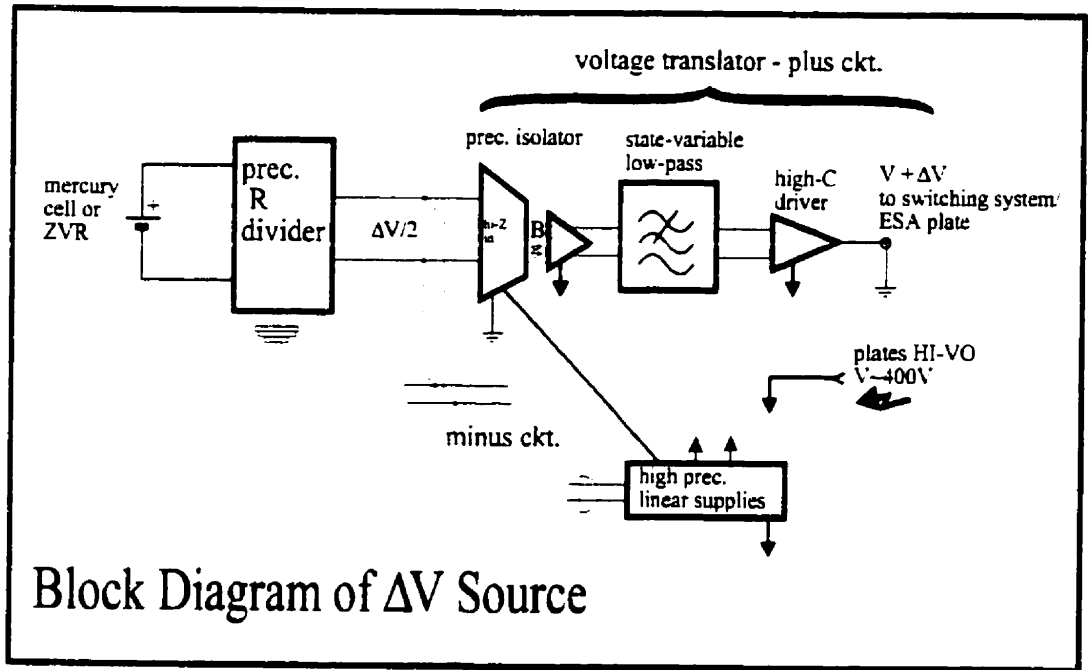
These requirements suggested a voltage translation circuit, basically one in which an isolation supply would accept a small ΔV value near ground and produce the same value at some high floating voltage. Ideally this ΔV would be switchable on time scales and with accuracy demanded by a peak matching approach. This involves switching periods of about 10 mS, but with the severe constraint of a sub-millisecond settling time to within $<1 \mu\text{V}$. The author hoped to achieve this with existing isolation-amplifier components, specifically one of the monolithic, FM-based linear isolation blocks offered by Burr-Brown, their 3656 module. The resulting circuitry is shown in Figures 5.5a,b,c and d, with schematics in Figures C-97-99 and C-98-5 and 6, and in simplified block-form in Fig. 5.4. The apparent complexity is mainly due to filtering and load-drive requirements.

It was quickly discovered, that although remarkably accurate and stable over the long term (> 10 seconds, say), these types of isolation-amplifier devices produce a switching noise ($f \approx 700\text{kHz}$) of a magnitude that was quite severe by our standards. The suppression of this noise by careless application of passive or linear electronic filters might have ruined any hope of fast switching a ΔV from within this circuit. (The component engineers could not offer an alternative for resolving our problem). The use of digital filter technique was not seriously considered because at this point one could more sensibly go over to a full digital D-to-A-based ΔV generation scheme: this indeed is the basis for a "next design" mentioned in the preamble to this section.

The solution achieved was more a matter of attention to detail throughout the design than any one special technique. As an example, a disturbing short-term drift was noticed. This was of order $20\mu\text{V}$, and with a quasi-random period of about 5 seconds - very disconcerting. Frequency measurement of the FM carrier mentioned above revealed this to be due to long period phase noise, meaning an undesired frequency shift due to component instability or electrical interference. It was finally determined that the problem was caused by the lack of power supply drift immunity when either side of the amplifier/modulator system in the 3656 devices was independently powered using "conventional" linear regulators, *e.g.*, the popular 78Mxx devices. Curiously, but conveniently, the 3656 is also capable of using a single supply through an internal transformer system. The first supply scheme was thus replaced with such a single, highly stable supply ($\pm 0.01\%$ short-term drift) using an AD581, precision 10 V reference (see Fig. C-98-6). This did the trick; therefore the stable supply itself requires a very good supply! This entire system thus consistently provides ΔV values steady to within about $1 \mu\text{V}$ or less between measurements. A record of a typical standard-cell voltage as translated by the system is shown in Appendix C.

A further example of the need for precision design practice is the filter system. It had to be a low-pass filter with a very sharp transition band, or at least good rejection in the carrier frequency range. The design chosen was a sixth-order state-variable active filter constructed with good quality passive components and OP-07 category operational amplifiers⁴. This design boasts over 60dB of rejection at 100kHz, with only a few dB loss at the crucial 13kHz corner frequency, and virtually no overshoot or oscillation. This met the requirement that a new voltage sent to the

⁴ Later replaced with quieter OP-37E devices.



Block Diagram of ΔV Source

Figure 5.4

system, say, by a low-voltage chopper, would settle within order of a few milliseconds. This exceeds the previously mentioned criteria, but was still workable with measurement-cycle phases of 20 - 40 ms.

As a great deal of time had been invested in solving these electronics issues (not to mention other mundane operational problems with the mass spectrometer), the decision was made to preserve as much of the "wiring-in-place" as possible. This meant that the short-term, conservative solution was to not switch this voltage at all at the low voltage input, but rather to dial in a desired ΔV from a convenient, good-quality, low-voltage divider and let the supply "sit" as a good, stable, low-impedance source to a high-voltage chopper, to be described below. This component had been designed into the system before the settling time problems with the ΔV supply had been resolved. Here, the ΔV s would be rapidly switched in and out of the circuit, as required, by solid-state switches operating at the high floating voltages at the ends of the ESA "stack".

The long-term plan is to replace this system with one possessing a true fast-switching capability. A proprietary RF-based system is in successful early trials: this is described in §8. The ΔV summing/synchronization configuration that ultimately resulted as a first re-design, and that was used in these studies, is shown in block form in Figure 5.6. As remarked before, the plus and minus plate voltages are now each processed separately in order to apply a system ΔV . The system is capable of delivering the $V+\Delta V$ values required both for a computer run, *i.e.*, a four-quadrant run in which data are accumulated in the MCA for off-line analysis, or a visual run, the simpler, 2-phase run, where a peak cancellation is attempted visually by the operator (as explained earlier). The latter involves the application of a single ΔV value, that is, a ΔV is added to the ESA voltage on alternate cycles. When a computer run is desired, the visual chopper is stopped with the contacts set to simply feed through whatever pair of voltages the "computer chopper" generates. Conversely, when the operator wishes to perform a visual match, the "computer chopper" is halted such that ΔV is available to be added to the plate voltages by the mechanical "visual chopper". This would correspond to the nominal (computer) phase 0 mentioned in §IV.3. At the same time, the "visual" chopper is set running. In this case, the latter performs a repetitive selection of V or $V+\Delta V$ (see Fig.C-95-7).

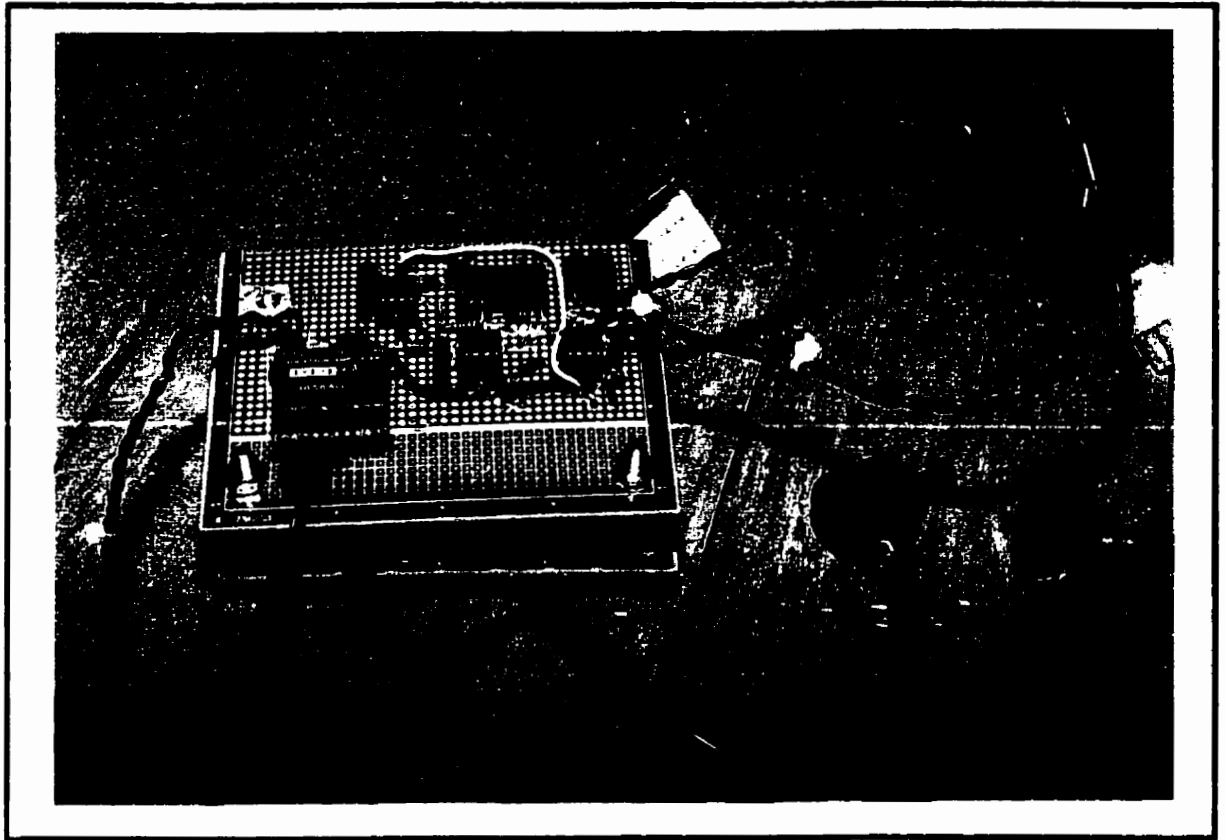


Figure 5.5a Dual $\Delta V/2$ supply boards, high voltage isolated from each other, ready for test.

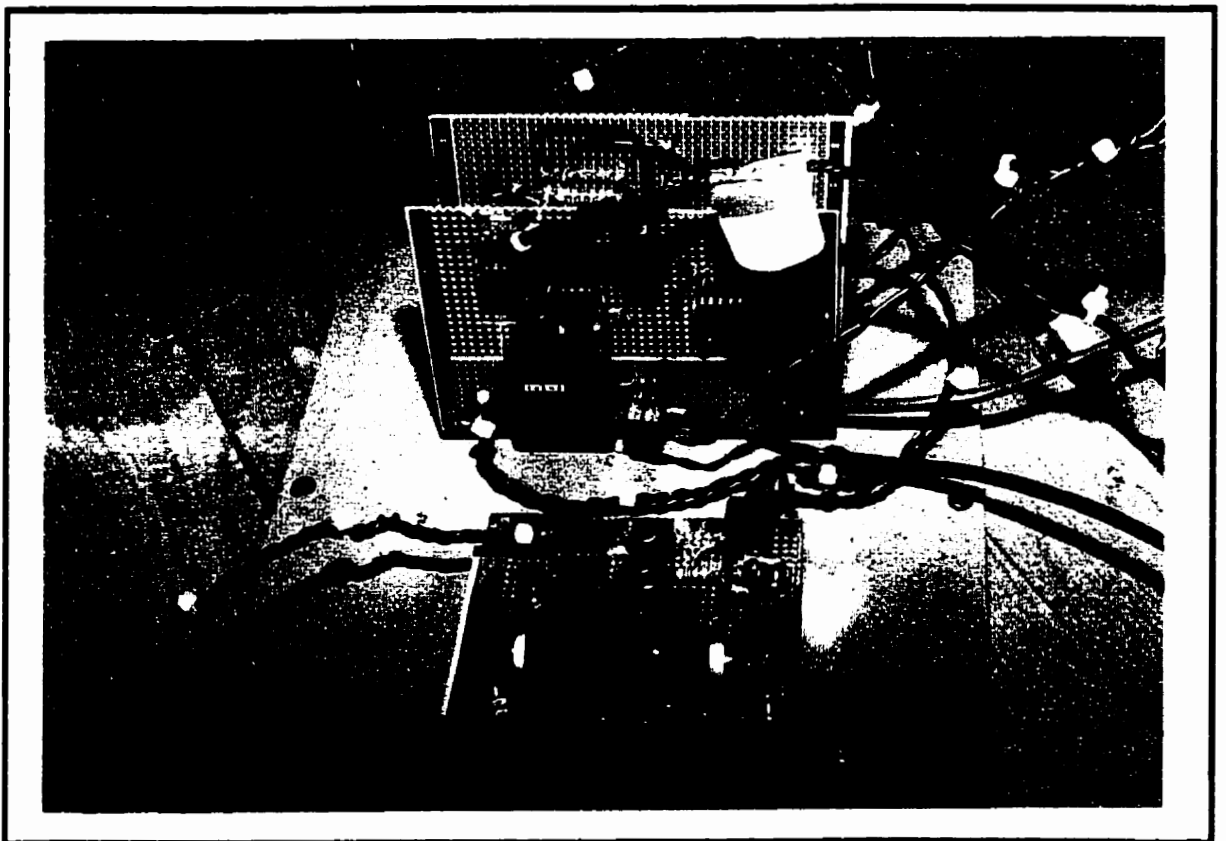


Figure 5.5b $\Delta V/2$ supply boards mounted along with their precision linear supplies.



Figure 5.5c Final installation: Kevin-Varley setup pot as well as thermal c and heater (resistor) are visible.

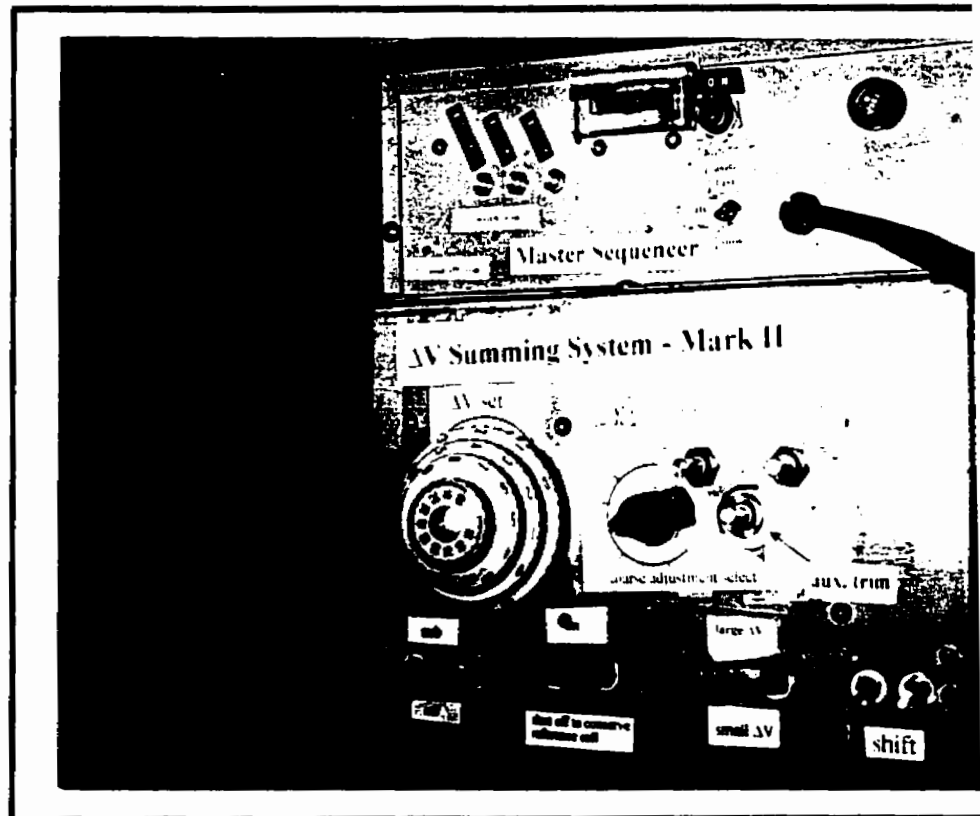


Figure 5.5d Unit with front controls shown in rack mount: also visible is the sequencer to which the system is synchronized.

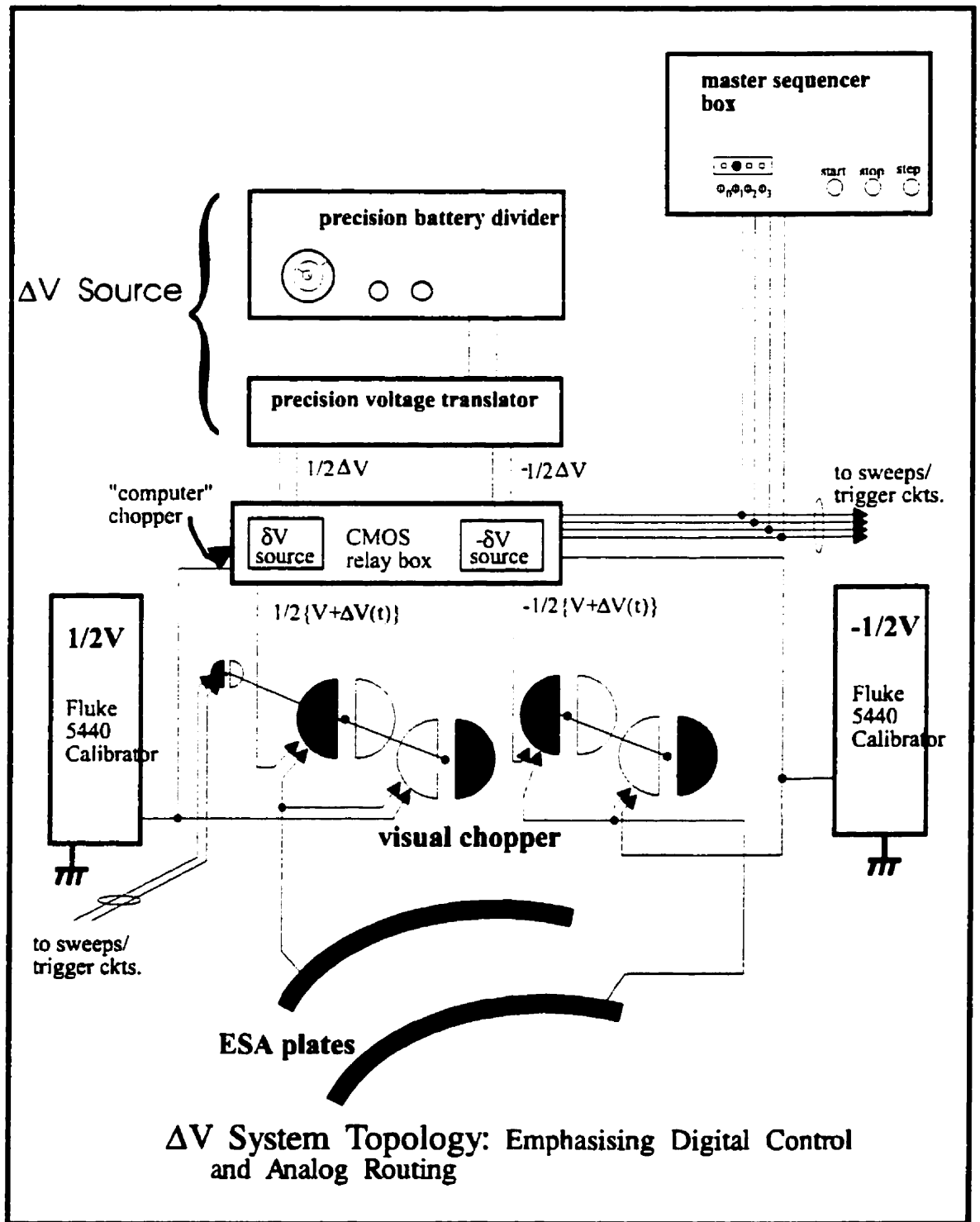


Figure 5.6

5. Digital Chopper System: Digital Sequencer and Solid-State Relay Subsystem

One of the key steps in upgrading the Manitoba II electronic infrastructure would be the replacement of the mechanical chopper system with a fully electronic switching system. This would eliminate problems with tuning the former ingenious but very finicky mechanical contrivance, and would also allow for a quick evolution to a fully computer controlled system. The latter should come to completion sometime soon after this study; however, for this work, a "hardwired" digital sequencer was designed.

The heart of the system, the "Master Sequencer", is visible in Figure 5.7, with a schematic of the electronics in Figure C-96-11. It serves to provide the four phases of the master system timing cycle, corresponding to the four phases of data collection at different potentials (in a "computer run": see Section IV.3 for details on the measurement cycle).

The device consists of fairly conventional TTL logic components, used to divide down a master 6.000 MHz crystal-derived clock signal to 4 periodic pulses, sequencing in a walking-ring cycle (see Figure 4.4). These pulses are about 10mS in duration and follow each other with a short time interval of about 50 μ S between them, to allow for settling/removal of applied Δ Vs in each phase. The pattern is fixed, as is the period. The operator can start, stop and single-step through the cycles using front panel push-buttons. This allows the Δ Vs to be measured potentiometrically at the end of each match. In practice, the beam is stopped, the timing cycle is halted by pressing "stop" and the applied Δ V measured, via the existing potentiometer circuit, at each phase of the cycle by "step-ping" through each phase in turn, *i.e.*, pressing the "step" button as required.

The four TTL pulses generated by the sequencer are hence used to switch solid-state relays based on MOSFET transistor technology. The relay circuit is shown in Figure 5.8, with a schematic in Figures C-97-5 through 6.7 and C-98-1. The system centres on the SW02 quad, digitally controlled MOSFET analog switch, made by Precision Monolithics Incorporated. Though a number of devices representative of this category of circuit have emerged from various semiconductor firms in recent times, this IC was one of the first precision analog switches available. It successfully routes the Δ Vs required for our matching purposes with very high precision and reproducibility, due largely to its low "on-resistance" and the very high impedance of the ESA plates. The TTL pulses, created for convenience near ground in the sequencer, are translated to the corresponding logic levels in the vicinity of the ESA supplies via opto-isolator ICs. These logic signals are then applied to the analog switch network, also floating at high voltage; the analog switches cannot be operated with logic signals that are near ground if the linear signals are at high voltage.

The 400V isolation required for each side of the plates supply is easily achieved through careful, but conventional, wiring practice with multiple isolated DC supplies. Low noise is achieved via isolation of AC lines, careful power supply by-passing and the use of RF shielding as required. As can be seen from the schematic, the small δ Vs used as the so-called "splits" voltages on computer matches are created locally, simply by using a large voltage divider with an alkaline dry-cell.

A further function provided by the switching circuitry is a so-called "wide-sweeps" sawtooth waveform, wherein the ESA voltage is swept by a few volts, in complementary fashion,

on each plate, in order to view a large mass range on the live display. With this range of potential change, the operator can see about a 1 u wide display. This sweep is implemented via a pair of LM555 monostable multivibrators driving a constant-current transistor as a capacitor charger (see Figure C-98-1).

6. Source Ion-Optics Electronics System Changes

The existing electronics for the supply and switching of potentials for the source quadrupole and deflection plate section of the mass spectrometer ion optics, and for the switching of the acceleration voltage, was basically sound, except that it made no *simple* allowance for subtracts-mode matching. In the old system, the timing signals by which the above mentioned potentials were shifted in order to satisfy Bleakney's theorem were simply inverted *in phase* whenever the operator switched to "subs" (*i.e.*, subtract) mode. This meant that the respective source ΔV s were positive when the ESA plates were at nominal potentials, and zero when the ESA plates were at nominal $-\Delta V$. This setup in turn required the operator to stop measuring and perform an energy refocus, especially in the case of a wide doublet, in which the ΔV shift was substantial (*e.g.*, approximately 120 V on the 20 kV acceleration potential for a 1 u "calibration" run). In practice this is highly inconvenient and error-prone.

As can be seen in the schematic Figures C-98-10 and -11, a single switch now controls a relay system that effectively performs a true reversal of the ΔV applied at the source. (The author credits his colleague, Mr. Joseph Vaz, for assembling the new sections of the C-98-11 circuit).

7. Source Electron-Emission Control

An extremely annoying aspect of source operation with certain chemical species is a drift in source electron emission. The source itself (excluding power supplies) is described in detail in a number of works (see, *e.g.*, [Ba(1971)]), but a schematic diagram is given in Figure 5.9. During operation, the filament is typically at white heat, and thus undergoes metallurgical changes resulting in flexing, sagging and effective emissivity change: (the heavy copper supports re-anneal and also flex with each heating cycle). Worse still, with a sample vapour such as WCl_6 , elemental tungsten infiltrates and deposits onto the filament; although this problem is greatly reduced by using tungsten ribbon rather than the usually superior rhenium material. The result is a constantly shifting electron emission, which taxes the patience of the operator and thereby may lead to lost time and error.

A steady electron emission is essential if the source condition existing when the system was brought to an energy focus is not to change. A change in source conditions can cause troublesome systematic problems ultimately due to violation of the Bleakney condition discussed in Section III. To this end, a feedback system was introduced into the ion-source power supply system whereby the emission of electrons could be sensed and corrected by manipulation of the filament current. Varying the electron acceleration potential (see Fig. 5.9) would not do, as this might take one away from some optimal bombardment energy as well as alter the location and energy of formation of the positive ions.

In detail, this subsystem (see Figure C-99-20) operates by sensing the voltage drop across a resistor in the return path between the accelerator supply and the reference point shown in Figure 5.9. This is compared to a setpoint potential: any difference is amplified by an op-amp and

the resulting output used as a correcting signal. This signal modulates a large-current transistor "pass-bank" in the filament supply circuit so as to minimize the original difference.

8. Future Enhancements

As mentioned above, a number of improvements to the ΔV sequencing and potential-measurement system were designed and brought to a prototype stage during this work, with a view to completion as time would allow. These are discussed here in order to show why they are desirable and to provide a record of work done.

Computer Sequenced Chopper/Measurement System

Presented here is an outline for a highly automated system to both conduct the voltage sequencing of a run in real-time, and to measure the run voltages thereafter. A substantial fraction of the time consumed in performing a run at present is due to manipulation of the potentiometer by hand. In course of determining each pseudo-battery and $\Delta V/2$ value, the operator hunts down a null on the potentiometer by setting the dials on a seven-stage Kelvin-Varley divider. A given match could require as many as eight such operations in order to record the $\Delta V/2$ value of each quad (*i.e.*, phase quadrant; see §IV.3), on each end of the ESA stack. (In practice, some effort is saved by noting which values are stable, and re-measuring only those potentials that tend to drift within a run). Although highly effective historically, the practice is still error prone and tiresome. Further, there are a number of advantages to be had in terms of flexibility of reconfiguration of certain run parameters, such as quad duration times (see Section III.3), or interchange of quad schedules for systematic checks (again, see Section III for an full explanation of the measurement cycle "phase quads"). An example of such checks would be to see if application of a large ΔV followed by a small ΔV yields systematically different results, say, due to electrical settling effects, than a cycle in which the order is reversed.

In the design presented in Figure 5.10, a server performs the voltage measurements through a high-precision digital voltmeter. The voltmeter is presented to the potentials of interest through a commercially produced, high-precision analog switching card. This card basically consists of sets of digitally switched low-thermal relays that route a number of signal pairs to a single output-pair terminal. The cards are specially designed to reduce thermal junction effects throughout, as well as to minimize such problems as heating of the relay contacts from the relay's own coil. Such cards can be distributed through another card to form a routing hierarchy if the complexity of the system demands it. This card(s) is in turn controlled by a National Instruments real-time Digital Input/Output (DIO) card. Thus the measurement server would select either a pseudobattery or $\Delta V/2$ measurement point, while the voltmeter would generate a value for telemetry. This value would be read, and the voltmeter operation controlled, in general, through a conventional GPIB⁵ link. The data could then be transcribed locally, or read by the Master Run Computer over an (Ethernet™) LAN⁶. The main problem to be resolved in the near term is how

⁵ General Purpose Instrumentation Bus, originally a proprietary Hewlett-Packard standard, now the IEEE 488.x

⁶ Local Area Network. Ethernet is a trademark of Xerox Corporation for a coaxial-cable-based high-speed local computer-communications technology (now IEEE 8803.x).

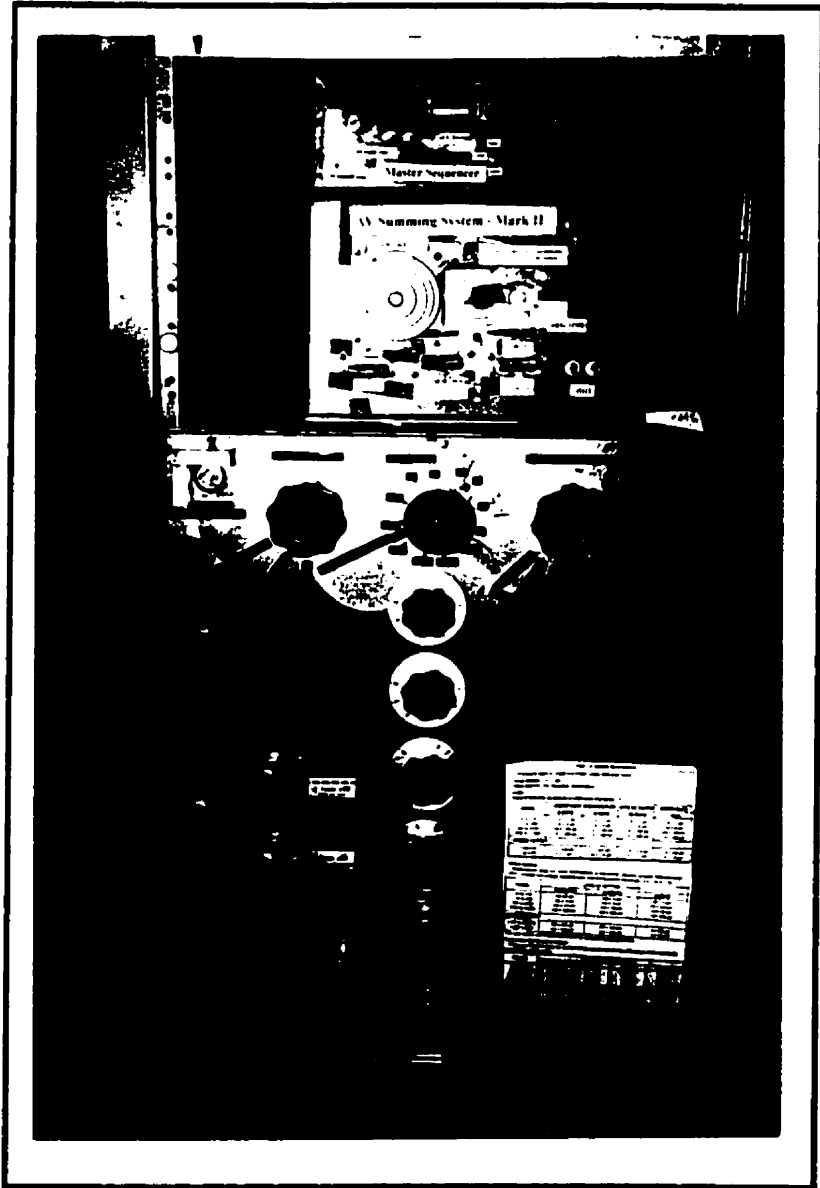


Figure 5 7 View of master sequencer. ΔV -summing and resistor/potentiometer boxes.



Fi



Figl

to perform a high-precision measurement of the pseudobatteries when the voltmeter itself presents a finite, albeit high, input shunt impedance to the circuit. A simple solution may turn out to be a calibration factor on each such measurement, produced by comparing the voltmeter reading with a standby, true potentiometer in the same system box.

The run-time operation, would involve sending the proper relay-setup signals to the existing ΔV solid-state relay system (see sections V.4. and 5 above). The timing requirements are not severe, in that a measurement phase quad typically lasts about 40 mS. Currently, the plan is to use the rather sophisticated timing sub-system which exists on the National Instruments DIO card. The measurement server merely presents the appropriate timing values to the internal timing registers in the card and initiates a timing loop. The card then presents the desired digital pulses to the inputs of the solid-state relay. The system at this point serves as the master sequencer for the entire measurement system, thereby replacing the digital chopper mentioned in section 5. above. As mentioned, an advantage to the computer-controlled approach is the ability to alter the sequencing, allowing for, say, stretching the duration of the phase quads, if settling time is an issue, or conversely shortening it to better average out random voltage variation. Further examples include varying the basic cycle time to find better anti-resonance frequencies with respect to electrical interference sources, such as the mains. Interchanging the assignments of ΔV values to the phase quads would also allow for added checks on the systematic effect of, say, the settling of a smaller δV value following a phase with a large ΔV .

An RF Approach to Real-Time ΔV Setup

A further refinement to the concept presented above would be to setup the ΔV values via digital control, eliminating the direct manual entry of values using conventional (precision) potentiometers. As with other enhancements discussed before, the objective is to automate as many tasks as reasonably possible to reduce operator workload.

A successfully tested prototype of such a design is shown in Figure 5.11. In this system, all switching of ΔV s is handled by a local microcontroller, which cyclically transmits FM-encoded ΔV values, in real-time, to a high-voltage receiver circuit. This scheme would therefore also entirely replace not only the analogue circuitry mentioned above, but also the solid-state switching system. The local control PC could be the same run-slave computer as shown in Figure 5.10, or yet another computer connected to the run master computer via Ethernet. At present, only a direct FM encoding has been used, in which the transmitter frequency (f) is simply proportional to the desired ΔV , *i.e.*, $\Delta V = k \cdot f + f_{base}$. (Further details will be provided in an article intended for publication, as this system was not used in the data collection for this work).

MCA Sampling System

Presented here is an outline for a new MCA system to replace the aging Fabritek device. As mentioned, this would be based on an internal MCA "card" for an AT-class personal computer (*i.e.*, Intel processor), specifically, an EG&G Nucleus MCA/MCS system card. This computer would host the card, but would serve as yet another run server in that, besides possibly providing a live display of the data during a match, it would also send back the data to the run master over the LAN. As the reader will note from Fig 5.12, the card itself would directly receive the

amplified pulses from the mass spectrometer ion detector, and store them in multiscaling mode. Channel advance signals are generated by a timer box which is, in turn, triggered by the system master timer, the latter creating the run phase pulses (see §IV.4). The main pieces of work involved here are creation of the network software required to read the card and fabrication of the timer box. The latter has actually been built in order to test the operation of the card in this sort of setup.

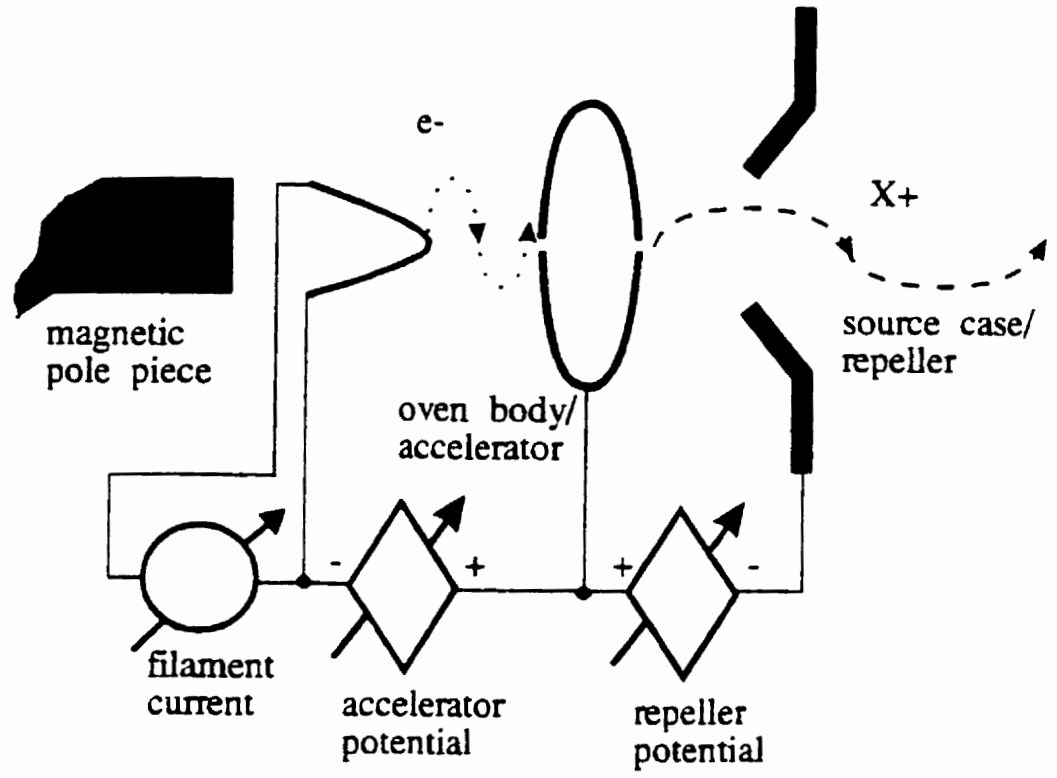


Figure 5.9 The potentials applied within the ion source.

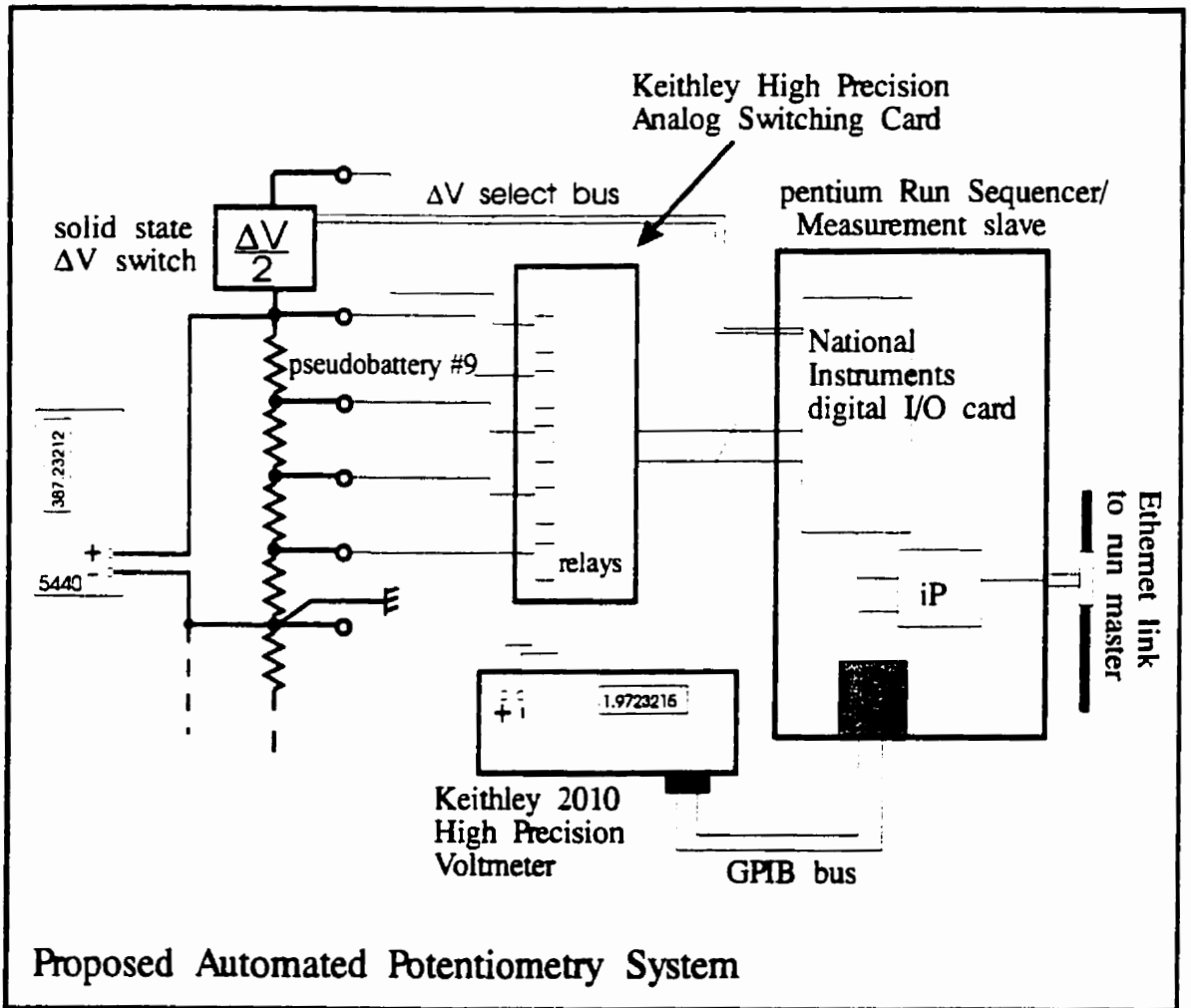


Figure 5.10

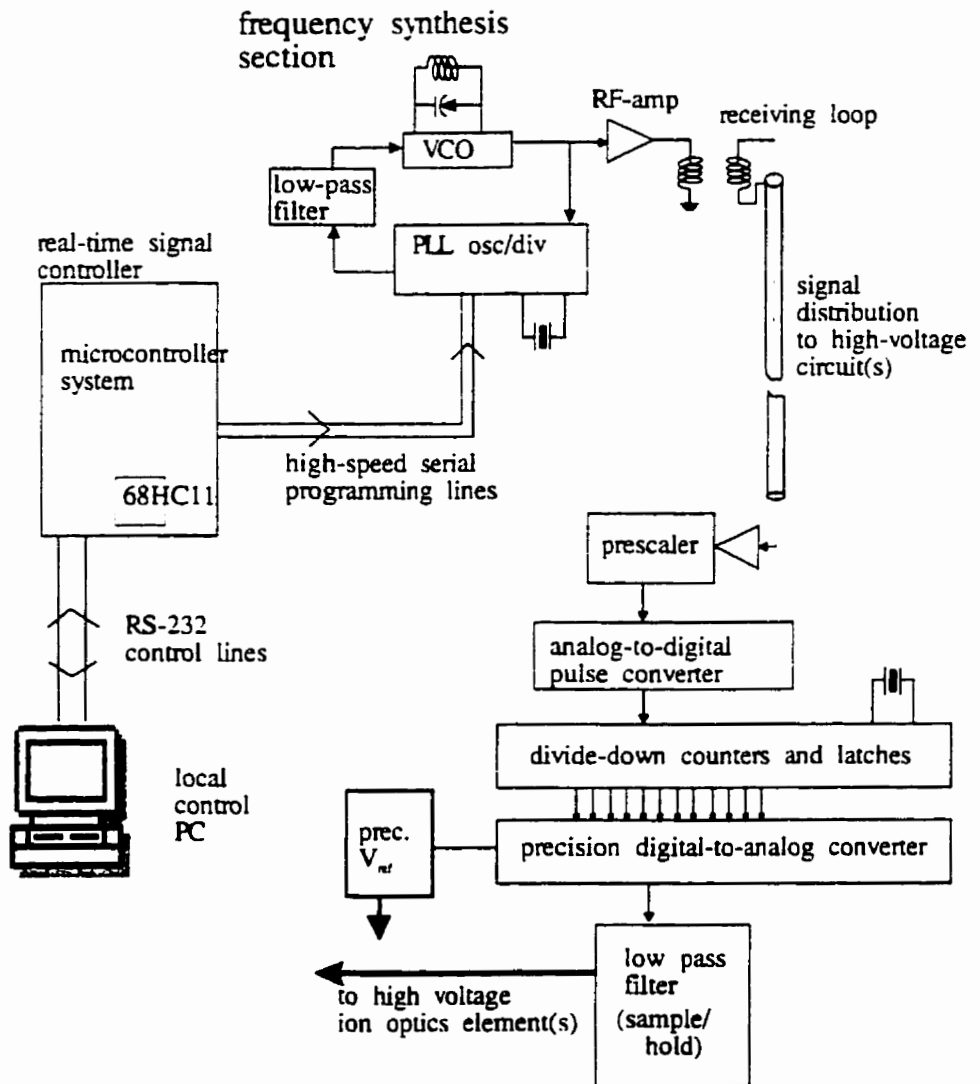


Figure 5.11 A ΔV summing system, based on an RF method, which has reached the working prototype stage.

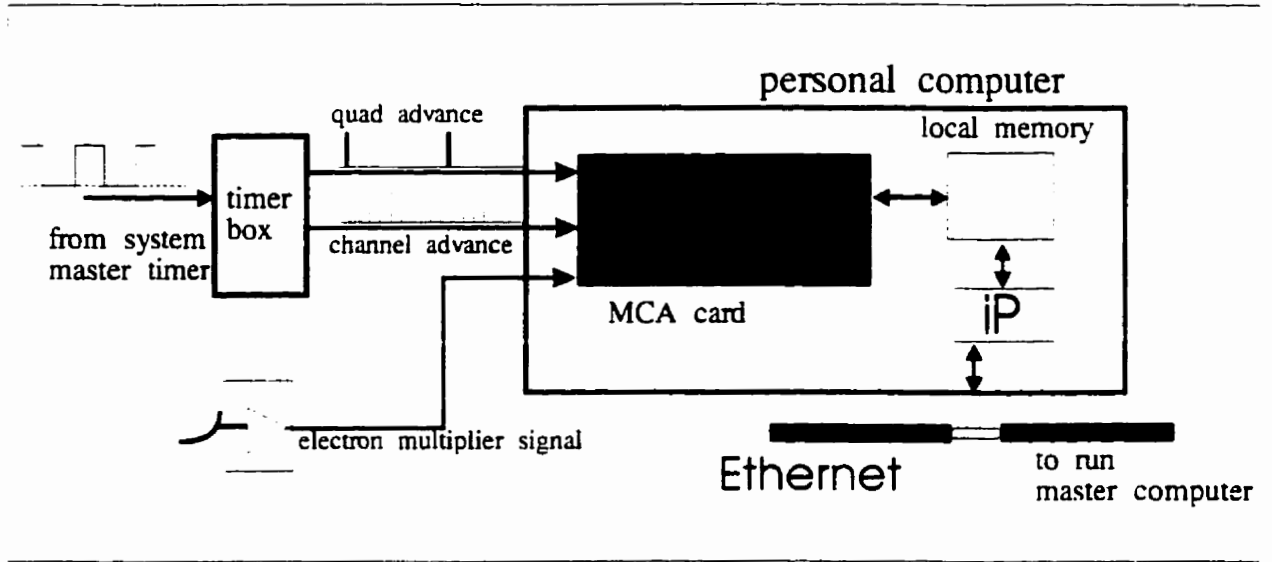


Figure 5.12 A new data collection system based on a commercially available MCA card for personal computers.

VI New Software for the Manitoba II Instrument

A brief description is given here of new software written for this study and for software being developed in conjunction with the on-going hardware enhancements outlined in §V.8 above. Further theoretical background for the analysis is developed in the next section, while a complete specification for the data analysis system is given in Appendix A

1. Digital/Computer Peak Matching – AMDPRIME⁷

Soon after embarking on the process of making mass measurements by the so-called "computer matching" method (Section III.3), this investigator found that the existing software and analysis system (core program name SPECTRUM), though sophisticated and tested, had a number of serious drawbacks for future use.

Since the principals involved in the later development of the existing analysis code (see [Hy(1991)]) had departed the lab, the system was largely a "black-box". Thus, although already documented on a functional and even on a source-code level in some theses, it was difficult to be sure of what precisely some portions of the analysis algorithm did. What was more worrisome, was the fact that the measurement process was changing as a result of hardware changes, invalidating some of the assumptions embedded in the existing code. Further, it was not clear to the author that the overall analysis methodology was what he would want or need, from a practical or philosophical standpoint.

The system had begun development at a time in the evolution of computer technology when the level of processing and the file overhead were suited only to a departmental-grade computer, using off-line processing of data. It was in practice quite a time-consuming chore to prepare and process the data through an analysis sequence consisting of a number of isolated stages.

It was largely because of the desire to have a streamlined data-acquisition/data-analysis system, one that was also more transparent to future developers and users, that the decision was made to write new code using new methodologies and aimed at a personal computer platform. Bearing in mind that the "PC" had so tremendously evolved in processing speed and memory capacity that by 1994 it surpassed, say, some early MicroVAX systems, and that this trend was bound to continue, it seemed eminently reasonable to fashion a piece of code for an Intel-based⁸ personal computer that could fetch the run data from MCA storage, and analyse it on the spot if desired. As part of a broader design strategy, it would likely form the basis for a more fully integrated measurement process in the future, parts of which are described elsewhere in this thesis.

⁷ *i.e.*, Atomic Mass Determinations group "''", as in second generation, or more generously, PRinciple Matching and Error analysis system.

⁸ The Intel bias was due strictly to the author's familiarity with 80x86 processors.

The software requirements drawn up were largely intended to preserve the basic functional aspects of the older program: these included:

- a) the capability to read out data stored in the Fabritek MCA data memory.
- b) the capability to present this data for processing based in part on visual interpretation
- c) the capability to store the raw and processed data
- d) the capability to select, parameterize and process mass peaks, and to find their centroids, possibly with the ability to use different algorithms, including the ability to re-analyse at will if a problem is spotted at this stage
- e) the capability to combine the centroid information with potential measurements to produce a doublet mass difference along with relevant statistics

However in line with the philosophy of tailoring the code to the needs of each investigator a worthwhile refinement of the basic χ^2 peak matching process was found and introduced as a novel analysis feature, as will be discussed in Section VII.

The software would also be more user-friendly by presenting a "windowing"-type graphical interface; indeed it was written for the Microsoft Windows[®] environment in C++, using the Borland 3.0/ 4.0 Windows/C++ development system.

The method of centroid estimation, centroid comparison and other statistical aspects of the analysis are developed in depth in the next chapter. As well, a concise functional specification for AMDPRIME5 is provided in Appendix A. Finally, a crucial check between results obtained using AMDPRIME and SPECTRUM on a sample data file is given in §VII.

Stages in the Peak Processing

Generally speaking, a "request" refers to "pressing" a virtual command button on a graphical display.

Upon completion of a single match, the MCA data are read from the Fabritek instrument by a simple download request. The data are presented immediately for confirmation. Typically, all eight matches are sequentially developed and collected, along with potentiometry measurements, before entering a storage request for offline processing and eventual archiving.

Data processing requires manual setting of markers to delimit the relevant background regions and the search areas for peaks. This is done in a peak-processing "workbench" window. Nominal peak limits are systematically found according to a specified peak height fraction. It is possible to request a fully automated search and layout of such parameters, but a manually guided approach is beneficial, since this entails a walk through all of the peaks, and bad match data can often be easily spotted by the human eye. It is precisely because all "auto-setting" algorithms have a problem with parameterizing noisy data typical of the real world that provision for systematic smoothing was provided in the system; this will be described in more detail later.

Once satisfied with the peak parameterization the user requests fits to each match to obtain the distance in channels, and hence voltage, between a mathematical null peak for the reference species and the peak for the comparison. Application of Bleakney's theorem, along with the correction mentioned earlier for non-ideal ESA properties, as well as a potentiometric correction, provides individual mass values.

Yet another request then combines these individual match values into one grand average for the run. For incomplete runs in which one or more matches are missing, the user may exclude those matches from the averaging process. Sufficient information is available from the analysis to provide a statement of both simple and weighted variances.

2. Magnet Control Software - BORIS

Many of the same arguments made for replacing the SPECTRUM system mentioned above applied to the existing analyser-magnet control program, though it was in a more primitive state of development. This software provided the operator with the means to set and slew the magnet field value in a fairly convenient manner from the run-control PC, rather than manipulating the difficult front panel controls of the Bruker high-current supply.

Motivated further by a hardware upgrade to the GPIB interface of the control PC and replacement of the magnetic field sensor voltmeter, the existing MAGNET code was rewritten for the graphical user environment and new GPIB high-level driver functions. The target system was again a Microsoft Windows® environment, with object-oriented coding practice and implementation in C++; using the Borland 3.0/ 4.0 Windows/C++ development system as before. The resulting human interface of BORIS (B-field Online Ramp, Increment and Set) provides a more comfortable set of virtual readout and input "devices", such as "tape gauges" and scroll controls.

(Since this is an auxiliary system, albeit an important one, and not analysis software, it is mentioned here as a record of work done, without further detail).

3. Computer-Measurement Control Software

A significant amount of development work was undertaken on software for the Automated Potentiometry System discussed in §5.8 (see Figure 5.10). The author credits Ken Aarts for producing, under the author's specification, Windows-based prototype code which could successfully run the Keithly High-Precision Analog Switch Card and Keithly 2010 High-Precision Digital Voltmeter. This work-in-progress is mentioned in this thesis for acknowledgement and documentation purposes, but will not be discussed further.

VII Peak Matching

This section describes the mathematical and empirical basis for the peak matching analysis.

Match peaks consist of four sets of doublets⁹ read from the multichannel analyser, each set being referred to as a quad, a reference to the 4 quadrants of the measurement cycle mentioned in §IV.3, (see esp. Figure 4.4). As explained there, the idea is to establish, through a set of changes in ΔV , what value of ΔV would be required for an exact overlap of test and neighboring reference peak in the doublet.

If one momentarily disregards the natural statistical fluctuation associated with the rate at which ion-beam particles individually arrive, a rectangular source and detector slit combination will under ideal circumstances produce isosceles-triangular peak shapes on the live display of the instrument, when the slit openings are of equal width (assuming the overall ion-optics magnification is unity for simplicity). If the slits are not set to equal width, one can easily see that a flat top will appear on each of the triangles, if one imagines how a wider rectangular beam will be "seen" when scanned across a smaller rectangular aperture, or vice versa. The actual peaks observed upon accumulation will be triangles with four primary extra characteristics

1. random fluctuation due to the inherently random nature of particle emission and detection, as alluded to above
2. further "smearing" of the accumulated peak due to a) changes to the magnetic field (*e.g.*, motion of a nearby steel elevator cab), stray AC electrical, magnetic and electromagnetic pickup, and damped oscillation of the table from mechanical building disturbances; b) nicks and burns in the source slit (which suffers by far the most of either slit from the 20keV source ion bombardment), as further discussed in [So(1973)]
3. spurious peak counts into the surrounding signal zone corresponding to actual particle deflection by residual gas molecules, space charge and high order image aberrations. Generally, there are systematically more counts on the low energy side of the beam as energy-degrading collisions are the common source for these counts.

Notice that some of the item 2.a) effects suggest a harmonic component to the time integrated beam profile; this will be discussed further below. One should also include non-ideal factors that are more immediately under operator influence,

4. poor focusing, which can produce asymmetric peaks and inadequate resolution
5. unstable source conditions associated with the discharge parameters in the source electrodes and vacuum.

⁹ In the case of a wide doublet, and for any reasonable resolution, the partner peak will of course not be visible in the data.

While these factors are relevant to both visual and computer-based peak matching, the rest of this section is devoted to the process of computer matching. Since many of the statistical formulae are quite conventional, they are documented in the Functional Specification of AMDPRIME5 in Appendix A.

1. Definitions and a Brief Review of Methods and Issues

The peak-matching process begins by an objective procedure to extract a "location" for each peak, such that a useful measure of peak distances can be derived in spite of the peak-distortion effects mentioned above. One can explicitly calculate such distances by the evaluation of a centroid for each peak or one can implicitly do this by performing a direct channel-by-channel comparison of suitably delimited, corresponding peaks in order to minimize some parameter of fit, such as a χ^2 , as a function of peak offset.

The word "centroid" by itself will be used to designate a measure of peak position as given by *any method*, whereas the term "centroid method" will specifically refer to the process of extracting the centre of mass of the peak:

$$7.1 \quad c_k = \frac{\sum_{i=1}^N f_i^{(k)} x_i^{(k)}}{\sum_{i=1}^N f_i^{(k)}} ;$$

where $f_i^{(k)}$ is the number of counts in channel i for quad phase k , and $x_i^{(k)}$ is the location of the channel, often just the value i itself; while the estimate of the standard deviation of c_k is given by,

$$7.2 \quad \sigma = \left[\frac{\sum_i^N f_i^{(k)} (x_i^{(k)} - c_k)^2}{\sum_i^N f_i^{(k)} \cdot \sum_j^N (f_j^{(k)} - 1)} \right]^{1/2}$$

Thus the distance between the peaks is simply,

$$7.3 \quad s_{12} = c_2 - c_1 \quad \text{with error estimate,}$$

$$7.4 \quad \sigma_{12} = [\sigma_1^2 + \sigma_2^2]^{1/2}$$

This was the first computer-based method used in this laboratory, beginning with the work of Meredith [Me(1971)] (see also Meredith *et al.* [Me(1972)]).

In this study, the “ χ^2 method” specifically refers to the calculation of peak position, relative to the comparison peak of quad number two, the measurement phase in which a nominal $\Delta V=0$ is applied, by minimization of the measure $[\chi^2(s,K)]$, *i.e.*,

$$7.5 \quad d[\chi^2(s, K)]^{(k)} = d \left[\sum_{n_1}^{n_2} \frac{(f^{(2)}(x_i) - K \cdot f^{(k)}(x_i - s))^2}{\sigma_i^2} \right] = 0$$

for which a sampling zone $[n_1-n_2]$ is specified around one of the peaks, and local variance (i is the Poisson-based value (*i.e.*, $f_i^{1/2}$)). Mathematically, the choice of reference quad is arbitrary, but it was easier to think in terms of a zero-voltage reference point in the design of the analysis algorithm. The use of this method in this laboratory began with the work of [Kozier(1977)]. From a rigorous mathematical standpoint, the method is not really applicable for data distributed according to counting statistics, but only to data which have a Gaussian distribution. However, as noted by Kozier, experience has shown this not to be an issue in practice.

A method deeply related to both visual peak cancellation and χ^2 , but explicitly using an error measure based on s-domain analysis of superimposed peak forms, has been used with success by the Minnesota group of Kayser and Johnson ([KaJ(1975)]). They define a "generalized error signal", a seeming misnomer since this mathematical object approximates the idealized, but unknown, "parent" shape of the signal plus noise. A minimization process on this measure extracts the desired separations and amplitudes of the peaks.

Both the centroid and χ^2 methods have advantages and disadvantages which have been carefully studied and reviewed in this laboratory by Sidky [Sy(1990)] or Hykawy [Hy(1991)]. In his review of the analysis process, Sidky provided comparative analysis results that showed no substantial difference between the two.

In view of the long-standing debate over the relative merits of the two methods previously used in this laboratory, the philosophy adopted in this study was to take advantage of the fact that the new implementation of the centroid and χ^2 analyses would be made with only a functional description of their operation, possibly avoiding problems related only to coding practice. Indeed, the AMDPRIME analysis system performs peak matching by employing the centroid method as an initial (and default) method, with refinement by a χ^2 method that did turn out to be algorithmically different from the existing software. This refinement process involves a direct search of the space of peak separation and relative size. A set of parabolic fits is made to the function $[\chi^2(s, K=const)]$, for some reasonable initial estimate of K (call it K_0), within a reasonable neighborhood of K_0 . The maxima are determined, stored in a table, and a parabolic fit made along the K parameter axis (see Fig. 7.9). The author calls the scheme "simplified interpolated sampling" or SIS, due to the fact that it avoids an explicit Taylor expansion of $[\chi^2(s, K)]$, and the matrix operations thereby entailed in finding the minimum from the resulting multi-variate analytic statement of the solution.

As an important aside, Sidky noted what was essentially an instability in the χ^2 algorithm in use up to that point (about 1988), in that, while a peak position given by the centroid method was always nominally correct, a bad choice of certain minimization parameters could result in "wild" individual match values for Δm when the refinement was made. In particular, the conclusion was that the program had no provision for adaptation to varying widths of the search valley for $\chi^2(c, r)$; c being the trial centroid and r the trial relative peak height. Thus the instability was the result of a hardcoded parameter which caused the program to occasionally try to perform

quadratic fits to a spuriously narrow search space. This provided assurance that the technique did not contain some fundamental flaw as far as application to this type of analysis, but did reinforce the general *caveat* that, as analysis algorithms become more complex, spurious looking results must be treated as a serious alert to such insidious bugs. One result was the incorporation of a Monte Carlo routine with which to create a variety of simulated data files.

In this connection, a strong theoretical re-assessment was not done in this work, however, some empirical arguments will be presented that, in the end, will be shown to mildly favour the χ^2 method. The tests described in this section served both the purposes of verifying program function and of helping to identify favourable aspects of each method.

It was important, first of all, to perform a comparison between the performance of the existing versus the new software on some common, representative run data. Six runs were selected for the test, three from the narrow doublet $^{201}\text{Hg}^{35}\text{Cl}_2 - ^{199}\text{Hg}^{37}\text{Cl}^{35}\text{Cl}$ comparison and three from the wide doublet $^{183}\text{W}^{16}\text{O} - ^{12}\text{C}_2^{35}\text{Cl}_5$. The analysis results are reported for both the centroid and χ^2 values, and in both simple- and weighted-average forms, for the output of each program. The tests with narrow doublets would exercise the mathematical peak-resolving capability of each program. The details of the method used in AMDPRIME are described later.

The results, as given below in Tables 7.1 and 7.2, show that, while the analysis output is not identical for each run, similar trends in Δm 's and associated error estimates do show up when using the χ^2 analysis, and that no significant differences should likely be attributed to the programs in respect to the overall average. The agreement using the simpler centroid method is not as good, and for the case of the narrow doublets, one can note a somewhat systematically higher result for the case of the narrow doublet study. The individual differences are arguably within the range of what one could expect from numerical processing by two pieces of independently written code running on different processors, involving a number of fitting stages and with results that are quite sensitive to centroid variation at the sub-channel level (approximately 15 μ per unit shift of channel number in the comparison peak would be typical).

A sample study on artificial peaks was conducted to examine whether either of the χ^2 or centroid methods offers an advantage as far as immunity to the effect of imperfect peak shapes (the origins of which were mentioned in above). For convenience, this test focused on one match mode, the Normal Adds Forward (NAF) match. As shown in Figure 7.1 the χ^2 matching of Monte Carlo-generated NAF peaks demonstrates some marginal improvement in the form of reduced sensitivity to peak skew and distortion, but at the price of a larger σ , even with some qualitative variation between peaks (*i.e.*, shape). This would naturally decrease the risk of systematic error. Figure 7.2 demonstrates the intuitively expected result that a similar skew on all peaks produces no significant systematic shift. The Monte Carlo routine which produced the skewed peaks was based on the nominal gaussian peak form (*sans* noise):

$$7.6 \quad f_i^{sm} = e^{-\frac{(i-c)^2}{\sigma^2}} \quad : (c-i) < 0$$

$$7.7 \quad f_i^{sm} = e^{-\frac{[(i-c)(1+\zeta)]^2}{\sigma^2}} \quad : (c-i) > 0 \quad \text{with } \zeta \text{ the skew factor.}$$

run i.d. by date	centroid: simple average, μ	centroid: weighted average, μ	χ^2 : simple average, μ	χ^2 :weighted average, μ
12FEB99 SPECTRUM	100 870.04 ± 31.08	100 902.42 ± 33.32	100 878.45 ± 23.95	100 895.18 ± 25.56
12FEB99 AMDPRIMS	100 899.58 ± 24.41	100 914.29 ± 39.00	100 885.37 ± 31.5	100 910.32 ± 39.0
23FEB99 SPECTRUM	100 859.81 ± 28.64	100902.87 ± 19.23	100 875.31 ± 20.04	100 891.97 ± 16.58
23FEB99 AMDPRIMS	100 872.60 ± 27.22	100 885.68 ± 37.21	100 881.18 ± 26.52	100 899.59 ± 34.03
24FEB99 SPECTRUM	100 891.71 ± 7.65	100 895.62 ± 5.52	100886.77 ± 8.43	100 885.66 ± 8.40
24FEB99 AMDPRIMS	100 844.39 ¹⁰ ± 8.13	100 888.86 ± 6.40	100878.54 ± 7.42	100 883.70 ± 6.92

Table 7.1 Comparison of results of analysis programs and methods on sample $^{183}\text{W}^{16}\text{O}-^{12}\text{C}_2^{35}\text{Cl}_5$ wide-doublet data.

run i.d. by date	centroid: simple average, μ	centroid: weighted average, μ	χ^2 : simple average, μ	χ^2 :weighted average, μ
27JAN98 SPECTRUM	4956.60 ± 3.79	4955.42 ± 3.62	4959.02 ± 7.89	4959.53 ± 6.71
27JAN98 AMDPRIMS	4965.51 ± 4.34	4965.81 ± 4.44	4963.36 ± 4.84	4963.87 ± 5.15
06FEB98 SPECTRUM	4964.19 ± 6.02	4962.70 ± 5.84	4970.12 ± 4.97	4969.10 ± 4.96
06FEB98 AMDPRIMS	4976.11 ± 4.77	4975.66 ± 4.69	4973.35 ± 5.01	4973.56 ± 4.94
10FEB983 SPECTRUM	4985.08 ± 9.46	4977.76 ± 9.44	4975.75 ± 5.19	4973.62 ± 5.22
10FEB983 AMDPRIMS	4980.77 ± 5.17	4980.86 ± 5.32	4980.68 ± 8.04	4978.50 ± 7.97

Table 7.2 Comparison of results of analysis on sample $^{201}\text{Hg}^{35}\text{Cl}_2 - ^{199}\text{Hg}^{37}\text{Cl}^{35}\text{Cl}$ narrow-doublet data¹¹.

In the case shown in Figure 7.1, the lack of great difference in the effect of unequal peak skew on the results of the two methods seems somewhat counterintuitive as the process of using the squares of channel count differences (cf. Eq. 7.5) would be expected to amplify any mismatch,

¹⁰ This would likely be classified as an outlier if unweighted averages were taken on the complete data set.

¹¹ The alert reader will note what *seems* to be a systematic change in run values with time. This is spurious in that these results are from a study in which many "outliers" were purposely hand selected from a large run result set. While the full set does show a mild chronological trend due to a few initial low values, with suspect calibrations, most of the later run averages had a healthy scatter about $\sim 4970 \mu$. The accidental choice of certain later *and* higher outliers adds to the impression of a strong trend here.

especially between peaks of very similar shape. Notice, however, that the variational per-channel weighting in the denominator of the standard χ^2 form weakens its rate of change with offset. In the absence of any systematic bias intrinsically associated with either method, the only advantage would be in seeking a reduction of variation that can be attributed to processing method, and so this became an added consideration.¹²

This absence of significant difference between the two methods is seen in the results of a number of noise tests conducted with the new analysis package on artificial data. The results below are given for a NAF match (cf. §IV.3) which was conducted on simulated data having varying amounts of excess noise, that is, scatter in the channel count over and above what one would naively expect from Poisson statistics on count number alone. Indeed simulated peaks constructed on this assumption have a much cleaner appearance than actual data, (enough so that a study was conducted by Meredith [Me(1971)] on this interesting matter; [Ko(1977)] also came to the same conclusion). The increase in noise was achieved by simply raising the value of the Monte Carlo peak-generator σ value. When applied to all 4 members of the match spectra there was no significant difference in either final Δm values or the variance. When a more realistic attempt was made to apply a systematic in the form of excess noise in only the first quad (in which the often weaker sample peak lay for the doublets in this work), the result became somewhat better for the centroid method in that it "moved" closer to the parent Δm value given as input to the simulator, although the variance was no better than the χ^2 result.

"excess" noise factor	average NAF Δm centroid method, μ , (10 trials)	average NAF Δm χ^2 method, μ , (10 trials)	difference cent. - Δm χ^2
2.3 x \sqrt{N} , all quadrants	120 552.73 \pm 15.5	120 552.71 \pm 16.6	0.02
2.0 x \sqrt{N} , all quadrants	120 554.53 \pm 13.26	120 547.24 \pm 13.80	7.29
1.7 x \sqrt{N} , all quadrants	120 559.77 \pm 16.54	120 551.18 \pm 8.72	8.59
1.5 x \sqrt{N} , all quadrants	120 558.54 \pm 8.41	120 553.97 \pm 8.90	4.57
1.3 x \sqrt{N} , all quadrants	120 558.57 \pm 7.55	120 550.10 \pm 9.98	8.47
1.0 x \sqrt{N} , all quadrants	120 557.67 \pm 5.05	120 553.87 \pm 7.7	3.80
0.7 x \sqrt{N} , all quadrants	120 559.06 \pm 2.47	120 553.33 \pm 6.50	5.73
0.5 x \sqrt{N} , all quadrants	120 558.73 \pm 4.70	120 552.05 \pm 4.16	6.68
2.3 x \sqrt{N} , quadrant 0 only	120 560.57 \pm 8.79	120 555.10 \pm 9.12	5.47

Table 7.3 Noise tests of the two analysis methods on artificial data. Parent (*i.e.*, input) Δm for Monte Carlo $\Pi_{NAF} = 120\ 561.08$ μ (skew factor = 0.1).

¹² The author would like to mention the valuable observation made by Dr. Kozier, as this work goes to press, that the reduced $-\chi^2$ on the best-peak-matching figure for a match is a useful indicator of peak-dissimilarity, and thus would be an important statistical object to make available in the run results for future studies on systematic effects and perhaps for use in generating a confidence measure on the match values.

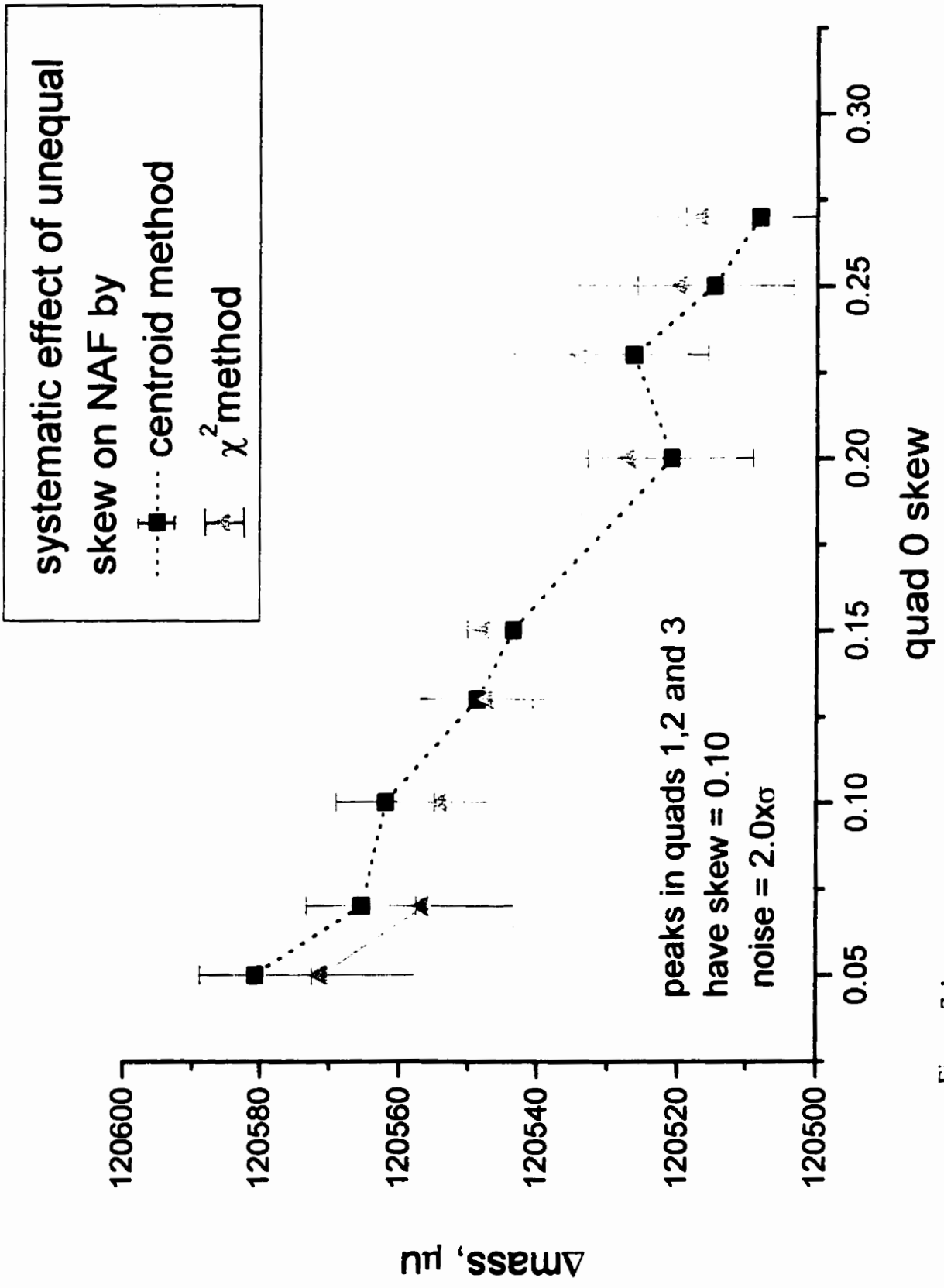


Figure 7.1

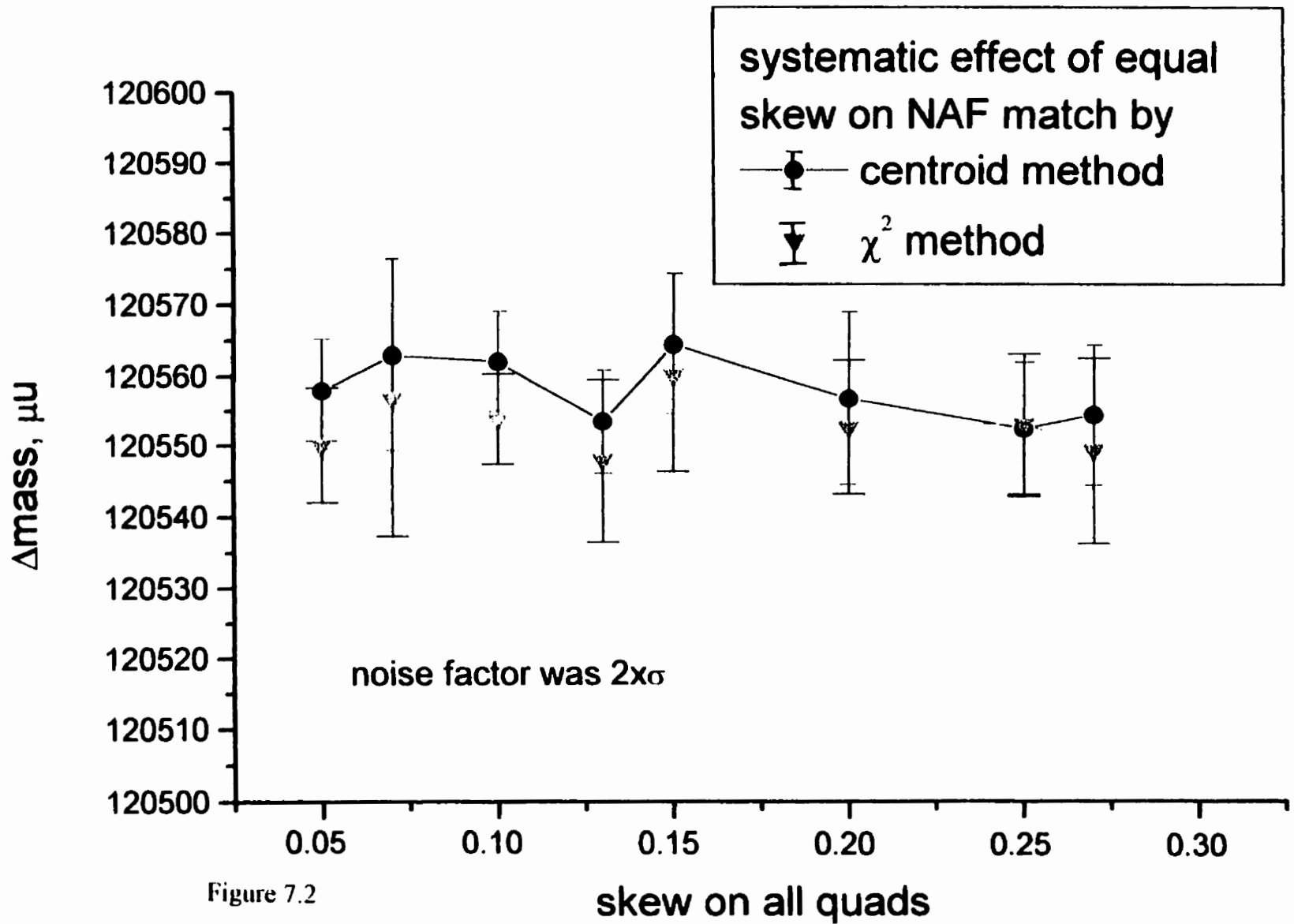


Figure 7.2

Clearly all of the results are systematically low: it is surmised that this is due to the skew factor kept for this analysis, since simulations involving all of the other match configurations seemed to produced complementary scatter about Π , (*i.e.*, the result on average over the 8 match modes being a good estimate of Π).

The main significant advantage that has been empirically noted in the course of this study with real data, for χ^2 over the centroid method, is the tighter clustering of results, especially when weighting is used: see, *e.g.*, Table 7.4. More significantly, the Birge ratio ($\sigma_{\text{ext}}/\sigma_{\text{int}}$) is closer to unity, suggesting that one has a better estimate of the uncertainty. The main disadvantage of the former has been the very pragmatic issue of it being algorithmically more troublesome to implement and verify. Thorough testing of a large piece of code is never a minor exercise. Further, this author finds the direct access to the "absolute" peak location in the centroid method very compelling. The user can often spot systematic problems in the data and/or analysis by comparatively comparing centroid motion under varying conditions at the peak processing virtual workbench mentioned in §VI. (Selection of a smoothing technique, to be discussed below, was aided by this process, for example). Thus in view of results seen, while there was little motivation to apply a more rigorously correct elaboration of the χ^2 method, such as maximum likelihood minimization (*e.g.*, see [Ko(1977)]), the results do somewhat favour the χ^2 approach.

analysis type	unweighted result as $\mu \pm \sigma$ ¹³	weighted result as $\mu \pm \sigma_{\text{int}} \pm \sigma_{\text{ext}}$
centroid	124 023.19 ± 5.78	124 023.25 ± 1.87 ± 4.07
χ^2	124 024.82 ± 5.20	124 017.19 ± 0.62 ± 1.48

Table 7.4 Analyses on actual data set for ¹⁹⁹Hg-¹⁹⁹(C₂Cl₅).

Finally, a test of the program on a full set of Monte Carlo-generated data provided what was considered to be confirmation of program function. A series of 10 files (BIGTESTx.DAT), each file being a complete simulated run, were created, with a noise factor of 2x the Poisson width and with a skew factor $\zeta = 0.1$ (appropriately reversed for reverse sweep matches: see §IV.4). These data corresponded to no real nuclei or compounds thereof, but had many parameters that were similar to the real comparison of ¹⁹⁹Hg versus ¹⁹⁹C₂Cl₅. The results after analysis by AMDPRIME are shown in Table 7.5.

analysis type	result on 10 "runs" with matches weighted	unweighted matches in each run
χ^2 , wtd. average	120571.13 ± 2.06 ± 2.26	120570.07 ± 2.12 ± 1.65
" , simple average	120571.82 ± 2.29	120570.45 ± 1.58
centroid, wtd. average	120568.58 ± 1.64 ± 1.28	120569.27 ± 1.77 ± 0.84
" , simple average	120568.43 ± 1.53	120569.58 ± 0.93

Table 7.5 Results of a validation run on AMDPRIME using 10 Monte Carlo runs. Parent (*i.e.*, input) Δm for Monte Carlo $\Pi = 120569.12\mu \pm 4.27 (\sigma)$ (on the 8 matches)

¹³ An underscore on σ is this author's choice of symbolism for the standard deviation of the mean.

The two processing methods comfortably straddle the input value, with the χ^2 results slightly high and the centroid method results either essentially right on or slightly low. Coincidentally, the weighted average of the weighted average results from the two methods was a nearly "perfect" 120 569.20.

Values Finally Reported

Clearly some final representative value from the eight categories of results has to be selected for reporting. The overall run averages turn out not to vary considerably between data averaged over the eight groups (see §VIII), that is, they were the same to within about $\pm\sigma$ (less than $\approx 4\mu$) for wide doublet comparisons. This is not by any means insignificant, as this is approximately the current typical confidence level for most high-precision mass measurements reported for stable nuclides. (As well, random errors have historically been considerably smaller for this instrument; this will be discussed further.)

The slight advantage for the χ^2 values was discussed above. There has been some discussion as to whether the weighting of matches within a run was statistically meaningful. As elaborated in the software functional specification (Appx. A, *Interpolation of the Matching ΔV , with Uncertainty Value*), an error on the match ΔV is available from the propagation of the error estimate on each centroid mean, through the linear regression on the match line (*i.e.*, through the $+\delta V$, $-\delta V$ and $\Delta V \approx 0$ calibration points), and on to the particular ΔV_i interpolation for the match. These individual σ_i values were plotted, as their squares, against the deviation of the corresponding Δm datum, c , from the simple, complete run average μ (of 8 match modes). As can be seen in Figure 7.3, there is a loose correlation of estimated "local" error to the deviance (regression $R = 0.413$), which confirms the casual observation that Δm values closest to the long run average generally have smaller standard deviations.

Therefore the choice was made that, until further motivating evidence was available from future studies, the *weighted* average of the matches would be used to define the value for a run. This statistically entails taking the weighted average of all runs as well, since there is no compelling reason to then drop the weights at the stage of taking the average of all runs without a better understanding of any variable systematic effects between runs. The last mentioned study (BIGTEST) weakly implied that the two methods may somehow complement each other as far as accuracy, but there was no reasonable statistical significance to this hypothesis for the sample size. It is not clear that a Monte Carlo calculation with a larger sample size would realistically go further towards resolving the issue until, among other factors, the issue of how true peak shapes arise (see, *e.g.*, Mc(1971)) is thoroughly understood. Thus, a grand weighted average of the χ^2 -method weighted-average run results is reported.

2. Processing Stages: Some Details

Stages in the computer processing leading to match and run results are described in some detail here. An analysis flow diagram is presented in Figure 7.10, while full details, including formulae, are to be found in Appx. A, the Functional Specification of AMDPRIME5.

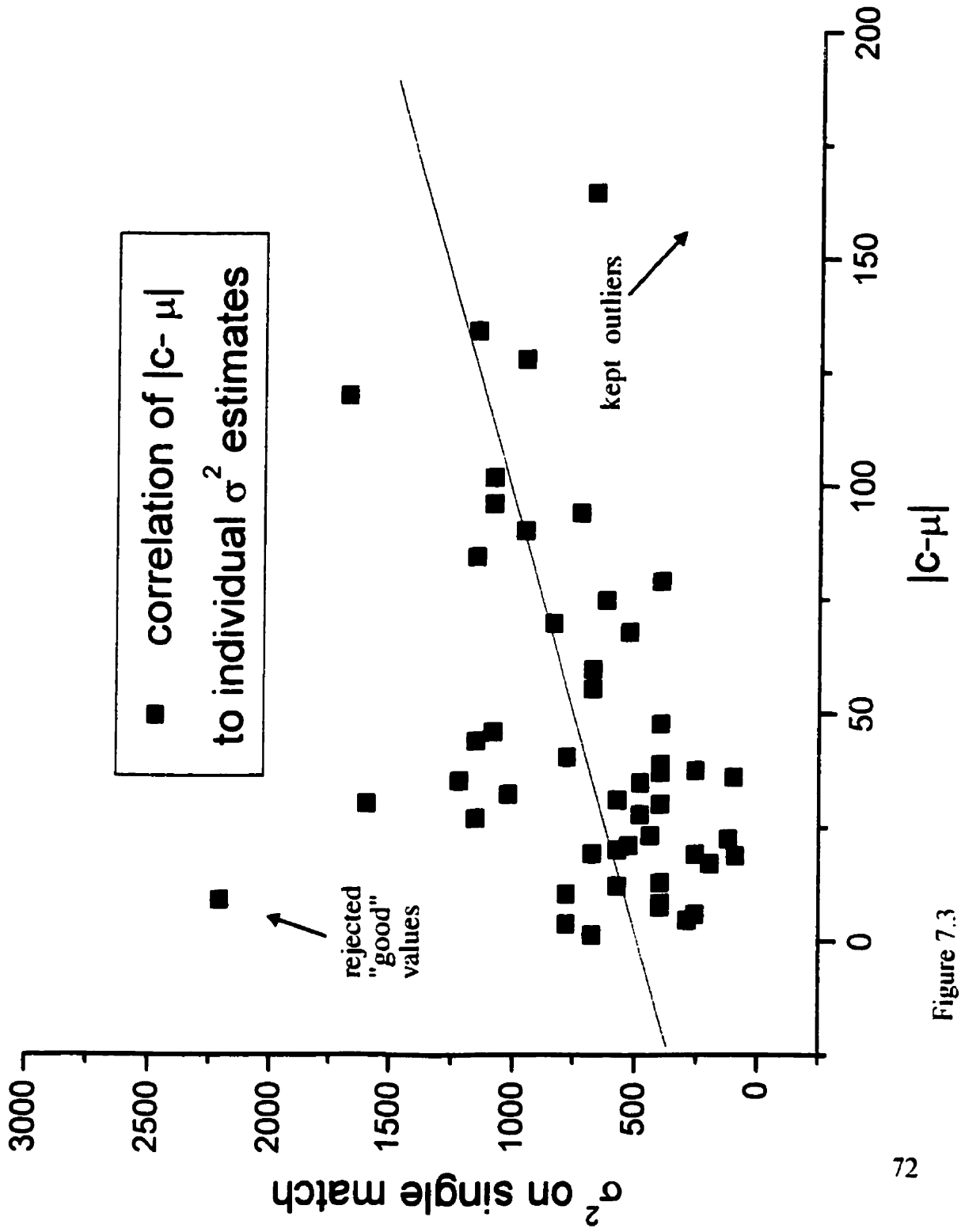


Figure 7.3

2.1 Smoothing and Deconvolution

The data collected are almost invariably "smoothed" before a staking-out of the critical peak limits is attempted. This is done by convolution with any reasonable sampling function, such as (a portion of) a harmonic function, in the s -domain. In the continuum description one simply multiplies,

$$7.7 \quad \Xi(s) = F(s) \cdot h(s)$$

where $F(s)$ is the Fourier transform of the data, and $h(s)$ the transform of the smoothing or sampling function of choice, such as a sine (actually, the first positive cycle):

$$7.8 \quad F(s) = \int_{-x}^x f(x) \cdot e^{2\pi s x} \cdot dx$$

$$7.9 \quad h(s) = \int \sin\left(2\pi \frac{x}{\lambda}\right) \cdot \Theta(\pi/2, \pi) \cdot e^{2\pi s x} \cdot dx$$

$\Theta(\pi/2, \pi)$ being the double-Heaviside function that is equal to unity in an interval π about $\pi/2$, and zero elsewhere.

The result upon inversion is a function, $\xi(x)$, in which all noise contributions to the peak spectrum below the characteristic size of the smoothing function have been suppressed.

The standard practice in this investigation is the application of a truncated sine function ($\pi/2 = 35$ channels) in the convolution on all of the match spectra. The discrete version of this process is shown schematically in Figure 7.4. The rationale is to greatly simplify the parameterization of a peak by the analysis system. It is extremely difficult to construct an algorithm to sensibly and with some notion of consistency set peak limits, for example, when random fluctuations and the occasional channel "spike" appear in the data. Further, the eye is better guided in the non-trivial task of setting background markers. The convolution is always "removed" when the peak marking is complete by simply reloading the raw data again.

The choice of convolution-smoothing, in particular an fast Fourier Transform (FFT) based discrete transform, is based on the fact that, as mathematically expected and as born out in trials, the peak centroids are not significantly affected. All the same, "removal" of the smoothing after demarcation of the peak(s) is important in that there is a residual systematic bias introduced into some matches evaluated using only the centroid method. A brief description of these trials is given in Appendix B.

One of the incidental benefits of applying a smoothing procedure before proceeding with the analysis is that bad data channels, *e.g.*, those that for reason of some equipment fault or noise hold a zero or an extremely large count ("spike"), stand out. A spike in the data spectrum, which is very hard to see on the graphics display¹⁴, gives rise to a concave lump, whereas a misplaced

¹⁴ The software was written to suppress spikes and zeros in the middle of a peak feature so that scaling of the plot would almost always succeed: this was deemed more useful to the user than a bad display due to a faulty channel.

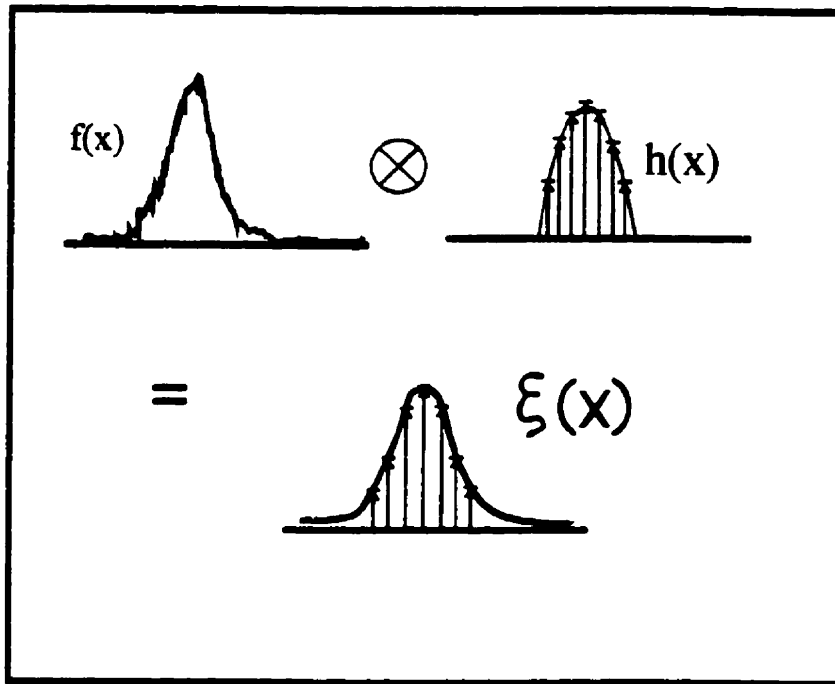


Figure 7.4 Discrete convolution of data to a smoothed representation.

zero gives the complementary hollow. Such data can generally be rescued by a "despiking" feature of the software. The hazard otherwise would have been a spurious centroid value that the user might not easily notice.

It should be mentioned that attempts to develop a means to extract the "original peak" shapes, *i.e.*, triangles, by deconvolution were made. Assuming that the bulk of the peak smear is due to some harmonic "system motion", trials were made with various harmonic sampling functions, such as pure cosines and cosines "diluted" with some percentage of a constant. None gave satisfactory results: this is a process that is unforgiving as far as the exact choice of sampling function. Since convincing centroid values were already being generated by this point, this line of investigation was left for a future date.

2.2 Backgrounds

There is a significant contribution to each peak in a close doublet from the counts of its partner. This is due to the problems mentioned in points 2. and 3. at the beginning of this section, *i.e.*, scattering and other sources of peak broadening. A suitable choice of background-subtraction method is thus essential if one is to approach micro-unit resolution in the analysis of a close doublet. Depending on the method chosen, the centroid calculated on a peak will shift by a good fraction of a channel, with the other member of the doublet shifting in a direction that does not compensate, but rather doubles the systematic motion; that is, the peaks on a quad data display will seem to either slightly "attract" or "repel". A centroid motion of a single data channel corresponds to a change of potential of about $40\mu\text{V} \approx 10\mu\text{u}$ at this mass. Thus a poor choice of subtraction method may lead to effective mass errors of the order of a few or several micro-units on a match in this study (at mass ≈ 200), since the systematic motion described will apply when considering the test versus reference peak positions across the four quads.

A simple-minded straight line applied to the base about each peak fails on this account: peaks will systematically "move" too far with respect to the untreated case since, as can be seen exaggerated in Figure 7.5, too much of the real peak is removed on one side of the maximum.

A nearly optimal solution, if one is confident that the members of the doublet have the *same parent distribution or shape*. AND if sufficient amounts of each peak are available in a data quad, is peak stripping. Referring to Figure 7.6, the idea is to take the tail of one peak, which is presumably far enough away from contamination by the partner peak to be fiducial, as a template to subtract background from the portion of the same peak in the zone between the doublet. Empirically, the method is highly useful in testing other baseline-removal techniques, since by using good quality data sets where all of the aforementioned criteria are met, a very high order of correction is achieved. This has been tested on synthesised data containing added noise, and has worked well when peaks have homologous shapes. This latter point is, however, the downfall of the method: one seldom has a good quality partner peak to the peak of interest in any given quad. There are, for instance, problems related to the value of data collected near the initial channels of the quad, when ΔV is known to be in the early stages of exponentially settling. Thus the method is used largely to help in studying other techniques and, indeed, the actual technique chosen was selected in part because of its indistinguishability from good quality peak-stripping results.

The background-subtraction technique used in this study is, in fact, a fairly straightforward quadratic fit to the relevant background zones in a quad. The operator selects 4 reasonably sensible locations for a least-squares fit to a hypothetical quadratic curve, (see Figure 7.7), meant to represent the very mild concave shape of the tail of the partner peak. The rules-of-

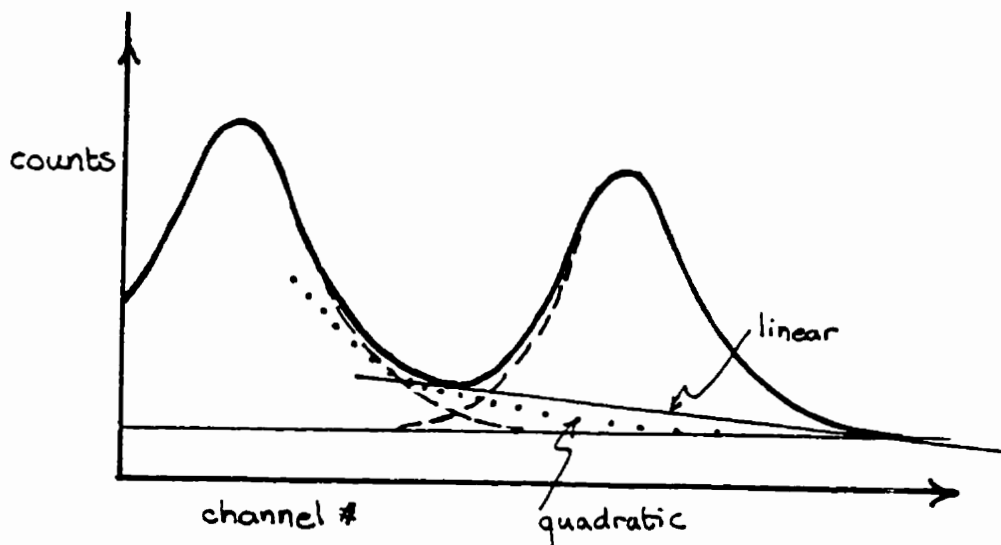


Figure 7.5 An exaggerated demonstration of the superiority of a parabolic fit.

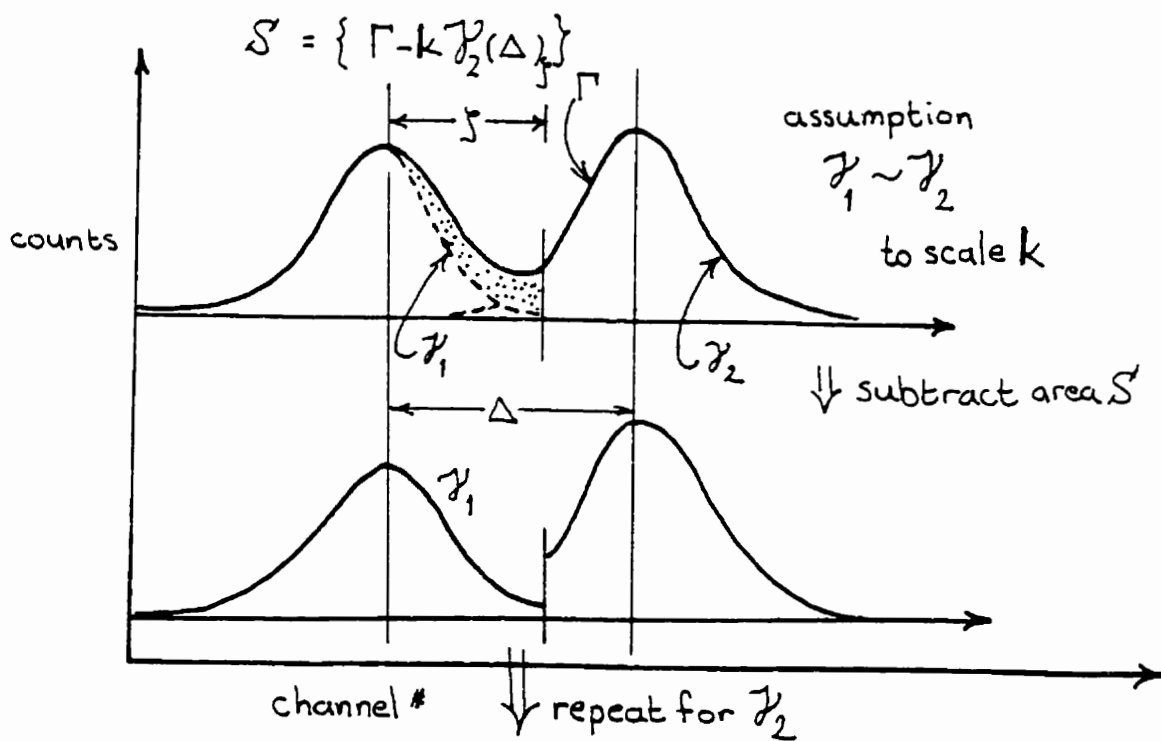


Figure 7.6 An idealized peak-strip operation on one member of a close doublet.

thumb, as incorporated in the fully automated match process, are to use the following points (again, see Figure 7.7):

1. one marker, [2], at the inter-peak centre
2. one marker, [4], at the extreme tail of the peak of interest
3. one marker each, [1] and [3], at the "sensible beginnings" of each peak on the appropriate sides, *i.e.*, marker [1] is at 2% of the peak height of the left-hand peak, based on a cruder straight-line fit, while marker [3] is at the conjugate point directly opposite the peak centroid (as far as can be determined by the initial centroid estimate). Markers [1] and [3] can be set up by a request to the program, after an initial manual placement near their respective "partners" [2] and [4].

As alluded to above, these criteria were established by experiment on synthesised peaks and comparison with good quality peak-stripped data. The software ensures, as far as it is reasonably possible to say, that equivalent portions of the peak of interest are sampled by always setting the inner peak background markers on the curve symmetrically with respect to the current estimate of the centroid.

2.3 The Match

As explained in §IV, a match between the members of a doublet is accomplished by interpolating a reference against a calibration line of δV versus channel number created using the test peak, or vice versa. Both cases, test versus reference peak motion deflection and reference versus test peak motion deflection, are set up during a single run as one of the 3 permutation categories of match parameters, described in §IV as Adds and Subtracts.

In essence, the centroids of one member of a doublet under a successively applied ΔV of $+\delta V$, $V \approx 0$ and $-\delta V$ provide three data points for a least-squares line. In a fourth quadrant, a larger ΔV is applied which nearly lines up the other member with the $\Delta V \approx 0$ peak of its partner, providing a peak that can be used to interpolate the "true" ΔV that would have been needed to achieve a match. The linear fitting and error calculation is quite conventional; see Appendix A for the formulae incorporated in the algorithm.

The calculation of a simple centroid, using peak limits established by height, begins the actual analysis for individual peak location. This provides an initial set of centroids, peak widths in terms of an effective standard deviation, etc.. These data is used immediately to provide an initial mass difference result, and a useful measure-of-goodness of the analysis in the form of a χ^2 on the three-point calibration line (not to be confused with the χ^2 method). Prior to some corrections mentioned below, this centroid-based value is actually the final one in the case of analysis by the centroid method.

In the case of the χ^2 method, processing continues: a process is begun whereby the peaks corresponding to an applied ΔV of "large ΔV ", $+\delta V$ and $-\delta V$ are more intensely compared to that of $V \approx 0$. The nominal centroids calculated as above serve as a starting point for searching, locally, the independent parameter space, s (shift) and K (scaling), of the measure of the minimum of χ^2 , given by $d\chi^2$ (see Eq. 7.5), with respect to the $V \approx 0$ peak. As shown schematically in Fig. 7.9,

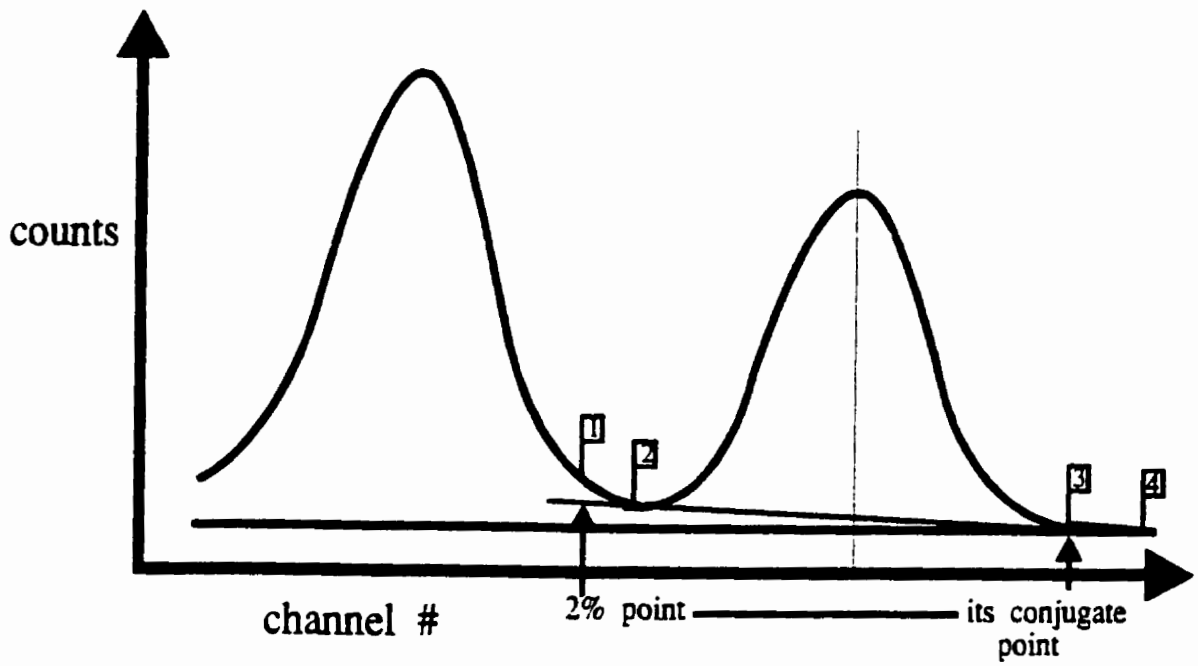


Figure 7.7 Setup of the key background position flags by computer guidance in preparation for a quadratic background fit.

when the overlap between the test peak and the nominal $V \approx 0$ peak has been optimized, there is a minimum. Thus a type of refinement to the initial peak positions is executed. The locations of three "voltage peaks" mentioned are thereby adjusted accordingly, *i.e.*, according to the δs that was found at the minimum.

It is entirely possible for χ^2 peak-to-peak fitting to fail, generally due to poor peak shapes or spuriously-large, single-channel values (spikes in the spectrum). This occurrence is usually quite obvious from the output of highly deviant results when the SIS algorithm begins, as the current value of the temporary χ^2 values are presented in a real-time processing display window. One of the incidental values of the χ^2 method is to call to the analyst's attention such problems (but see also comments on smoothing above). Naturally a deformed peak is of questionable value, even if accepted under the centroid method, but spiked data can often be repaired as mentioned earlier.

2.4 Corrections

An important correction applied at this point is a "thermal subtraction." A close examination of Figure C-95-7 shows that one essentially has two measurement configurations when taking a ΔV , as shown in simplified form in Figure 7.8. The idea is that one always includes a finite contact potential in measuring some ΔV that, although initially unknown in this circuit topology, is small and constant in a statistical sense. As this indicates, this contact potential, say $\epsilon+$ when measuring some $\Delta V > 0$, cannot be assumed to be the same when measuring $V < 0$; in this case call it $\epsilon-$. This is because there is a change in the particular contact set. Now, if all of the ΔV s in a match are measured one way, we would not be aware of such a potential and it would have no effect on the peak match. If some measurements are made with the potentiometer reversed, however, as when examining the "splits" potentials, then one or the other set must be offset: not correcting for this clearly leads to a bad three-point fit on the calibration line, for example. This correction is made by reading the nominal $\Delta V/2 = 0$ potential both in the forward and backwards potentiometer setting. Here, very close to zero, one can fairly easily read both a positive and minus offset on the system null meter. An algebraic solution of the equations that account for all of the known and unknown circuit drops in each configuration then gives both $\epsilon+$ and $\epsilon-$. The final form of the expressions used to give the estimated true ΔV s are summarised in Appendix A.

A "calibration" is also needed for any run, largely to cope with the otherwise unknown, small, added surface potentials that inevitably develop on the ESA plates. This long-recognized problem is known to be caused by extremely thin dielectric coatings, made up largely of such material as back-drifting diffusion pump oil, that deposit on the plates and there accumulate charge (see, *e.g.*, Petit-Clerc and Carette's work [Pe(1968)] which first investigated this effect in some depth). After thorough cleaning of such electrostatic elements, for instance by use of a glow discharge, the charges seem to nearly disappear, but form again over the space of days. If there is no "upset", that is, a sudden spurious electrical change that spatters the ion beam about, a stable charge tends to build up over this time, and can be dealt with by calibration.

A calibration is a run on a well known wide doublet at or near the mass region of interest. An example is a pair of the isotopic compositions of $C_2Cl_5^+$ for the $A=200$ region, perhaps 1 u apart. The discrepancy on the ΔM found for such a pair is then used, arguing a linearity of the

systematic effect, to scale the ΔM found on the narrow doublet of interest. The arguments for the legitimacy of this calibration are not presented here: the interested reader is referred to [So(1973)].

2.5 Run Results

As explained several in this work, a run consists of eight matches corresponding to the permutation of 3 matching conditions. Thus 8 peak separations in terms of potential are available to form a single run average, as a ΔM between the doublet members examined. This may be of significance in and of itself as a scientific datum, much as a reaction Q-value might be, or may be combined with the reference mass (M_R) to produce an absolute atomic mass value $M = \Delta M + M_R$ on the test species. Since the reference is typically a hydro-chlorocarbon, and the masses of H, Cl and ^{13}C are known to extremely high accuracy (the mass of ^{12}C is of course defined as 12), the only important error is from the ΔM value in this case.

The two forms of error estimate known as "external" and "internal" errors are computed, (see Birge [Be(1932)] or Meredith *et al.* [Me(1972)], and the Functional Specification in Appendix A). The former is a measure of the variation between the values of the members of a run.

$$7.10 \quad \sigma_{\text{ext}} = \sqrt{\frac{\sum_j^N [\Delta M_j - \overline{\Delta M}]^2}{(N-1) \cdot \sum_i^N \frac{1}{\sigma_i^2}}}$$

while the latter is explicitly only a summary of individual uncertainties, *i.e.*, an aggregate of σ in quadrature weight,

$$7.11 \quad \sigma_{\text{int}} = \frac{1}{\sqrt{\sum_i^N \frac{1}{\sigma_i^2}}}$$

A comparison of the two becomes a useful local consistency measure on errors. As well, the larger of the two error estimates is the quoted error in logged results.

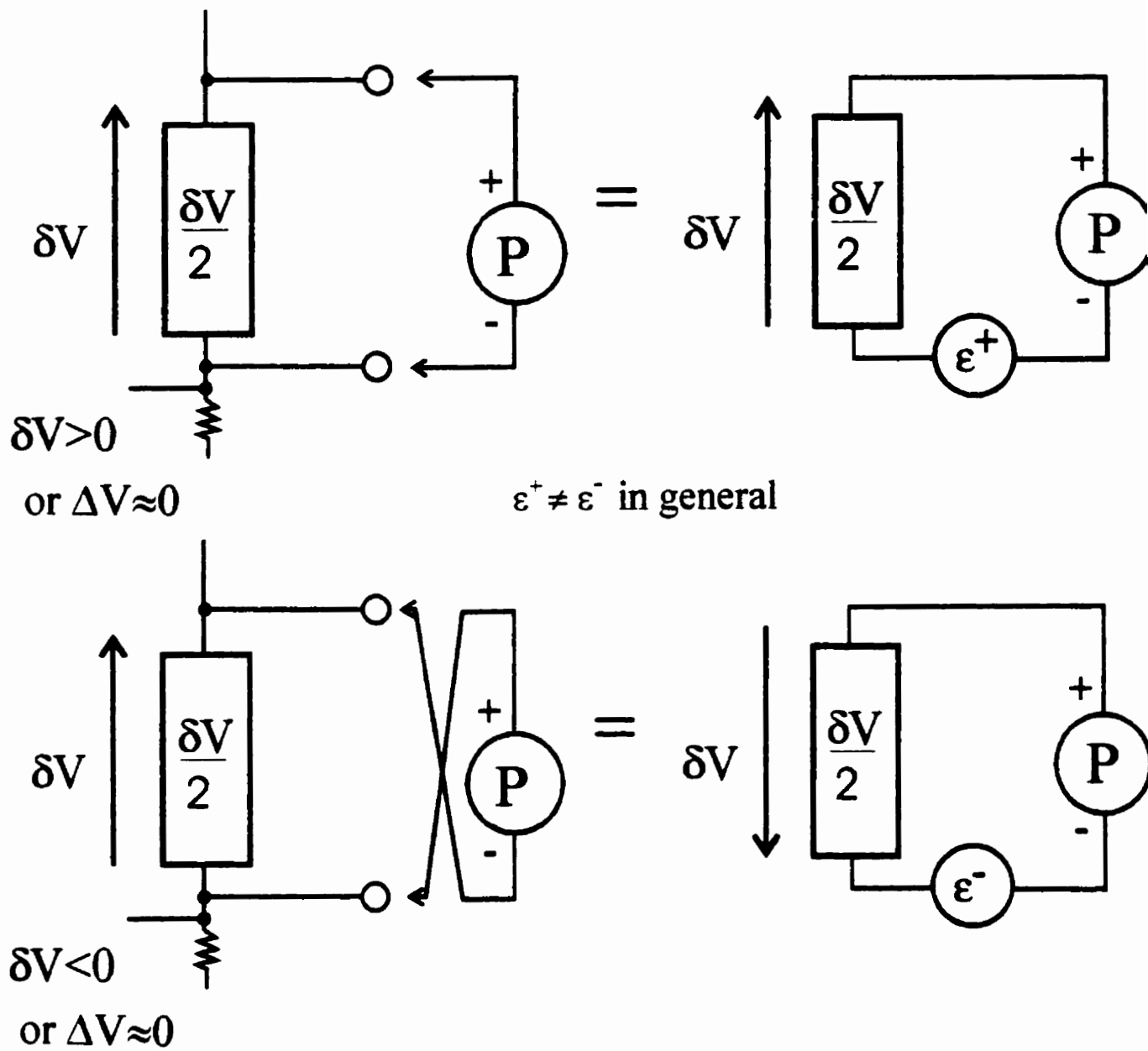


Figure 7.8 Using potentiometer switch reversals when $\delta V \neq$ nominal 0 (and when it is) to establish the contact potentials of the measurement circuit.

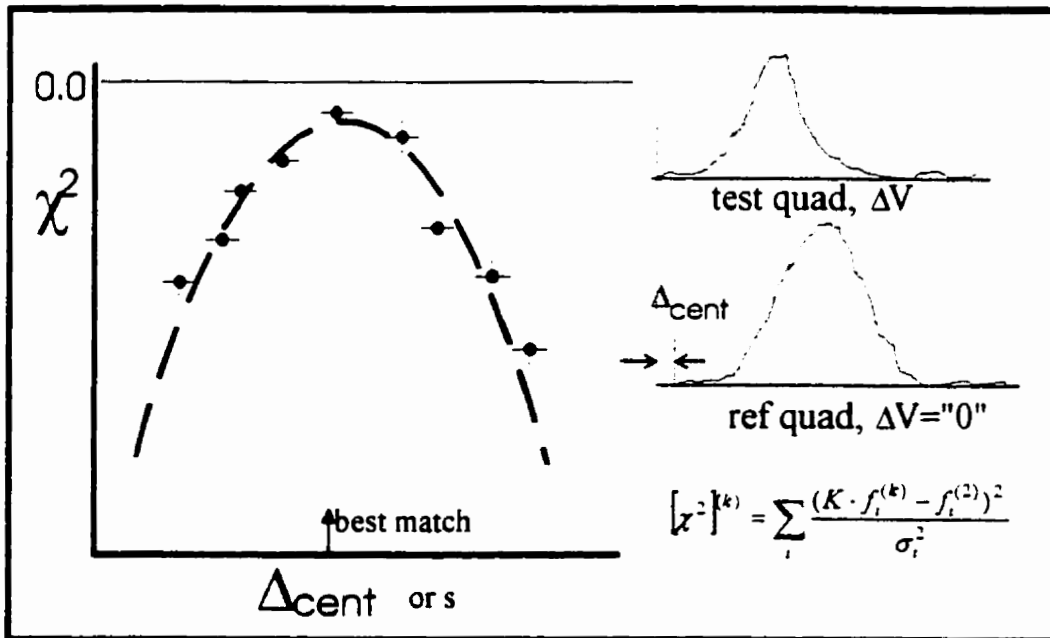
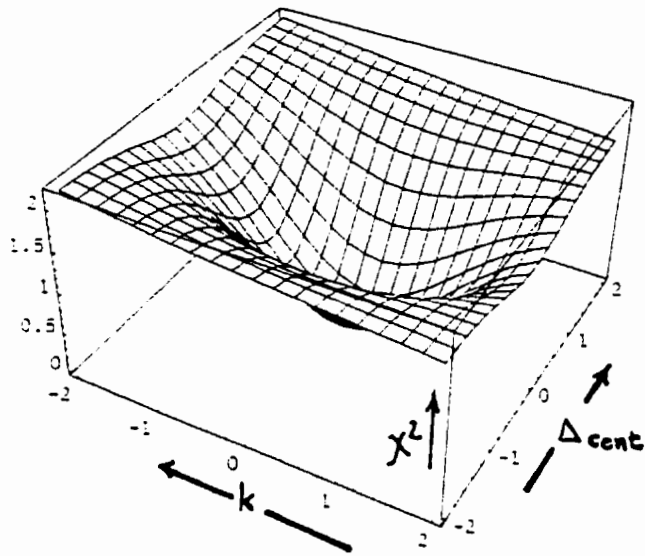


Figure 7.9 A “model” of the chi-square search in $(k, \Delta_{\text{cent}}, \chi^2)$ space, and a slice showing a 1-dimensional search for best centroid for a given relative height k .

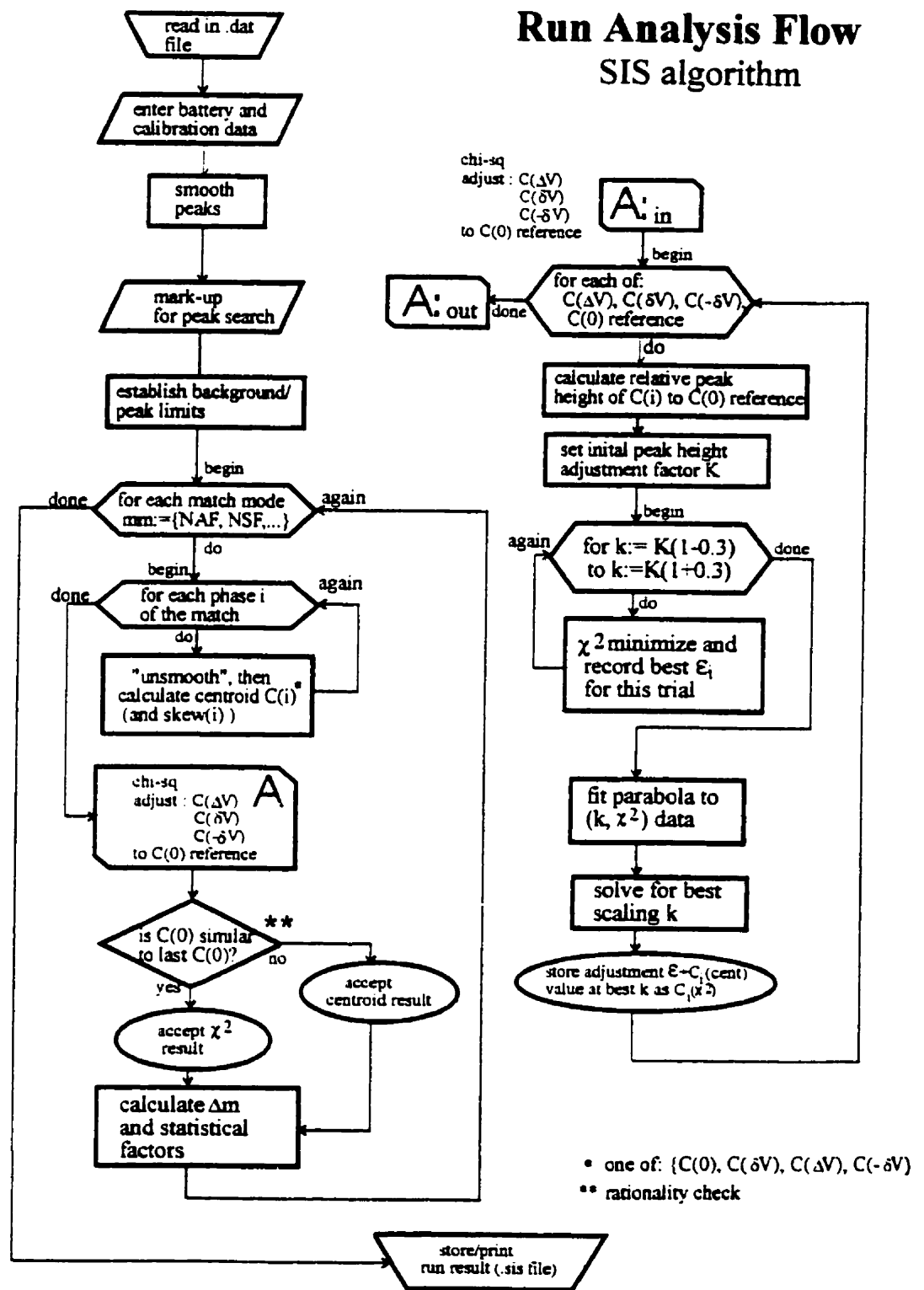


Figure 7.10

VIII Results of Measurements on the Mercury-Tungsten System

1. Assessment of the Data Quality

Given the order of magnitude of precision required for a useful mass table re-adjustment, that is, of the order of a few micro-units, the mass values produced in this study required some objective assessment of accuracy. The Manitoba II instrument has routinely offered up meaningful mass values to several parts in 10^9 mass values when operated with care and when systematics were well controlled. In the case of this study, where new potentiometry systems have been introduced and where relatively wide doublets are under scrutiny, little can be taken for granted in the avoidance of systematic effects. As discussed in chapter II, and again below, the ultimate check on the data is its fit within the network of other presumably reliable data, though there are clearly no guarantees. It is in this vein that the author chose to perform a local least-squares adjustment in the vicinity of the tungsten-platinum groups in the valley of beta stability (approximately $A=180$ to 200)¹⁵. A meaningful interpretation can then be made of the new data as far as its impact on the consistency of the member nuclide masses in this analysis.

Within the scope of these measurements, however, there are a number of assessments for data accuracy. One of the most important on-going checks is built into the measurement protocol, that is, the permutation of match configurations discussed in §IV.4. As mentioned there, the reversal of some key run configurations can be diagnostic in finding instrumental biases.

Some of the effects examined in determining the ΔM s for this study were:

- rapid changes in ion source conditions.

Here, the object distance (in the sense of ion optics) and characteristics of the ionization region will change. Often this will mean a drift in the energy focus of the system, and a systematic effect on the measurement of chemically dissimilar doublets.

- current leakage in the potentiometry circuit.

As a rough calculation, notice that at 400 V, a leakage resistance of 400 G Ω can allow up to 1 nA to flow through the potentiometer. At an input impedance of 1 M Ω (Keithley Instruments Model 155), this corresponds to a voltage drop of 1 mV! Thus special care was taken in the fabrication of all circuit sections which handled ΔV at high voltages in regard to proper insulation.

- unbalanced ΔV supplies

This violates the operation suggested by Bleakney's theorem. This can arise with poorly trimmed op-amp circuitry in the ΔV voltage-translation system.

- choice of thresholds for peak analysis; see Appendix B.

- unusual peak shapes (*i.e.*, far from the ideal triangular shape), especially within a given match.

¹⁵ The author acknowledges the direct assistance and valuable experience of his supervisor in constructing and interpreting this analysis.

A sign that the ion beam is not optimally aimed, that transport paths in the machine are not equivalent for the two members of a doublet or that EM or mechanical interference is "moving" the beam about; all capable of adding a systematic factor to the respective peak locations.

- large difference in intensities between reference and test peaks.

- "charge-up" on the potentiometer during measurement.

This list is not all-inclusive, but comprises effects observed both in the course of this and previous work. All were carefully monitored once understood or at least identified.

2. The Results

The results obtained in this study are shown here. As the reader will note, the first three mass differences constitute a closed numerical loop. Indeed, inspection of the data indicates loop closure to within the loop error. The last doublet was measured largely as a test of the system after the electrical reconstruction (but see below).

doublet	values, μu	errors	other authors
A. $^{199}\text{Hg}^- - ^{199}(\text{C}_2\text{Cl}_5)^-$	124 017.19	± 1.48	Kozier <i>et al.</i> 124023.43 ± 0.53 [Ko(1980)]
B. $^{199}\text{Hg}^- - ^{199}(\text{WO})^{-16}$	23 145.55	± 3.65	Calculated from input data of [Au(1993)] w. Ir linkages 23113.55 ± 3.93 (!) w.o. Ir linkages 23134.47 ± 6.0 (see Table 8.3 and text)
C. $^{199}(\text{WO})^- - ^{199}(\text{C}_2\text{Cl}_5)^-$	100 870.48	± 3.09	$100 875.3 \pm 3.0$ (adj. value of Audi <i>et al.</i>) [Au(1993)]
D. $(^{201}\text{Hg} \ ^{35}\text{Cl}_2)^+ -$ $(^{199}\text{Hg} \ ^{37}\text{Cl} \ ^{35}\text{Cl})^+$	4 971.8	± 1.0	Kozier <i>et al.</i> $4 972.65 \pm 0.37$ [Ko(1980)]

Table 8.1 Final doublet Δm results from this study (no adjustment): simple loop residual ϵ_r on [A.-B.-C.] = $1.16 \pm 4.78 \mu\text{u}$ (largest σ for any two loop member σ 's combined)

As discussed in §VII.1, these data are calculated as the weighted average of run analysis values obtained using the weighted average of match values from the χ^2 method. The data linkage is shown in the diagrammatic form introduced in §II.2, in Figure 8.1, with the reference $^{199}(\text{C}_2\text{Cl}_5)^-$ taken as a "virtual" nuclide for convenience.

¹⁶ Almost exclusively $^{183}\text{W}^{16}\text{O}$, with the rare ^{17}O (0.038 atom %) dimer, $^{182}\text{W}^{17}\text{O}$ (1:1500 atom mixture). A small correction has been applied to the figures for ^{199}WO , by remove the weighting of the latter species on the doublet spacing in $\Delta M_{\text{apparent}} = c_{183}\Delta M_{183} + c_{182}\Delta M_{182}$, c_i being the atom fraction of component i .

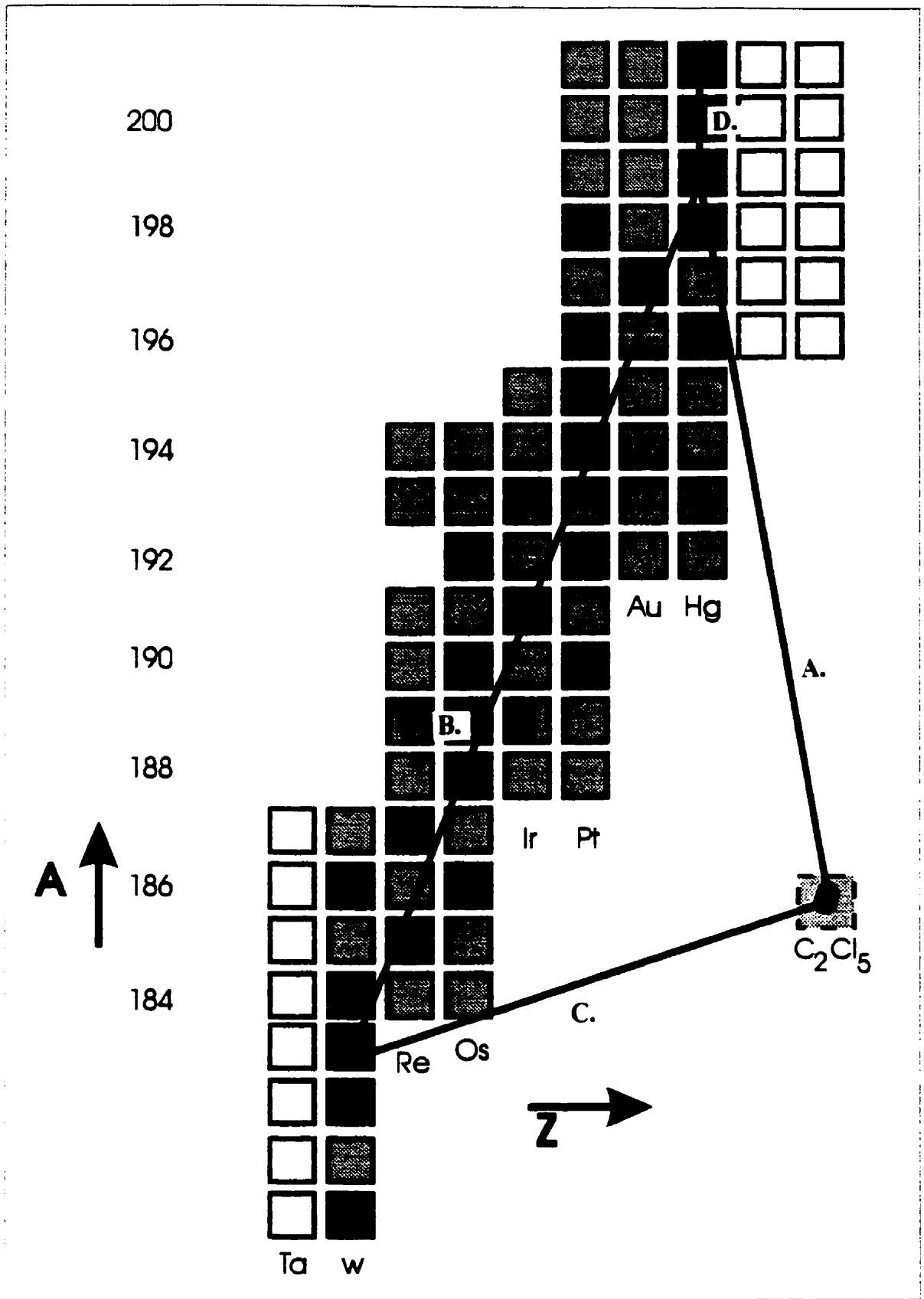


Figure 8.1 The mass table between tungsten and mercury with the linkages measured in this work.

The closure of the measurement loop on chemically dissimilar doublet measurements provided confidence that potential systematic problems, common with such determinations, and which are difficult to specifically characterize, were under control. The assumption is that the factors addressed in §1 were the critical ones. The main concern was the relatively wide data scatter that led to such large standard deviation values, *i.e.*, large *external* errors not necessarily accompanied by commensurate *internal* errors (see §VII.2.4). As discussed earlier, the errors for this experiment have historically been smaller, typically by a factor of 5 or more with respect to the standard deviations presented above. Clearly a variability had appeared with changes to the system.

In detail, a comparison with similar data obtained by previous investigators on the older system revealed that similar data scatter was present between run match values on wide-doublets. However, the match averages from run to run had a smaller scatter. The implication is that run-to-run related factors were changing. The main observable that had changed with time was a large increase in the systematic correction, previously discussed in §VII.2.4. Previous investigators found typical $ESA_{cal} \approx 30 - 130\text{ppm}$, while currently, measurements on $^{201}\text{(C}_2\text{Cl}_5) - ^{199}\text{(C}_2\text{Cl}_5)$ ($\Delta m \approx 2\text{ u}$) often give ESA_{cal} as high as 700ppm on some days. This is stable within a given run if there are no "upsets", electrical disturbances that would spatter ions in the ESA or other parts of the ion optics. (as also mentioned in §VII.2.4). Such corrections obviously have a proportionately large effect on wide doublet values. The author suspects that variability in this factor is an important component of the overall variability, though, due to the practical difficulties in calibrating the systematic error through the course of a run, this has not been conclusively shown.

It should be mentioned that attempts were made to clean the ESA plates by discharge. Pure argon was slowly allowed to leak into the system while a high AC voltage from a Tesla coil was applied to the ESA plate terminals. As the pressure rose through the "glow discharge region", at approximately several millitorr, it was expected that such a discharge would indeed be established and persist for a few minutes. There was, unfortunately, no resulting significant decrease in the calibration value from the previously measured $ESA_{cal} \approx 450\text{ppm}$ following this treatment. It was decided that further, more aggressive measures involving direct chemical wiping of the plates would risk incurring more problems, and that the problem would be best dealt with by more frequent calibration checks, exploiting the various match configurations available on a visual run to examine the calibration data for problems.

In order to help resolve the overall variability issue, an experiment was conducted in which a series of NAF matches were made in succession on a wide doublet. The assumption was that any intrinsic variability, that is, not having to do with changes to the match mode, would be isolated as the short-term drift component. This would be repeated a few days later to check for similar variances. The results for one trial set are given Table 8.2. A similar set of measurements made before and after the indicated date showed no significantly different results, especially with respect to the error estimates. (The systematic offset between methods is obviously undesirable, but is known to be averaged out through the use of 8 match configurations when the known error sources are well controlled). As mentioned previously, the internal errors are based on the propagated effect of the values of the standard deviations of the peaks on their linear regression error within a match. The former are given by:

$$8.1 \quad \sigma = \frac{W}{\sqrt{24N}} \text{ for triangular peaks (see, e.g., Meredith [Me(1972)])}$$

W being the base width and N the total of all channel counts

W is typically 200 to 400 channels, depending on the operator's ability and machine performance, while N is largely dependent on beam intensity, (as traded against resolution): of order 10^5 is typical on a good accumulation. Thus $\sigma \approx 0.2$ channels is a typical uncertainty on centroid position. For 8 identical matches such as these, one would expect from the source of randomness indicated (*i.e.*, statistics of a steady beam) a magnitude of external uncertainty value similar to the historical norm (hence in formal terms, the χ^2 measure should approximately equal the number of degrees of freedom). Clearly a source of variability had appeared within the system.

analysis method	average of 8 NAF matches as one run (07JUL99.DAT)
centroid, simple avg.	124 014.00 \pm 7.97 μu (σ)
centroid, weighted avg	124 012.04 \pm 1.90 \pm 8.17 (as $\pm\sigma_{\text{int}} \pm\sigma_{\text{ext}}$)
χ^2 , simple avg.	124 001.67 \pm 6.70
χ^2 , weighted avg.	124 002.52 \pm 1.89 \pm 6.79

Table 8.2 A study on actual data to examine variability in the (^{199}Hg - $^{199}\text{(C}_2\text{Cl}_5)$)⁻ doublet values using the NAF match.

It was also clear to the operators that the resolution routinely achieved on Manitoba II had degraded with respect to some earlier benchmarks (see esp. *e.g.*, [Ko(1977)]). From this consideration, the overall effect is one of trying to make a precise measurement with a "blunter" instrument. More precisely, since a $1 \mu\text{u}$ resolution in a doublet spacing measurement corresponds to mathematically establishing peak positions to approximately 1:1000 of the peak width, certain effects start to become troublesome. Very small variations introduced at the analysis stage, for instance, such as peak-threshold settings, now have stronger effects on the match value scatter.

The other issue that has been raised is the dynamic stability of the ΔV supplies. When the switching ESA potentials are observed on an oscilloscope, one can observe an exponential settling after a transition with a characteristic time of about 0.3ms (refer to Figures 4.3 and 4.4). After 12 or more e-folding times, the new potential *should* be well within the tolerance for the desired value, the assumption being that this asymptotic value is stable and reproducible on a cycle-to-cycle basis. This is extremely difficult to verify, as even a very good quality oscilloscope has an effective resolution of 1% of full scale. A worthwhile future test may be possible with the construction of a specialized voltmeter that could digitize to a 1-in- 10^6 or even only a 1-in- 10^5 resolution in about 3ms.

As a matter of record, the sources of variability mentioned in Section I and in the introduction to §VII, were each addressed in turn. One other suggestion is that the increased variability is perhaps related to some recent beam-tube modifications that had been attempted in order to make the instrument more suitable for special low-A studies (as has been raised as a possibility by Sharma [Sh(1997)]). The idea is that the beam tube portion that sits in the magnetic analyser pole gaps is somehow off of the optimal B-field region as far as uniformity. Unfortunately, as of the completion of this work, no conclusive explanation is yet at hand.

3. Local Least-Squares Adjustment of the Results

Local least-squares adjustments on the mass table were performed in order to obtain a measure of the goodness-of-fit of the data obtained in this work within the network of nearby, higher-reliability nuclide mass/energy difference values.

Study A (alpha) comprises the loop data of Table 8.1 (and Figure 8.1) as well as a subsidiary connection through ^{185}Re . An unpublished ^{201}Hg - ^{185}Re - ^{16}O measurement [Ba(1999)] was available that allowed the construction of the subsidiary loop.

The results are:

link	doublet input value, μu	output network A adjustment (ϵ)	source
A. $^{199}\text{Hg}^- - ^{199}(\text{C}_2\text{Cl}_5)^-$	124 017.19 ± 1.48	124 017.11 (-0.084)	this work
B. $^{199}\text{Hg}^- - ^{199}(\text{WO})^-$	23 145.55 ± 3.65	23 146.26 (+0.706)	this work
C. $^{199}(\text{WO})^- - ^{199}(\text{C}_2\text{Cl}_5)^-$	100 870.48 ± 3.09	100 870.85 (+0.370)	this work
D. $(^{201}\text{Hg } ^{35}\text{Cl}_2)^- -$ $(^{199}\text{Hg } ^{37}\text{Cl } ^{35}\text{Cl})^-$	4 971.80 ± 1.0	4 971.81 (+0.014)	this work
E. $^{201}\text{Hg}^- - ^{185}\text{Re} - ^{16}\text{O}^+$	22 439.80 ± 5.4	22 439.39 (-0.415)	unpublished result from this lab. [Ba(1999)]
F. $^{185}\text{Re} - ^{35}\text{Cl}^- - ^{183}\text{W} - ^{37}\text{Cl}^-$	5 678.70 ± 1.0	5 678.69 (-0.014)	sum of tungsten linkages $^{183}\text{W} - ^{184}\text{W} -$ $^{185}\text{W} - ^{185}\text{Re}$ from input data of [Au(1993)]; used in part 2 of Table 8.3 below.

Table 8.3 Results of Study A (Figure 8.2). The loop residual on [A.-B.-C.] = $0.26 \pm 4.78 \mu\text{u}$
overall $\chi^2 = 0.061$

4. Implications for the Mass Table

Some evidence has already been presented in this work supporting the accuracy of certain previous results on the mercury system, *i.e.*, those of Kozier *et al.*. Wapstra and Audi have indicated a number of times ([Au(1993)], [Wa(1985)]) that the “absolute” Hg mass values involved would, if retained with a high confidence factor in their mass adjustment, systematically push most of the nuclide masses between mercury and the actinides towards values significantly beyond the error envelope for the region. This envelope is the contiguous estimated error line bounding their least-squares adjustment values for nuclides in the valley of β -stability. They have indicated that many nuclides in this region would be up to $20 \mu\text{u}$ heavier than an adjustment based on the reaction data suggests. The information here suggests that the problem lies

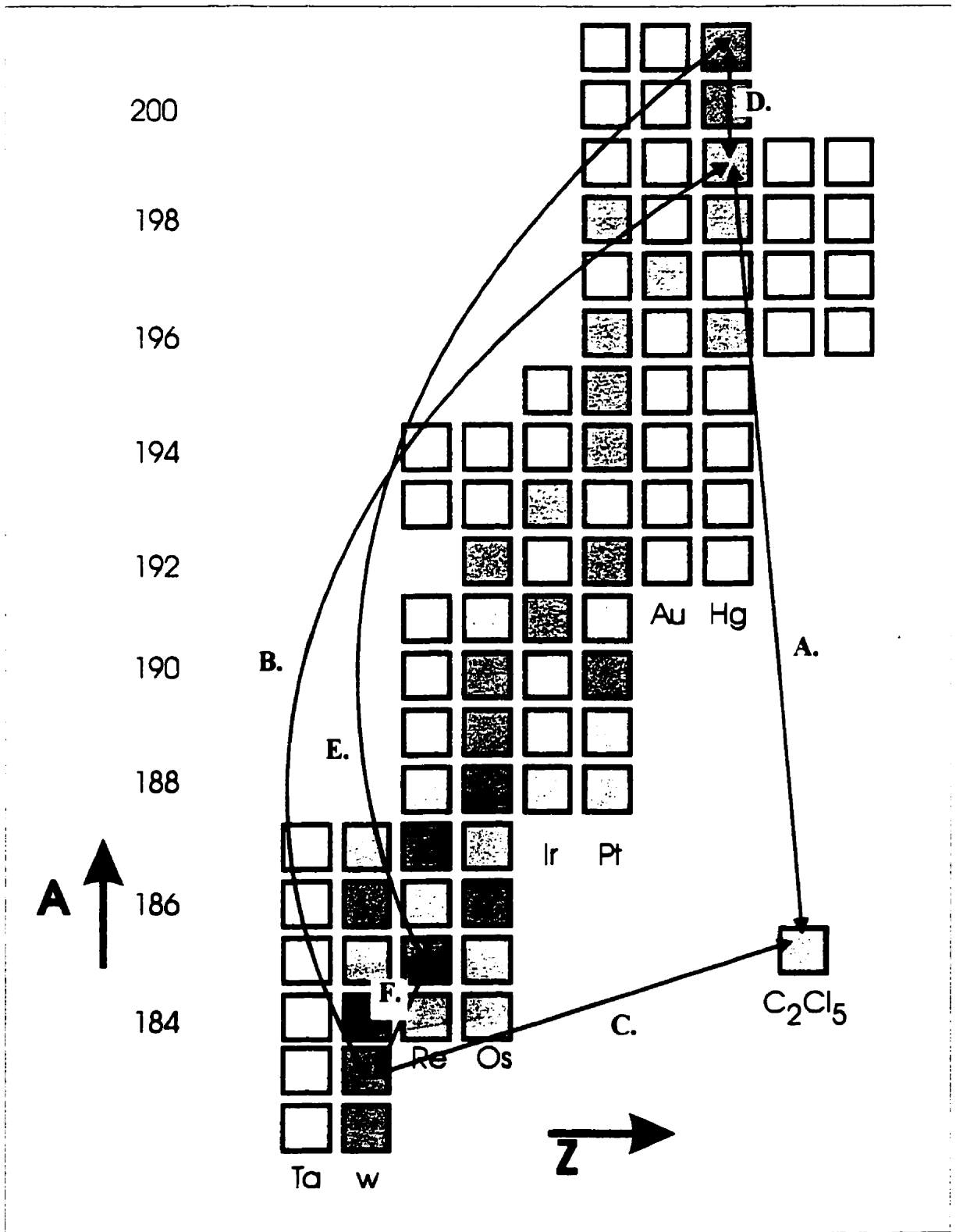


Figure 8.2 Least Squares Study "A"

elsewhere, *i.e.*, that there is no substantial error in the absolute masses of mercury as measured by Kozier. In that study, the entire set of stable Hg isotopes was examined by using chloride doublets where equal-A species could be found, such as $^{201}\text{Hg}^{12}\text{C}_2^{35}\text{Cl}_2$ - $^{199}\text{Hg}^{12}\text{C}_2^{37}\text{Cl}^{35}\text{Cl}$. A very tight set of mass spectrometric linkages was thereby established (and confirmed by (n, γ) linkages), thus a good re-measurement of the absolute mass of one of the members reflects on the accuracy of all absolute values reported.

If one assumes that the direct mass spectrometric (m.s.) linkage from tungsten to mercury as determined in this work is indeed correct, then it raises the possibility that one or more short m.s. linkages or Q-values belonging to the network in-between have been mismeasured (although nuclides above and below this region can have an influence as well: indeed newer high-accuracy measurements on the actinides in the '70s produced the first significant shift in this section of the mass table [Wa(1985)]). In §II.2, the hypothesis was presented that one or both of the literature values (input to [Au(1993)]) for the (n, γ) connections for ^{182}Ir - ^{183}Ir and ^{183}Ir - ^{184}Ir have an error of order 10 μ u. In order to examine this possibility further, the $^{199}\text{Hg}^-$ - $^{199}(\text{WO})^-$ connection was calculated using mass-table input data along various paths (from [Au(1993)]). The choice of paths was naturally constrained by the availability of experimental values. However, two major groups of paths were found for this study: these are presented in some detail in the dual listings of Table 8.3, while Figure 8.3 presents the component connections on the mass table visually.

In the first group, a key mass spectrometric doublet for $^{185}\text{Re}^{35}\text{Cl}^-$ - $^{183}\text{W}^{37}\text{Cl}^-$ is used to make the jump in a favourable direction from ^{183}W to an A= 185 nuclide. As can be seen from Table 8.3, all of the resulting equivalent $^{199}\text{Hg}^-$ - $^{199}(\text{WO})^-$ values were relatively low with respect to the figure from this work. The chains $\Omega 1$ and $\Phi 1$ (of Block 1) both came out peculiarly low; the first avoiding the m.s. doublets in the Re and Os region and the second avoiding the Ir connections mentioned above. The difference of about 30 μ u between these values and that reported here is interesting in that it corresponds to the downward local mass table shift that [Wa(1985)] indicated would occur if Kozier's mercury absolute mass data were used in their adjustment.

When the calculations were repeated using only reaction data to make the ^{185}Re - ^{183}W jump (the Block 2 group), the results rose across the board by about 20 μ u. Notice that the reported errors, summed in quadrature, indicate an uncertainty considerably smaller than this. Interesting as well, the average of the Block 2 values is approximately equal to the result of the new measurement, *i.e.*, ~ 23145 μ u.

These results do not conclusively isolate the problem; however, certain links that would otherwise appear to be reliable (*e.g.*, the (n, γ) reactions mentioned) cannot be supported by other linkages in the local network. If the problem *is* entirely with an (n, γ) value, this would be a significant error in that such data are often reliably precise to better than 1keV. Wapstra *et al.* do point out however that gross errors resulting from misidentification of nuclear levels are not rare (see, *e.g.*, the case of Raemy and $^{191}\text{Ir}(n,\gamma)$ ^{192}Ir discussed in [Wa(1985)]). It should be noted as well that Audi *et al.* have performed numerical studies in which the (n, γ) linkage between the two platinum isotopes ^{194}Pt and ^{195}Pt was dropped. Their results show a substantial improvement in the behaviour of the actinide masses, as far as closing the discrepancy in question, when examined as α -decay chain members.

In concert with the new measurements from this work, there is ample motivation for a new examination of a number of Q-values and doublets for nuclides in the valley of β -stability belonging to the platinum metals group.

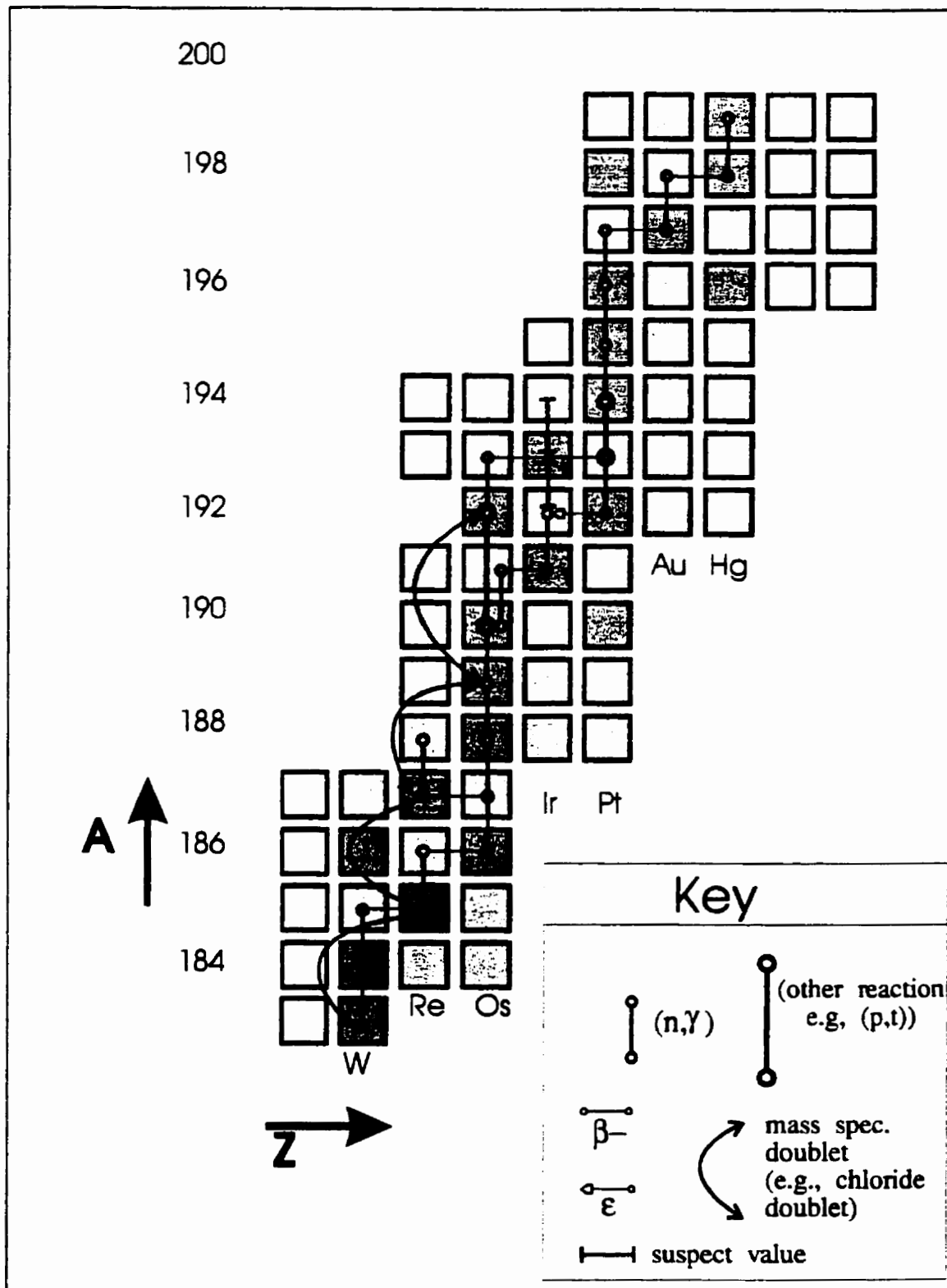


Figure 8.3 Some Linkages Leading from ^{183}Re to ^{199}Hg
(ref. [Au(1993)])

5. Conclusions

The data obtained in this study supports the 1977 results of Kozier (*et al.*) on the absolute masses of the stable mercury isotopes, in that, while uncertainties are somewhat larger than hoped for, the data has definitely converged on that result. This result is supported by the closure of the loop members measured and the independent loop via ^{185}Re . The simultaneous closure of the loops greatly increases confidence in the linkages in the face of the test that they are mass spectrometric doublets of

- 1) chemically dissimilar species, which carry some risk of idiosyncratic systematic measurement effects for the unsuspecting investigator
and
- 2) same-A species with widely disparate doublet spacings.

That the data were obtained using new critical electronic internals, as well as slightly modified machine optics (see comment above) and generally an instrument that was otherwise heavily used in the interim since 1977, suggests further that there was no overall systematic effect at play as far as contributions from the core experimental components.

This study adds further weight to the call for re-measurements of the linkages in the region of the platinum metals, if the backbone of the mass table is to serve as a fiducial reference at a level of precision now technologically achievable.

Appendix A: Functional Specification for AMDPRIME5

A.1 Terms

Focus: in a message-based, GUI system, the program will at any point be expecting input from one graphical interface window: the *focus* is said to be in this window

Background Markers: graphical user interface objects, with the appearance of square banners, used to mark and reference data in a visual presentation of a data quad. They can be manually or automatically positioned, depending on the operation in question. The semantics include: channel location of data largely composed of "uninteresting" events, in a statistical sense, and the number of events associated with that channel.

Peak Markers: graphical user interface objects, with the appearance of circular banners, used to mark and reference data in a visual presentation of a data quad. They can be manually or automatically positioned, depending on the operation in question. The semantics include: channel location of data largely composed of "interesting" events, in a statistical sense; the number of events associated with that channel.

Peak-of-interest: each quad contains precisely one member peak of a doublet that is to be parameterized; this is the peak-of-interest. The other member of the doublet may be visible, and is referred to as the partner or..

Partner peak: the member of a doublet, visible in the quad data, that is NOT being parameterized.

Peak-free zone: a contiguous portion of the data spectrum not containing any "substantial" peak components

Interpeak-zone: a contiguous portion of the data spectrum between a doublet, possibly containing a portion of either peak.

A.2 Symbols:

$x \equiv$ <graphical interface name> := default

The mathematical variable on the left is set to the value entered via the graphical user interface object on the right of \equiv , with the "safe" default after the :=

[activity] The user performs a set of graphically oriented functions interactively with the program; this is described in outline.

{ guideline for sensible program operation }

<fx> A subsidiary algorithm.

A.3 Graphical User Interface Control Panels

A.3.1 Startup Window

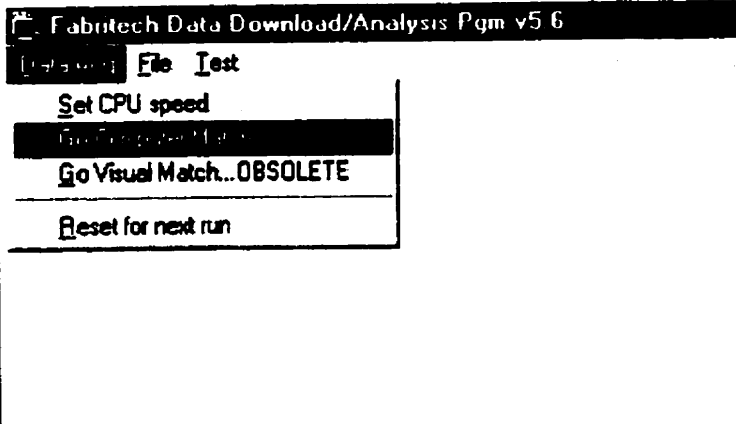
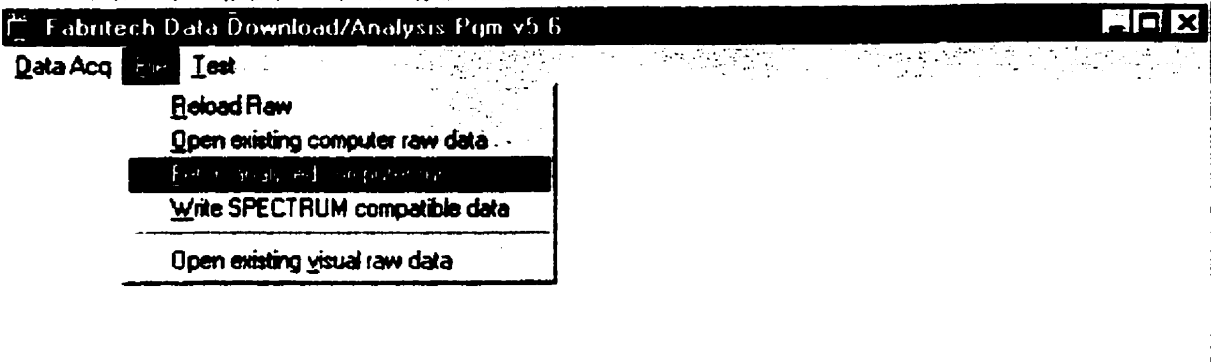


Figure A.4-1 User select major functions.

A.3.2 Download Window

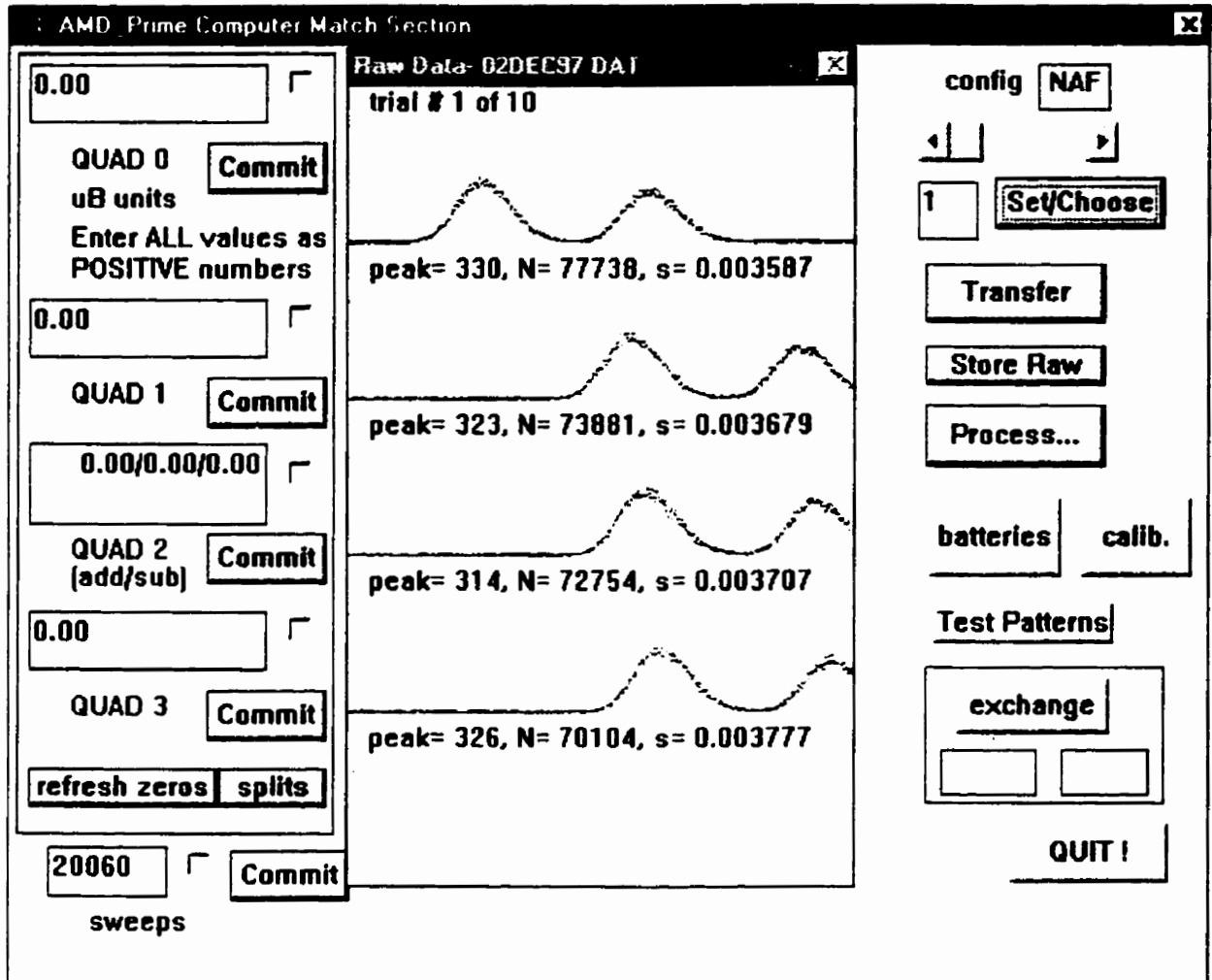


Figure A.4-2 Screen presented to user during a run (one match shown), and before start of analysis session.

A.3.3 Main Analysis Dialog

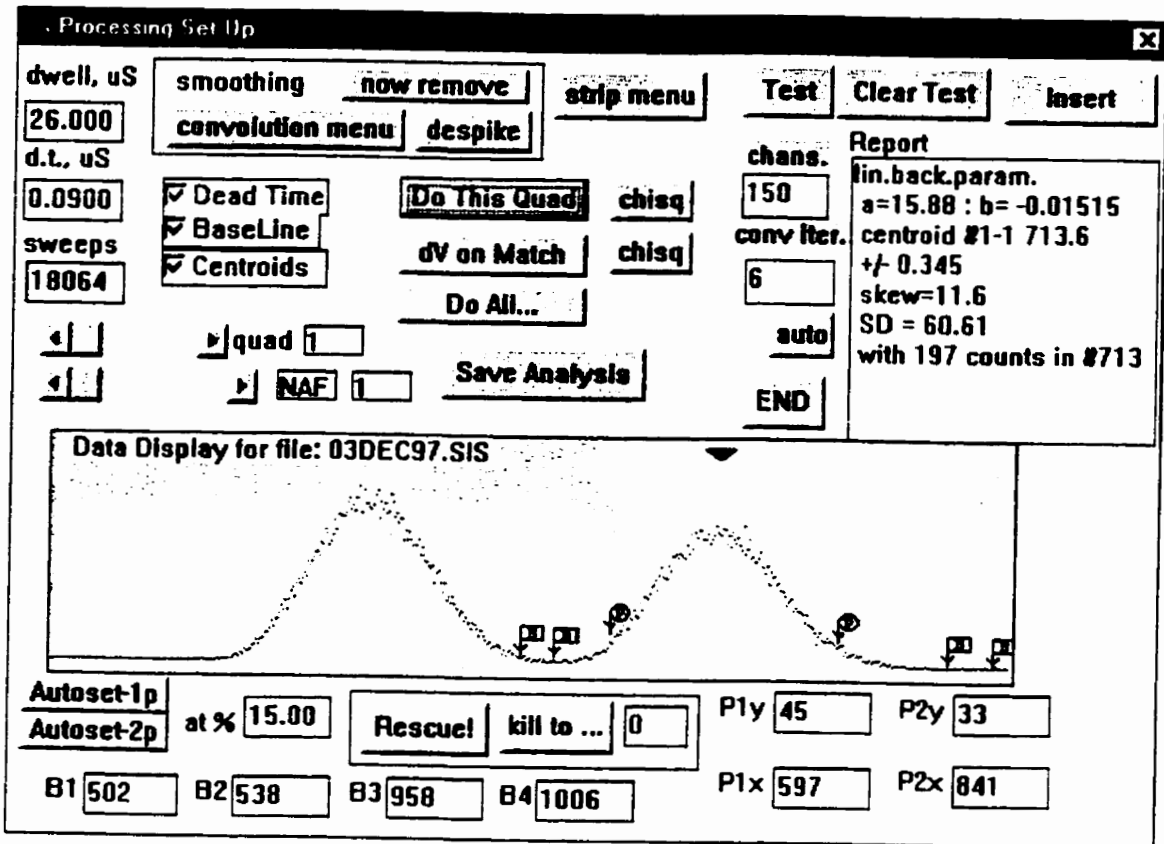


Figure A.4-3a Data analysis on a close doublet.

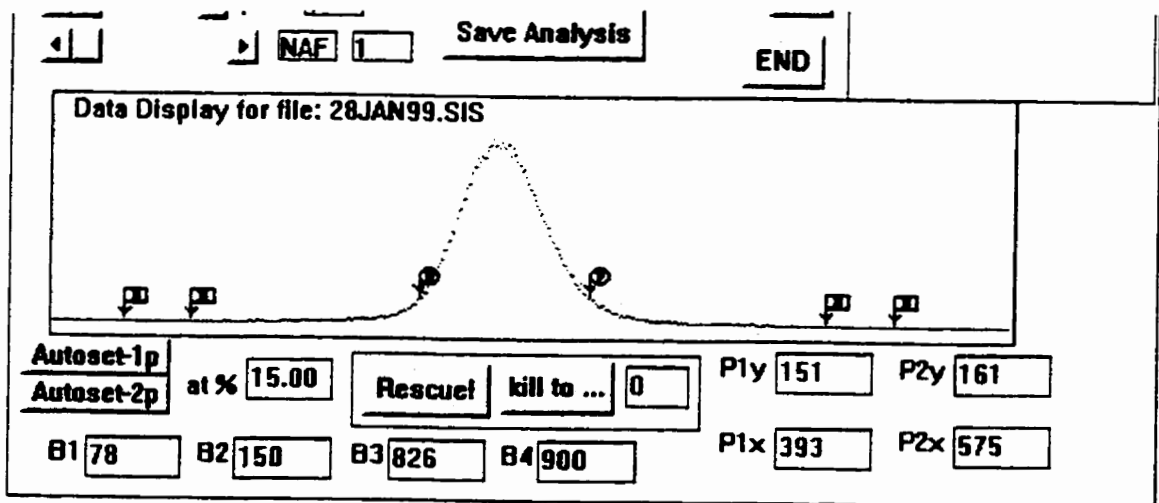


Figure A.4-3b Data analysis on a wide doublet (other peak not in this quad).

A.3.4 Convolution Processing Window

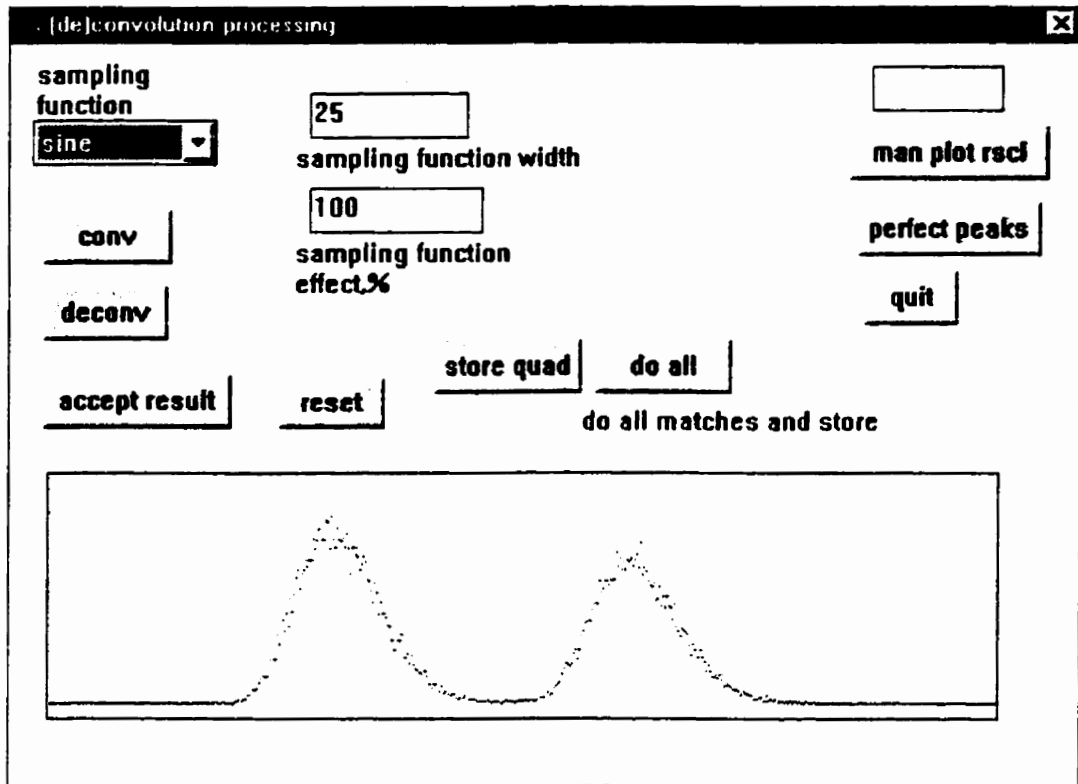


Figure A.4-4 Data before smoothing in the De/Convolution Dialog.

A.3.5 Auxiliary Windows: (pseudo)Battery Measurements

Battery #	Label	Value	Checked	Commit	Notes
1	BATTERY #1 or NAF uB units	0.000000	<input checked="" type="checkbox"/>	Commit	
2	BATTERY #2 or NSF	619393.000000	<input checked="" type="checkbox"/>	Commit	
3	BATTERY #3 or NSR	619072.000000	<input checked="" type="checkbox"/>	Commit	
4	BATTERY #4 or NAR	618774.000000	<input checked="" type="checkbox"/>	Commit	
5	BATTERY #5 or BAR	619120.000000	<input checked="" type="checkbox"/>	Commit	
6	BATTERY #6 or BSR	618551.000000	<input checked="" type="checkbox"/>	Commit	
7	BATTERY #7 or BSF	618966.000000	<input checked="" type="checkbox"/>	Commit	multi use as separate batteries
8	BATTERY #8 or BAF	618990.000000	<input checked="" type="checkbox"/>	Commit	
9	BATTERY #9	618667.000000	<input checked="" type="checkbox"/>	Commit	uni use as parts of one
10	BATTERY #10	0.000000	<input checked="" type="checkbox"/>	Commit	

DONE

Figure A.4-5 "Excess" portion "b" of pseudo-battery voltages are entered in this dialog: full battery voltages are actually $B_i = 25,000,000 \text{ units} + b_i$.

A.3.6 Auxiliary Windows: Calibration Information

The screenshot shows a window titled "Calibration Data" with a close button (X) in the top right corner. The window contains several input fields and checkboxes, each with a "Commit" button next to it.

At the top, there are two rows of input fields:

- Row 1: "add" field with value "526.000000", a checked checkbox, and a "Commit" button. To the right, a field with value "198.843715" and a "Commit" button.
- Row 2: "sub" field with value "526.000000", a checked checkbox, and a "Commit" button. Below this, the text "Calibration avg. ppm under" is displayed. To the right, a field with value "reference mass, (u)" and a checked checkbox.

A horizontal line separates this section from the "Resistor Calibration section" below.

The "Resistor Calibration section" contains several input fields and checkboxes, each with a "Commit" button:

- Field with value $-7.000000e-07$, checked checkbox, and "Commit" button. Below it is the label "dial/temperature factor, uB".
- Field with value $-7.400000e-06$, checked checkbox, and "Commit" button. Below it is the label "factor C".
- Field with value 0.200000 , checked checkbox, and "Commit" button. Below it is the label "temperature systematic, uB".
- Field with value $-5.000000e-06$, checked checkbox, and "Commit" button. Below it is the label "factor C1".
- Field with value $-1.660000e-05$, checked checkbox, and "Commit" button. Below it is the label "factor C2".

At the bottom left of the section, there is a "DONE" button.

Figure A.4-6 Resistor chain thermal and matching factors are entered here, as are the ESA calibration factor and the reference peak mass (ionized).

A.3.7 Select Dialog for Match Average

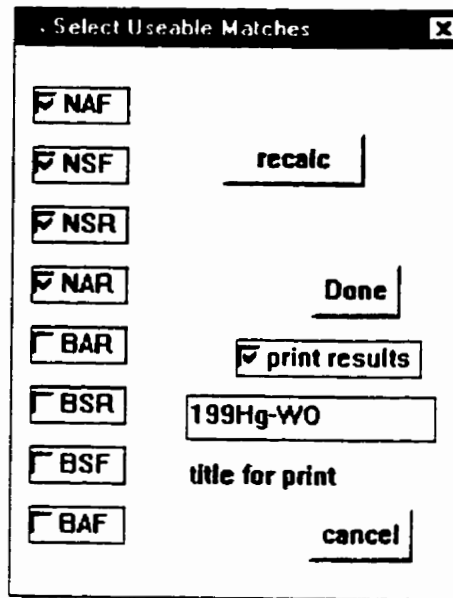


Figure A.4-7 User selects which matches to re-analyze, average or print together.

A.4 Processes:

A.4.1 Reading in an UnAnalysed Computer Match File

Actions:

The user selects file from the main menu.

The user then selects open existing raw computer data.

A standard file selection dialog is presented.

All files with extension *.dat are presented by default: the user may, however, select any file.

Actions:

The user selects a file.

The chosen file is "opened".

The following contiguous pieces of data are read until complete or a file-read error is detected.

Appropriate error messages are posted with the occurrence of any read problem.

DATA FORMAT: COMPUTER RUN RAW DATA (uB \equiv micro-"Bishop", internal unit)

Fabritek data	short	1024 x 4 x 10	x(2 byte)
quads voltages (uB)	double	10 x 4	x(8 bytes)
aux. quads voltageB (uB)	double	10	x(8 bytes)
sweep counts	int	10	x(2 bytes)
battery volts (uB)	double	10	
calib'n voltages(uB)	double	8	x(8 bytes)
			(obsolete! : now used for aux. quads voltageC)
calibration masses(u)	double	2	x(8 bytes) (obsolete!)
reference mass(u)	double	1	
analysis flag	char	1	

FILE SIZE raw =

82,509 bytes

If an analysed data marker is read as "true", the user is warned that analysis data were detected and are being read as well; see below for the analysis data format.

A.4.2 Reading in an Analysed Computer-Match File

Assumptions:

The user selects file from the main menu.

The user then selects open existing raw computer data.

A standard file-selection dialog is presented.

All files with extension *.sis (for "simplified iterated sampling") are presented by default: the user may, however, select any file.

Assumptions:

The user selects a file (see a reference such as Petzold[JJ])

The chosen file is "opened".

The data set mentioned in the Section **Reading in an UnAnalyzed Computer Match File** is read until complete or file read error is detected. This will read in data totalling.

FILE SIZE raw = 82,509 bytes

The analysis flag is read: if TRUE, the system proceeds to read the further analysis data below; if FALSE, a "data missing" message is posted and further reading of the file aborted. Appropriate error messages are posted with the detection of any read problem.

with analysed data

all background marks	markers_tag	11 x 4	x(20 bytes)	
all peak marks	markers_tag	11 x 4		
centroids	double	10 x 4	x(8 bytes = double)	
ext E flag	char	1		(obsolete! : now used for background shape type
ext E add(dim'less)	double	1	x(8 bytes)	(obsolete!)
ext E sub	double	1		(obsolete!)
autolevel(%)	float	1	x(4 bytes)	
centroid analysis				
flags	char	10 x 4		
centroid errors	double	10 x 4	x(8 bytes)	
dial/temp factor	double	1	x(8 bytes)	
temp. systematic	double	1	x(8 bytes)	
factor C	double	1	x(8 bytes)	
factor C1	double	1	x(8 bytes)	
factor C2	double	1	x(8 bytes)	
ESA calibration -ADD	double	1	x(8 bytes)	
match flags	match_tag	8 x 1		
ESA calibration -SUB	double	1	x(8 bytes)	

2525 bytes

FILE SIZE full analysis = 85034 bytes

A.4.3 Manual Setup of Background Marker Locations for Centroid Calculation

Assumptions:

The focus is the main analysis dialog.

{The background markers should stradle the peak of interest at points corresponding to visual estimates of the locations calculated by the autoset algorithm below }

[The user "picks up" and places the round-flagged peak markers as desired]

A.4.4 Manual Setup of Peak-Marker Locations for Centroid Calculation

Assumptions:

The focus is the main analysis dialog.

{The peak markers should stradle the peak of interest at the threshold levels of choice, as visually estimated - NOT RECOMMENDED for precision work - use Autoset (see A.4.5)}

[The user "picks up" and places the round-flagged peak markers as desired]

A.4.5a Autoset of Background and Peak-Marker Locations for Centroid Calculation on a "Wide Doublet"

Action: Autoset-1p is pressed

Assumptions:

The focus is the main analysis dialog.

Only one peak is present.

{ Peak can be smoothed or unsmoothed, though smoothed data is recommended at this stage of processing }

A peak threshold has been entered as a percentage. {15% is typical}

The peak markers are set to the peak-free-zones stradling the peak of interest.

A Background mark (1) is set in the left-hand peak-free zone by visual inspection, at a point as free of counts as possible.

Another Background mark (2) is set in the immediate vicinity of this point, the idea being to average (1) and (2) as representative of the left-hand peak-free area.

Another Background mark (3) is set in the right-hand peak-free zone by visual inspection, at a point as free of counts as possible.

As in the case of (1) and (2), the last Background mark (4) is set in the immediate vicinity of point (3) in the right-hand peak-free zone.

An average of the first two markers mentioned, $(1) \oplus (2)$, is taken, with respect to both abscissa and ordinate.

An average of the last two markers, $(3) \oplus (4)$, is similarly taken.

A straight line is mathematically drawn through the two averages to serve as the only estimate to the background; see **Calculation of Background for Centroid Calculation**, "linear background" case. This estimate is plotted for confirmation.

A maximum on the peak, or "peak centre", is estimated by a search algorithm, <f1>

The peak markers are now set by a slope searching algorithm <f2>. This estimate is plotted for confirmation.

A flag is set to indicate "linear background" in use.

A.4.5b Autoset of Background and Peak-Marker Locations for Centroid Calculation on a "Close Doublet"

Action: Autoset-2p is pressed

Assumptions:

The focus is the main analysis dialog.

A double peak is present on the display (with reasonable separation).

A peak threshold has been entered as a percentage. {15% is typical}

The peak markers are set to the peak-free-zones straddling the peak of interest.

A Background mark (1) is set at the minima of the inter-peak zone by visual inspection.

Another Background mark (2) is set in the immediate vicinity of this point, towards the partner peak..

Another Background mark (3) is set at the extreme of the peak-free area such that it and the inter-peak mark bracket the peak of interest.

The last Background mark (4) is set in the immediate vicinity of this point.

Ref Fig, A.4-8

An average of the first two markers mentioned, (1) \oplus (2), is taken, with respect to both abscissa and ordinate.

An average of the last two markers, (3) \oplus (4), is similarly taken.

A straight line is mathematically drawn through the two averages to serve as the first estimate to the background.

A maximum on the peak, or "peak centre", is estimated by a search algorithm, <f1>.

At the base of the partner-peak on the side nearest the peak-of-interest, at a point estimated to be 2% of the peak height with respect to the nearby inter-peak zone is then estimated using this baseline. The marker (2) is hence "moved" there.

The last Background mark is set in the peak-free zone at a point roughly symmetrically opposed, with respect to the peak-of-interest centre, to the "2% marker" mentioned above. The exact empirical rule is:

$$\text{last marker abscissa} = \text{peak centre} \pm (|[\text{distance from marker (1) to (2)}] \times 2 + |\text{distance from peak centre to marker(1)}|)$$

the \pm indicating that the appropriate direction be chosen based on the side of the partner peak with respect to the peak of interest. The above calculation may produce a value below zero or the maximum channel number, thus the following check is performed

if "last" marker belongs on the left of all other markers
 last marker abscissa = max(0 + noise margin, last marker abscissa)
 else
 last marker abscissa = min (maximum channel number - noise margin, last marker abscissa)

The marker (4) is hence moved there.

An refined estimate to the background is now calculated by least-squares estimate to a parabola formed by these markers. as detailed below in **Calculation of Background for Centroid Calculation, "parabolic background" case.**

This estimate is plotted for confirmation.

The peak markers are now set by a slope searching algorithm <f2>.

This estimate is plotted for confirmation.
 A flag is set to indicate a "parabolic background" in use.

A.4.6 Calculation of Background for Centroid Calculation

The following is performed under a request for a quad centroid: Do This Quad

Action: **Do This Quad** is pressed

Assumptions:

The focus is in the main analysis dialog.

The background markers have been set up by a preferred method.

{ for close doublets, where a parabolic fit is preferred, markers should have the dispersement that will sensibly result in a mild concave curve below the peak of interest }

if background type is "linear background"

A simple linear fit to the background is estimated as:

$$Bk(x) = mx + b$$

using:

$$m = \frac{y_b - y_a}{x_b - x_a}$$

$$b = \frac{x_a y_b - x_b y_a}{x_a - x_b}$$

$$y_b = \frac{y_4 + y_3}{2} ; y_a = \frac{y_1 + y_2}{2}$$

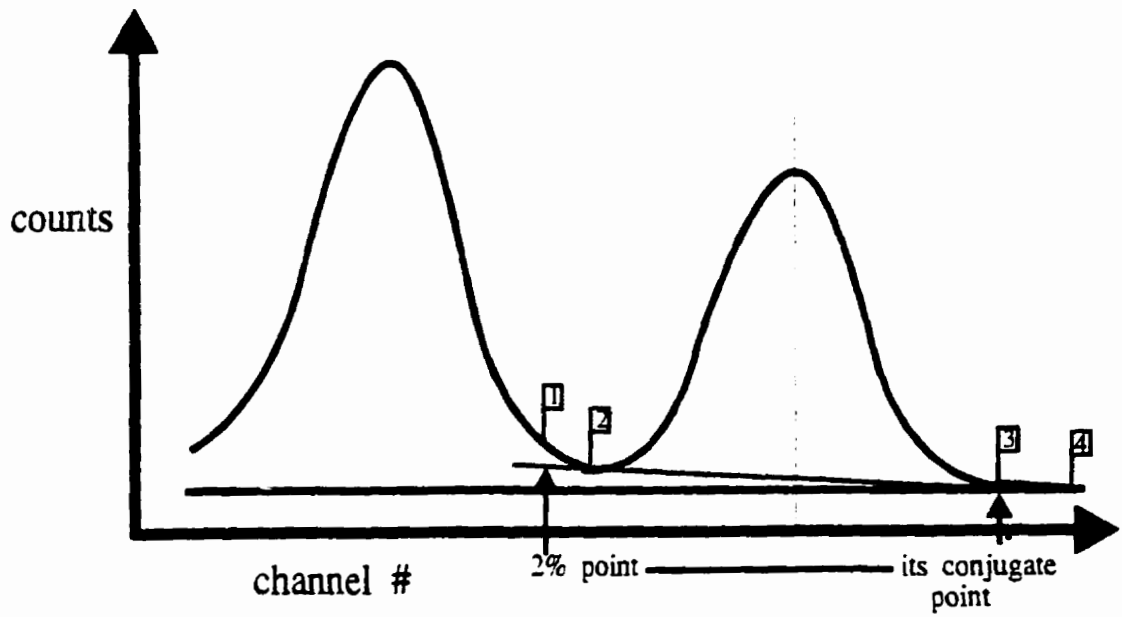


Fig. A.4-8 Background marker setup for peak matching on narrow doublets.
 (Identical to Fig. 7.7; reproduced here for convenience)

$$x_b = \frac{x_4 + x_3}{2} ; x_a = \frac{x_2 + x_1}{2}$$

y_i being the background marker ordinate, and x_i the associated abscissa

else (a "parabolic background" is assumed)

The ordinates, y_i , and abscissae, x_i , of the four background marks are used to estimate a best parabolic fit, $Bk(x)$, to the discrete function $y_i(x_i)$:

$$Bk(x) = a + bx + cy^2$$

using:

$$a = \frac{1}{\Delta} \bullet \begin{vmatrix} \sum y_i & \sum x_i & \sum x_i^2 \\ \sum x_i y_i & \sum x_i^2 & \sum x_i^3 \\ \sum x_i^2 y_i & \sum x_i^3 & \sum x_i^4 \end{vmatrix}$$

$$b = \frac{1}{\Delta} \bullet \begin{vmatrix} N & \sum y_i & \sum x_i^2 \\ \sum x_i & \sum x_i y_i & \sum x_i^3 \\ \sum x_i^2 & \sum x_i^2 y_i & \sum x_i^4 \end{vmatrix}$$

$$c = \frac{1}{\Delta} \bullet \begin{vmatrix} N & \sum x_i & \sum y_i \\ \sum x_i & \sum x_i^2 & \sum x_i y_i \\ \sum x_i^2 & \sum x_i^3 & \sum x_i^2 y_i \end{vmatrix}$$

where

$$\Delta = \begin{vmatrix} N & \sum x_i & \sum x_i^2 \\ \sum x_i & \sum x_i^2 & \sum x_i^3 \\ \sum x_i^2 & \sum x_i^3 & \sum x_i^4 \end{vmatrix}$$

here, $N=4$ and all sums run from 1 to 4.

Reference : Bevington [Be(1969)] eqn. (8-6)

Calculation of Each Peak Centroid

Assumptions:

Peak markers have been set to desired peak flanking locations, *start* and *stop*, by any method.

Calculate the value:

$$cent_{q,m} = \left. \sum_{i=start}^{stop} \frac{f_i x_i}{N_c} \right|_{q,m} \quad N_c = \sum_{i=start}^{stop} f_i$$

where *q* is the quad identity and *m* is the match identity, and X_i are the background-subtracted channel contents:

$$f_i = f_i^{raw} - Bk(x_i)$$

Calculate the statistical uncertainty on the centroid as:

$$\sigma_{q,m}^2 \cong \frac{1}{N_c^2} \sum_{i=start}^{stop} (x_i - cent_{q,m})^2 \cdot f_i$$

It is empirically known that convolution produces a rescaling of the spectra by about 1:17, therefore the uncertainty on the centroid must be increased by $\sqrt{17}$ when dealing with smoothed data.

A.4.7 Calculation of the Δm on the Match

The following is performed under a request for a single match value: dV on Match

Action: dV on Match is pressed

Assumptions:

The focus is in the main analysis dialog.

The centroids on the match have been calculated by a preferred method, OR have been read into the system from an analysed file.

{ missing centroid values will generate an error message to prevent run-time calculation traps }

Calculation of Thermal Corrections for Each Quad

Thermal potentials contained in the readings of ΔV are to be compensated as follows:

NAF

$$e_0 = \Delta V^+$$

$$e_1 = \delta V_1^+$$

$$e_2 = V_0^-$$

$$e_3 = \delta V_3 + V_0^+ + V_0^-$$

where δV_1 and δV_3 are the potentiometer readings on quad 1 and 3, respectively, (starting at 0), V_0^+ is the reading on nominal zero, using the "plus" setting of the potentiometer V_0^- is the reading on nominal zero, using the "minus" setting of the potentiometer, the sign read from the null meter indication, and NOT necessarily the actual polarity.

NSF

$$e_0 = -\Delta V + V_0^{+-} + V_0^{-}$$

$$e_1 = \delta V_1$$

$$e_2 = V_0^{--}$$

$$e_3 = \delta V_3 + V_0^{+-} + V_0^{-}$$

where ΔV is the reading taken from the potentiometer on the "minus" setting, thereby recorded as an positive number, and appropriately set to a negative value here (see also other notes above).

NSR

$$e_0 = -\Delta V + V_0^{+-} + V_0^{-}$$

$$e_1 = \delta V_1$$

$$e_2 = V_0^{--}$$

$$e_3 = \delta V_3 + V_0^{+-} + V_0^{-}$$

NAR

$$e_0 = \Delta V$$

$$e_1 = \delta V_1$$

$$e_2 = V_0^{--}$$

$$e_3 = \delta V_3 + V_0^{+-} + V_0^{-}$$

(see comments under NAF)

BAR

$$e_0 = \Delta V$$

$$e_1 = \delta V_1 + V_0^{+-} + V_0^{-}$$

$$e_2 = V_0^{--}$$

$$e_3 = \delta V_3$$

(see comments above)

BSR

$$e_0 = -\Delta V + V_0^{+-} + V_0^{-}$$

$$e_1 = \delta V_1 + V_0^{+-} + V_0^{-}$$

$$e_2 = V_0^-$$

$$e_3 = \delta V_3^-$$

(see comments above)

BSF

$$e_0 = -\Delta V + V_0^- + V_0^-$$

$$e_1 = \delta V_1^- + V_0^- + V_0^-$$

$$e_2 = V_0^-$$

$$e_3 = \delta V_3^-$$

(see comments above)

BAF

$$e_0 = \Delta V$$

$$e_1 = \delta V_1^- + V_0^- + V_0^-$$

$$e_2 = V_0^-$$

$$e_3 = \delta V_3^-$$

(see comments above)

Calculation of a Linear Fit to the Three Quad Centroids

Calculate the regression to the three calibration quadrants,
where

$$y_m = a_m + b_m x$$

using :

$$a_m = \frac{1}{\Delta} \begin{vmatrix} S_y & S_x \\ S_{xy} & S_{xx} \end{vmatrix} = \frac{S_y S_{xx} - S_x S_{xy}}{\Delta}$$

where

$$S_y = \sum_{q=1}^3 \frac{cent_q}{\sigma_q^2}$$

$$S_{xy} = \sum_{q=1}^3 \frac{e_q \cdot cent_q}{\sigma_q^2}$$

$$S_x = \sum_{q=1}^3 \frac{e_q}{\sigma_q^2}$$

$$S_{xx} = \sum_{q=1}^3 \frac{e_q^2}{\sigma_q^2}$$

$$\Delta = \begin{vmatrix} s & S_x \\ S_x & S_{xx} \end{vmatrix} = sS_{xx} - S_x^2$$

(extra subscripts, such as m , are left off when it is clear that we are dealing with a single match)

where

$$s = \sum_{q=1}^3 \frac{1}{\sigma_q^2}$$

and

$$b_m = \begin{vmatrix} s & S_y \\ S_x & S_{xy} \end{vmatrix} = sS_{xy} - S_x S_y$$

(reference : Bevington [Be(1969)], eqns. 6-12)

The error and covariance of the regression parameters are also required in order to estimate the error in the interpolation of the line; these are computed as

$$\sigma_a^2 = \frac{S_{xx}}{\Delta}$$

$$\sigma_b^2 = \frac{s}{\Delta}$$

$$\text{cov}(a_m, b_m) = \frac{-S_x}{s \cdot S_{xx} - S_x^2}$$

(reference: Press *et al.* [Pr(1988)], 14-2)

Two "goodness of fit" measures are provided to the user, a correlation coefficient,

$$r_m = \frac{NS_{xy} - S_x S_y}{\sqrt{NS_{xx} - S_x^2} \cdot \sqrt{NS_{yy} - S_y^2}}$$

and chi-squared value

$$\chi_m^2 = \sum_{q=1}^3 \frac{1}{\sigma_{q,m}^2} [y_{q,m} - \text{cent}_{q,m}]^2$$

Interpolation of the Matching ΔV , with Uncertainty Value

Using the calibration line generated as above, for any category of match configuration, the value of ΔV is interpolated as,

$$\Delta V_m = \frac{cent_{0,m} - a_m}{b_m} + e_{0,m}$$

The error on this is estimated as

$$\sigma_{\Delta V_m}^2 = \frac{1}{b_m^2} \cdot [\sigma_0^2 + \sigma_a^2 + \frac{\sigma_b^2}{b_m^2} (a_m - cent_m^0)^2 - \frac{2}{b_m} \cdot (a_m - cent_m^0) \cdot cov(a_m, b_m)]$$

Calculation of the Single Δm on the Matching ΔV and Its Correction

Assumptions:

A set of rational pseudo-battery potentials as well as calibration parameters exist, otherwise the procedure is here aborted, and an error message provided, in order to avoid numeric processing faults.

ESAcad ≡ <Calibration avg., ppm>:=230
M_{ref} ≡ <reference mass>
f_{dt} ≡ <dial/temperature factor, uB>:= -0.7x10⁻⁶
f_{temp} ≡ <temperature systematic, uB>:= 0.2
C ≡ <factor C> := -7.4x10⁻⁶
C1 ≡ <factor C1> := -5.0x10⁻⁶
C2 ≡ <factor C2> := -16.6x10⁻⁶
pseudo-batt_i ≡ <BATTERY #i> := 0

ΔM is then calculated using the corrections embodied in this pseudo-code:

A preliminary $\Delta M/M$ is calculated:

$$\frac{\Delta M_m}{M_{ref}} = \frac{\Delta V_m}{V}$$

where

$$V = (200,000,000 + \sum_{i=1}^{10} pseudo - batt_i) / C$$

{ pseudo-batteries 1 and 10 don't exist in the current setup, thus default zero values are used for these }

$$\text{if } \frac{\Delta M_m}{M_{ref}} < \frac{2}{10^4}$$

$$\Delta M_m = M_{ref} \cdot \frac{\frac{\Delta V_m + f_{temp}}{V}}{1 + \frac{ESAcad}{10^6}}$$

else if $\frac{\Delta M_m}{M_{ref}} < \frac{2}{200}$

$$\Delta M_m = M_{ref} \cdot \frac{\frac{\Delta V_m + f_{temp}}{V} \cdot [1 + f_{dt}]}{1 + \frac{ESAcad}{10^6}}$$

else if $\frac{\Delta M_m}{M_{ref}} < \frac{2}{100}$

$$\Delta M_m = M_{ref} \cdot \frac{[(\Delta V_m - 10^6) \cdot (1 + f_{dt}) + 10^6 \cdot (1 + C_1)]}{V \cdot (1 + \frac{ESAcad}{10^6})}$$

else

$$\Delta M_m = M_{ref} \cdot \frac{[(\Delta V_m - 2 \cdot 10^6) \cdot (1 + f_{dt}) + 10^6 \cdot (1 + C_1 + C_2)]}{V \cdot [1 + \frac{ESAcad}{10^6}]}$$

The error on ΔM is calculated in simplified fashion as:

$$\sigma_{\Delta M} = \sigma_{dV} \cdot \frac{M_{ref}}{V}$$

A.4.8 Calculation of ΔM for a Run

The following is performed under a request for a single match value: Do All...

Action: **Do All...** is pressed

Assumptions:

The focus is in the main analysis dialog.

A number of ΔM_m , i.e., doublet mass differences for match configuration m have been calculated

{ they cannot be read in from an analysed file, but must be generated in each case by a call to dV on Match, see A.4.7 }

A subset of these is chosen via the **Select Useable Matches** dialog for averaging.

{ the system shall attempt to detect unavailable ΔM_m values from the set chosen; missing values will generate an warning message and will be skipped over }

Action: Done is pressed

Calculate the run-averaged mass difference for a doublet using the weighted average of the matches:

$$\Delta M = \frac{1}{\sum_{i-\text{avail}} \frac{1}{\sigma_i^2}} \sum_{i-\text{avail}} \frac{\Delta m_i}{\sigma_i^2}$$

the notation "i-avail" to signify available matches, for the case where a match is not available on a run, but result based on a partial data set is chosen.

There are two error values calculated, an "internal" error and "external" on the run,

$$\sigma_{\text{int}} = \frac{1}{\sqrt{\sum_{i-\text{avail}} \sigma_i^2}}$$
$$\sigma_{\text{ext}} = \frac{\sqrt{\sum_{i-\text{avail}} \frac{(\Delta M - \Delta m_i)^2}{\sigma_i^2}}}{(N-1) \sum_{i-\text{avail}} \frac{1}{\sigma_i^2}}$$

Ref : (original) Birge [Be(1932)]; (recent) Kozier [Ko(1977)]

The above three values are printed in a message box.

Assumptions: The print check-box has been selected in the Select Useable Matches dialog.

The following data are printed on the line printer,

ΔM and the centroid channel for the relevant phase 0-peak , for each match, with statistical uncertainty, χ^2 and correlation coefficient on the match slope.

The reference mass.

The ESA calibration factor.

The thermal and "self-calibration" factors for the measurement potentiometer.

The weighted run average and errors as indicated above.

Auxiliary Algorithms

<f1> Searching maximum of a peak	Ap. A-24
<f2> Searching for threshold level on the rising slope of a peak	Ap. A-25
<f3> Searching for threshold level on the falling slope of a peak	Ap. A-26
<f4> FFT-based peak spectrum smoothing	Ap. A-27

Auxiliary Algorithms

Presented here are the auxiliary algorithms used in the data processing which the author felt were important enough to provide for reference purposes, as they reflect a choice of method and not simply implementation detail.

<f1> Searching maximum of a peak

Given

a storage array `store[i]` of N elements.
a variable `maximum`

Initialize a 5 point running average `run_av` using elements `store[0-4]`, excluding any element `store[i]` for which `store[i] ≥ store[i+1]` ("despiking").

Starting at $i=0$, to $i=N-i$,
check each `store[i]` so that

```
    if
      (store[i] > maximum )
    then if
      (store[i] < 6 x maximum ) OR
      (store[i] < maximum +10)
      : more despiking
    then
      maximum := store[i]
    else if
      (store[i] > run_av) AND
      (store[i] < 4 x run_av)
      : more anti-spiking
    then
      maximum := store[i]

  if the count i has exceeded the startup length 5
  then
    recalculate a new running average based on the last 5 store[i]
    quantities and set run_av to this value

  continue
```

<f2> Searching for threshold level on the rising slope of a peak

Given

a storage array `store[i]` of N elements, a specified `start_level`
a specified background `type` and `back` curve parameters object
a specified `scatter_window` to establish an abscissa acceptance window
a specified `height_window` to establish an abscissa acceptance window

the `glitch_level` is set to $1.7 \times \text{start_level}$

if `type` of background is *parabolic*

the `back` object is to be interpreted as a parabolic formula parameter set

Starting at $i=0$, to $i=N-i$,
check each `store[i]` so that

```
if
((store[i] - local background {back}(parabolic)) > start_level)
AND
((store[i] - local background {back}(parabolic)) < glitch_level)
```

then : begin an examination of a scatter window
: where every member of store from i to $i+j$ must exceed the window base

Starting at $j = i$, to $j = i + \text{scatter_window}$.

```
if
check each store[j] so that  $\forall j$ 
```

```
((store[i] - local background -{back}(parabolic)) >
(start_level - height_window))
```

```
then
return i as the start point
```

```
else continue
perform the above with {back}(linear)
```


<f3> Searching for threshold level on the falling slope of a peak

Given

a storage array `store[i]` of N elements, a specified `stop_level`
a specified background `type` and `back` curve parameters object
a specified `scatter_window` to establish an abscissa acceptance window
a specified `height_window` to establish an abscissa acceptance window

the `glitch_level` is set to $1.7 \times \text{stop_level}$

if `type` of background is *parabolic*

the `back` object is to be interpreted as a parabolic formula parameter set

Starting at $i=0$, to $i=N-i$,
check each `store[i]` so that

```
if
  ((store[i] - local background {back}(parabolic)) <= stop_level )
  AND
  ((store[i] - local background {back}(parabolic)) < glitch_level)
```

```
then : begin an examination of a scatter window
      : where every member of store from  $i$  to  $i+j$  must exceed the window base
```

Starting at $j = i$, to $j = i + \text{scatter_window}$.

```
if
  check each store[j] so that  $\forall j$ 
```

```
((store[i] - local background - {back}(parabolic)) >
 (stop_level - height_window))
```

```
then
  return  $i$  as the stop point
```

```
continue
else
  perform the above with {back}(linear)
```

<f4> FFT-based peak spectrum smoothing

This has been well described in Press *et al.* [Pr(1988)], who devote an entire section to smoothing by convolution, with FFT as an efficient implementation. The reader is directed there for an excellent introduction, pseudocode and C code listing, the latter having been “lifted” directly for use in AMDPRIME.

Appendix B: Some Data Analysis Studies

The Effect of Smoothing and Threshold Choice on Peak Motion and Analysis Results

Presented here are the some of the result on a study made to ascertain the effect of smoothing on peak positions. The term "peak position" is somewhat ambiguous in that it refers to a quantity indicating the position of peak in relation to other peaks, each ideally having the same parent distribution or "shape" between them due to the similarity in physical process involved in generating them, and derived according to an explicitly stated rule. The most common of these is the "centroid", calculated as given in Appendix A, via a formula like

$$B.1 \quad cent_{q,m} = \left. \sum_{i=start}^{stop} \frac{f_i x_i}{N_c} \right|_{q,m}, \quad N_c = \sum_{i=start}^{stop} f_i$$

$$B.2 \quad \sigma_{q,m}^2 \equiv \frac{1}{N_c^2} \sum_{i=start}^{stop} (x_i - cent_{q,m})^2 \cdot f_i$$

where stop and start are reasonable choices of thresholds denoting where the significant portion of a peak begins and ends (implicit in this discussion is that backgrounds have been "adequately" treated).

Since finding such peak limits is quite a difficult proposition with raw data, all work in this study begins with peak marker placement after smoothing using FFT convolution (as mentioned previously, with a some reasonably wide sine function). The interest is in whether centroids evaluated as stated "move" significantly when smoothing is "removed". The tables presented below for representative actual data show that while there is a mild effect, generally some fraction of a channels difference, when B.1 is applied to individual peaks, the cumulative effect on the match is usually to slightly raise the value of the mass difference on a close doublet, such as that of $HgCl_2^+$ at $A=271$, as shown in Figures B-1 and B-2.

A further interesting, though not surprising result, is that ΔM varies severely with threshold, though settling out at about 15%. This is a commonly used value (see, *e.g.*, [Ko(1977)]), and makes statistical sense in that at 15%, one obtains σ s that equal the theoretical result for a triangular peak accumulated under Poisson statistics, as mentioned in §VIII.2.

Table B.1

Detailed Evaluation for 09FEB98.SIS - NAF match,

usm = "unsmoothed",

sm = "smoothed", centroids in channel numbers; 1024 total channels per quad

typical peak width $\sigma = 65$ channels

threshold %	type	quad 0 centd.	quad 1 centd.	quad 2 centd.	quad 3 centd.	Δm
4	usm	571.4 ±.37	550.2	563.0	574.5	4980.20±5.1
	sm	571.2±.37	549.8	562.5	573.9	4984.47±5.1
5	usm	571.2±.37	550.1	563.1	574.5	4977.68±5.0
	sm	571.0±.37	549.7	562.6	573.9	4981.22±5.0
6	usm	571.1±.37	550.1	562.9	574.6	4976.19±4.9
	sm	570.7±.37	549.7	562.4	574.0	4977.61±5.0
7	usm	570.8±.36	550.1	562.7	574.4	4974.91±4.9
	sm	570.4±.36	549.7	562.2	573.9	4975.83±4.9
8	usm	570.4±.36	549.9	562.6	574.3	4971.78±4.8
	sm	570.1±.36	549.5	562.1	573.9	4973.28±4.9
10	usm	570.2±.32	549.4	562.3	573.8	4974.23±4.8
	sm	569.9±.32	549.1	561.9	573.3	4975.58±4.9
12	usm	570.1±.35	549.1	562.2	573.4	4977.00±4.8
	sm	569.7±.35	548.7	561.8	573.0	4976.80±4.8
15	usm	569.6±1.4	548.4	561.4	572.8	4978.51±4.8
	sm	569.4±1.4	548.1	561.1	572.4	4980.04±4.8

Table B.1 continued

threshold %	type	quad 0 centd.	quad 1 centd.	quad 2 centd.	quad 3 centd.	Δm
17	usm	569.3 \pm .37	548.8	561.4	572.8	4974.94 \pm 4.7
	sm	469.1 \pm .37	548.1	561.1	572.4	4976.39 \pm 4.7
19	usm	568.8 \pm .34	548.0	561.0	572.2	4975.26 \pm 4.6
	sm	568.6 \pm .34	547.7	560.7	571.8	4976.91 \pm 4.7

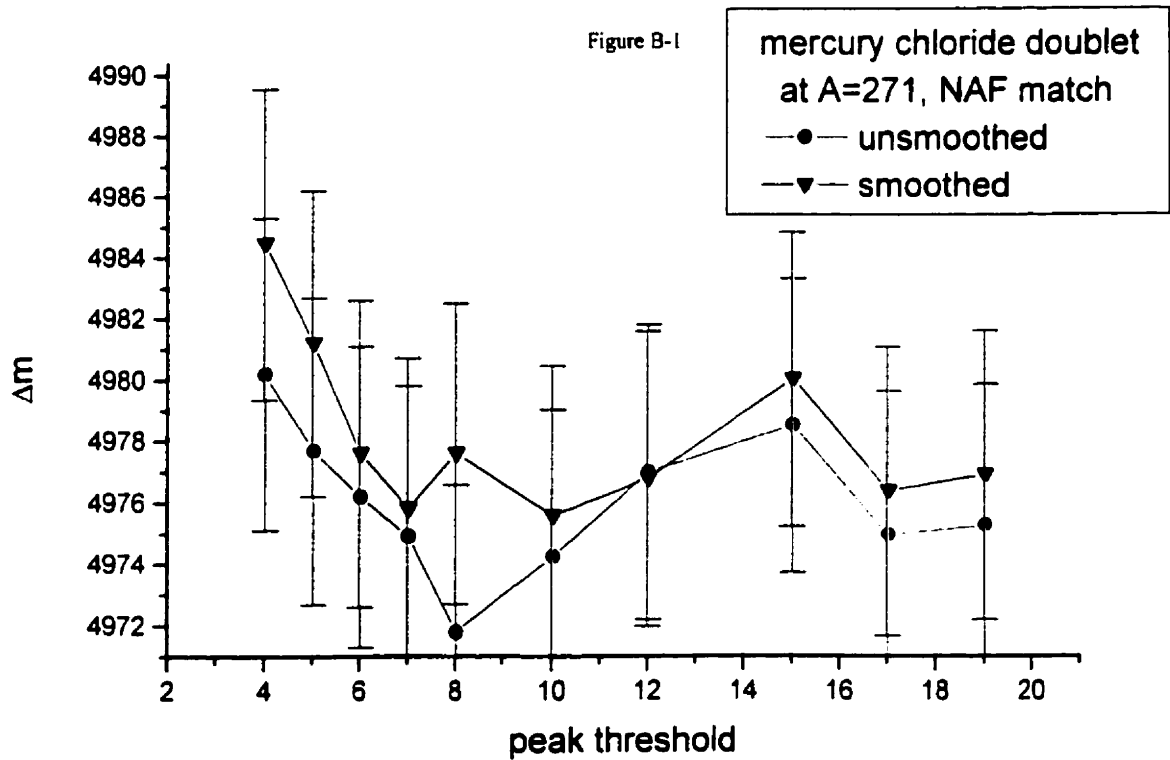


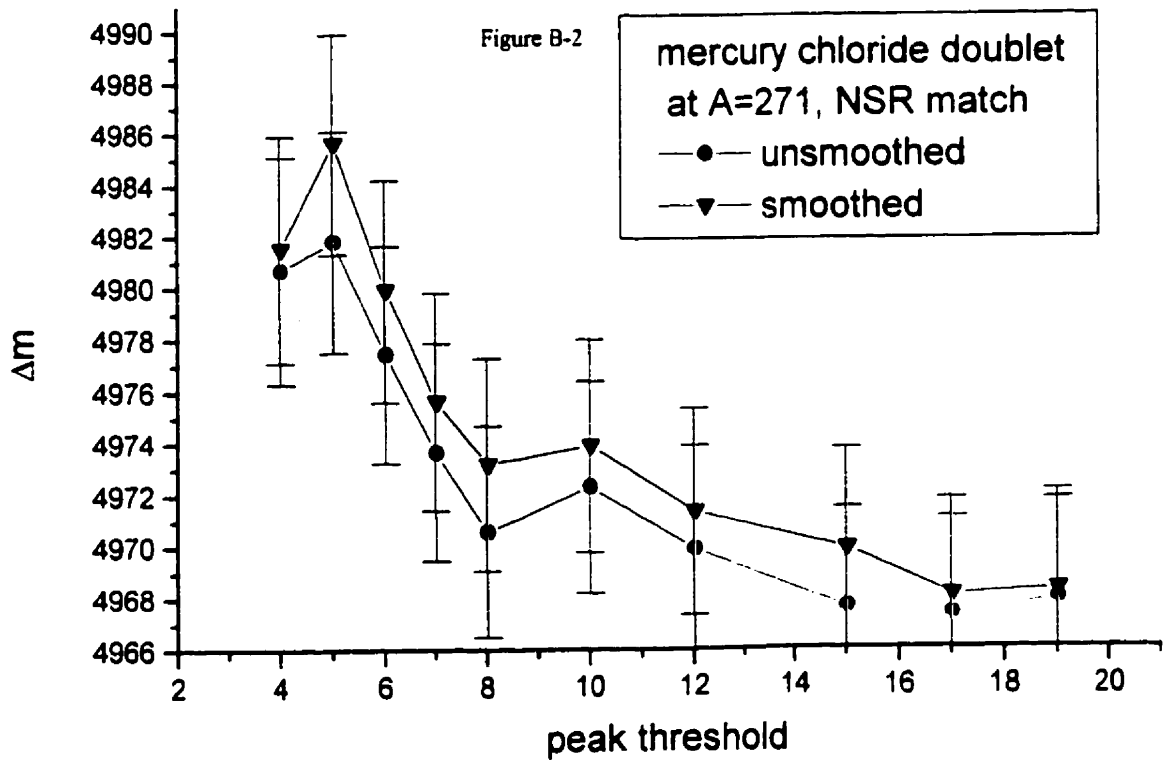
Table B.2

Detailed Evaluation for 10FEB98.SCS - NSR match,
 usm = "unsmoothed",
 sm = "smoothed"

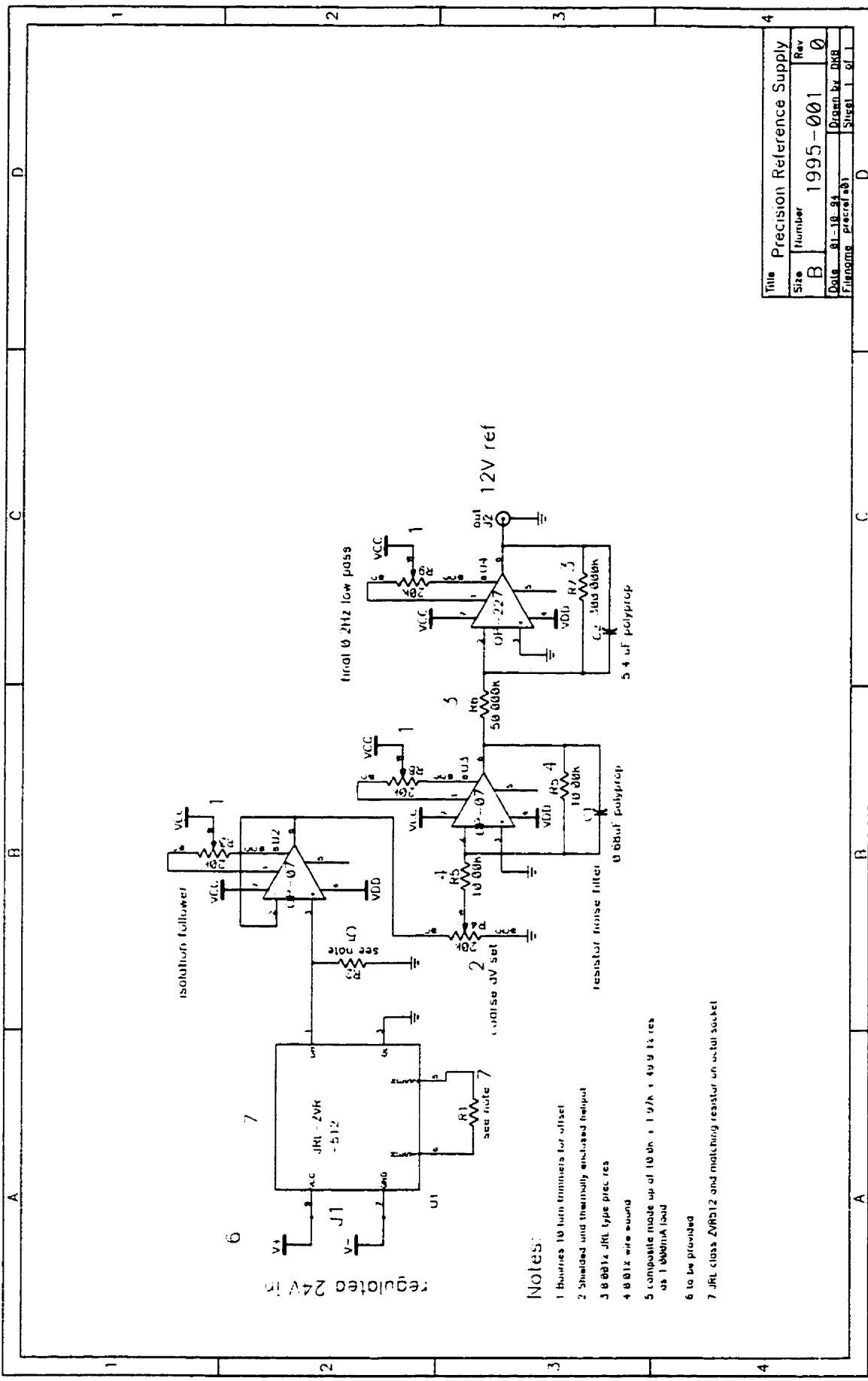
threshold %	type	quad 0 centd.	quad 1 centd.	quad 2 centd.	quad 3 centd.	Δm
4	usm	576.9 ± .31	583.1	568.7	558.1	4980.70 ± 4.4
	sm	576.5 ± .31	582.7	568.4	557.4	4981.54 ± 4.4
5	usm	577.3 ± .31	583.4	569.1	557.7	4981.81 ± 4.3
	sm	577.2 ± .31	583.0	568.7	557.5	4985.64 ± 4.3
6	usm	577.1 ± .31	583.6	569.3	557.8	4977.44 ± 4.2
	sm	576.9 ± .31	583.2	568.9	557.7	4979.93 ± 4.3
7	usm	576.9 ± .31	583.8	569.5	558.4	4973.66 ± 4.2
	sm	576.7 ± .31	583.4	569.1	557.8	4975.63 ± 4.3
8	usm	577.0 ± .30	584.1	570.2	558.3	4970.58 ± 4.1
	sm	576.8 ± .31	583.6	569.7	557.9	4973.19 ± 4.1
10	usm	577.4 ± .30	584.3	570.3	558.9	4972.29 ± 4.1
	sm	577.2 ± .30	584.0	570.0	558.5	4973.90 ± 4.1
12	usm	577.6 ± .30	584.8	570.5	559.3	4969.91 ± 4.0
	sm	577.3 ± .30	584.4	570.1	558.7	4971.37 ± 4.0
15	usm	577.8 ± .29	585.4	570.7	559.5	4967.62 ± 3.9
	sm	577.6 ± .29	585.0	570.4	559.0	4969.94 ± 3.9

Table B.2 continued

threshold %	type	quad 0 centd.	quad 1 centd.	quad 2 centd.	quad 3 centd.	Δm
17	usm	578.1 \pm .29	585.7	571.1	559.7	4967.32 \pm 3.8
	sm	577.9 \pm .29	585.4	570.8	559.5	4968.08 \pm 3.8
19	usm	578.4 \pm .28	585.7	571.7	560.2	4967.91 \pm 3.9
	sm	578.1 \pm .29	585.4	571.4	560.0	4968.27 \pm 3.9



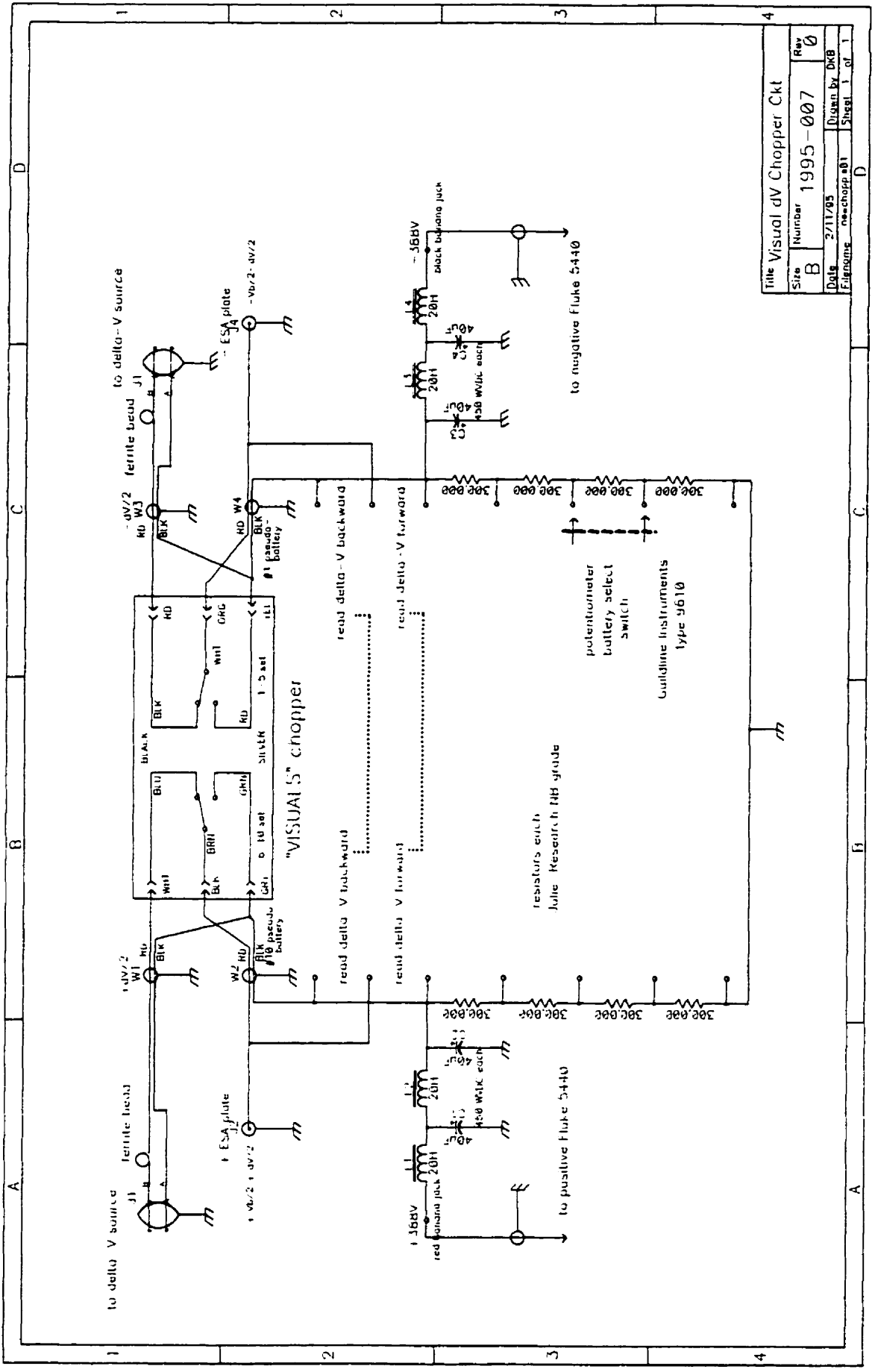
Appendix C: Circuit Schematics



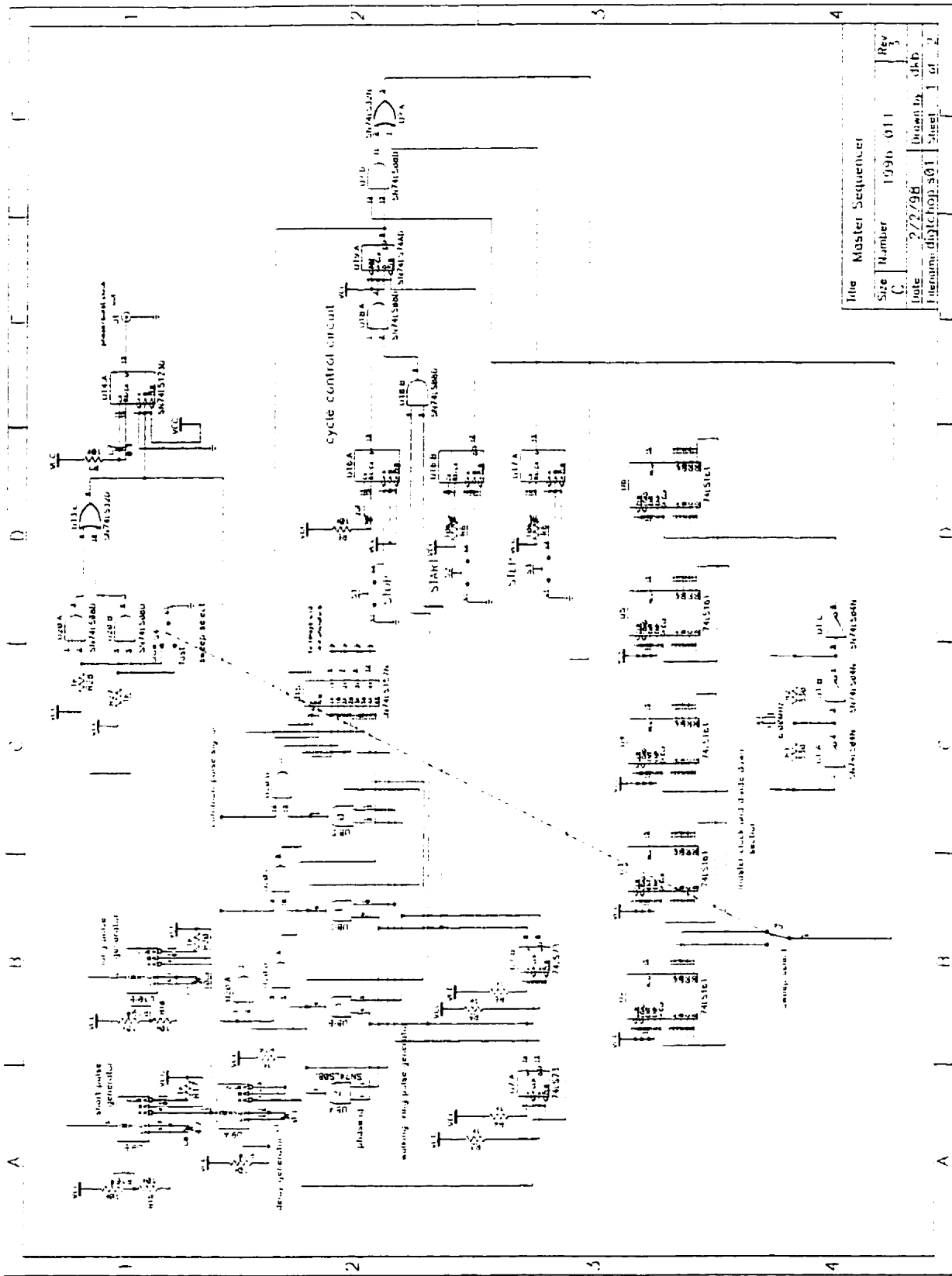
Notes:

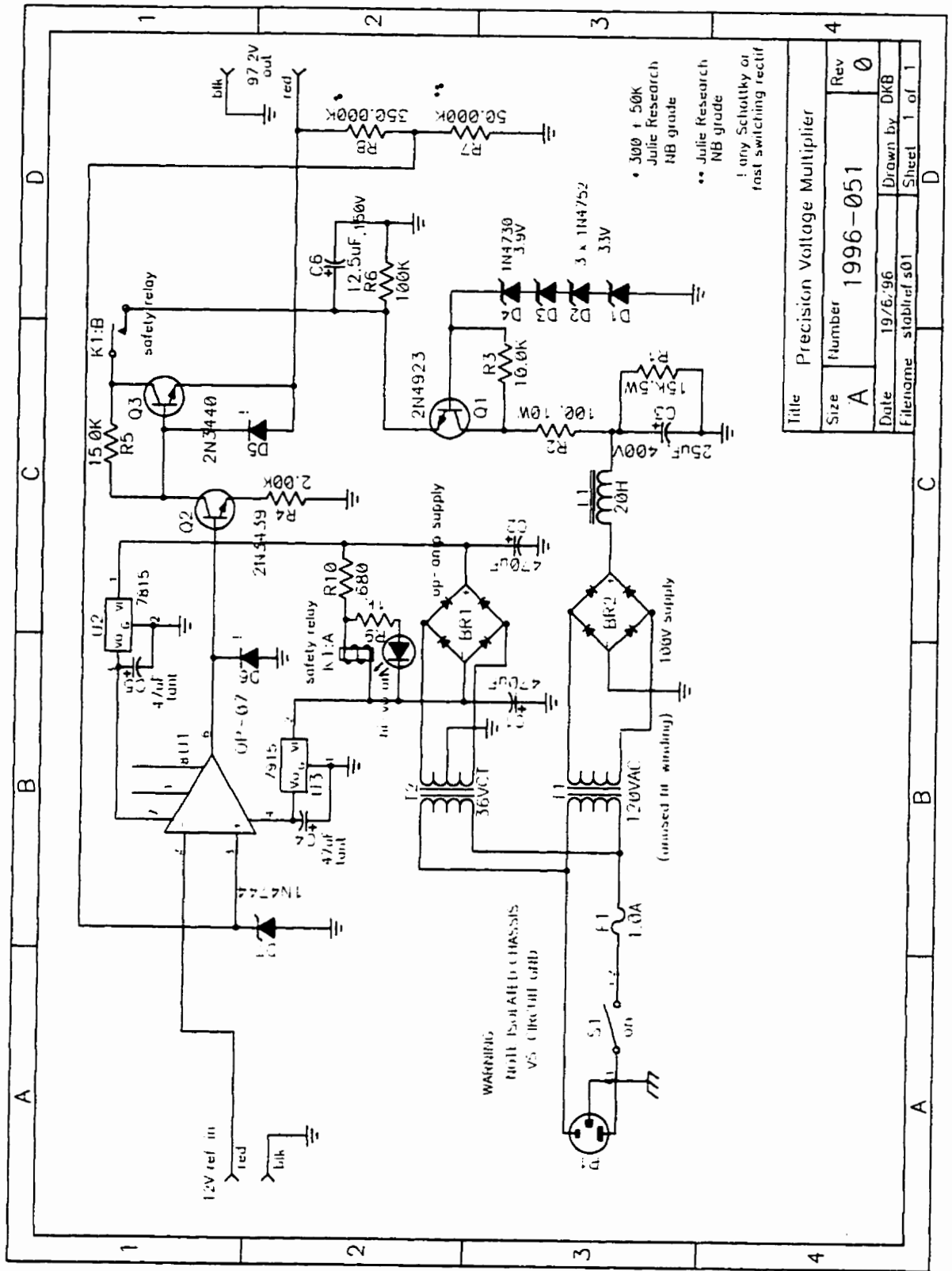
- 1 10 turn trimmer for offset
- 2 Shaded and thermally enclosed input
- 3 0.001% JRL type prec res
- 4 0.01% wire wound
- 5 composite made up of 10 0k + 1.97k + 49.9 1% res as 1 000mA load
- 6 to be provided
- 7 JRL class 2VR512 and matching resistor on octal socket

Title		Precision Reference Supply	
Size	Number	1995-001	Rev 0
Date	01-10-94	Drawn by	DKB
File name	prec.ref.sch	Sheet	1 of 1

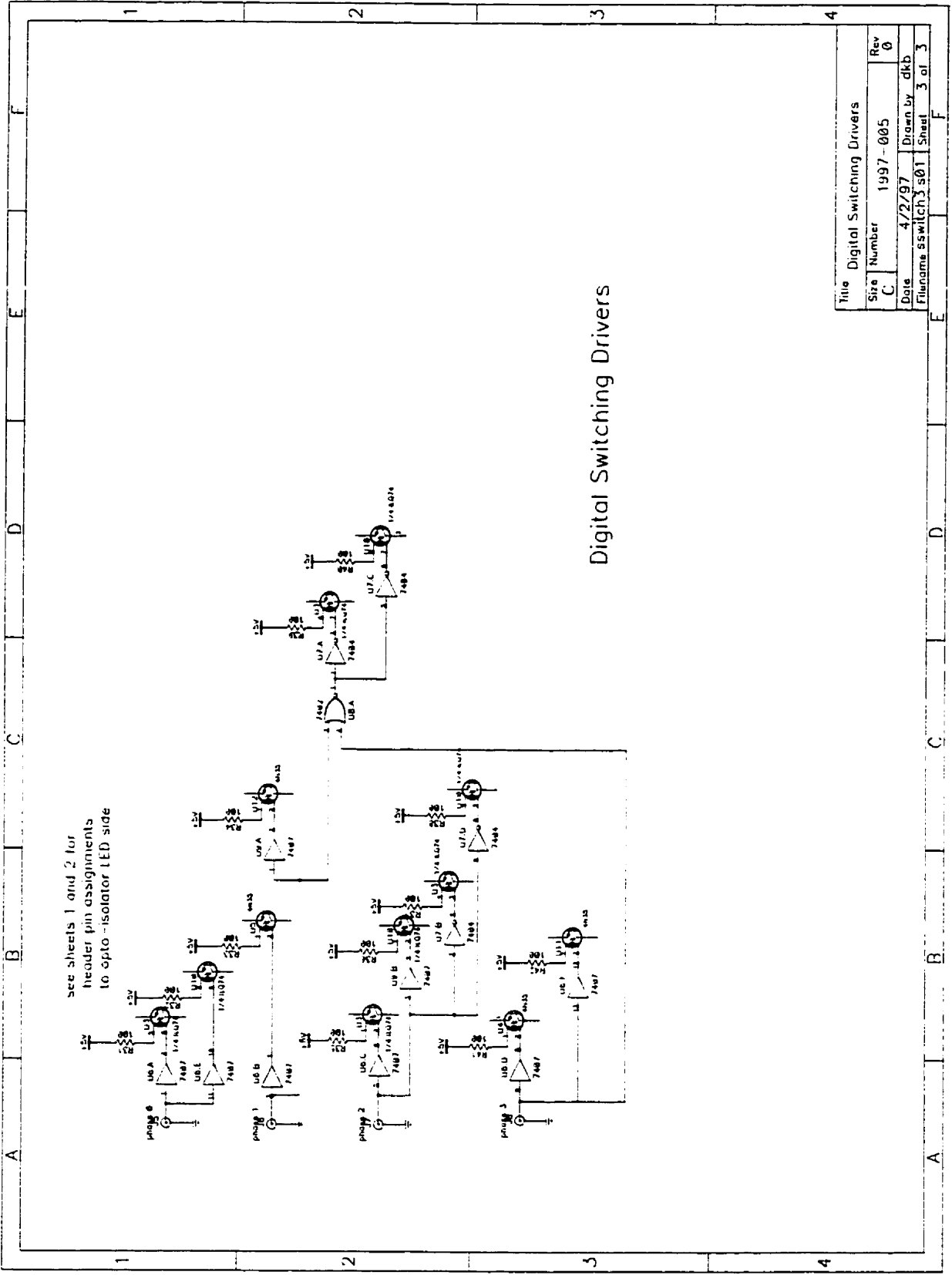


Title Visual dV Chopper Ckt			
Size	Number	Rev	
B	1995-007	0	
Date	2/11/95	Design by	DCB
Filename	res-chopp.a81	Sheet	1 of 1





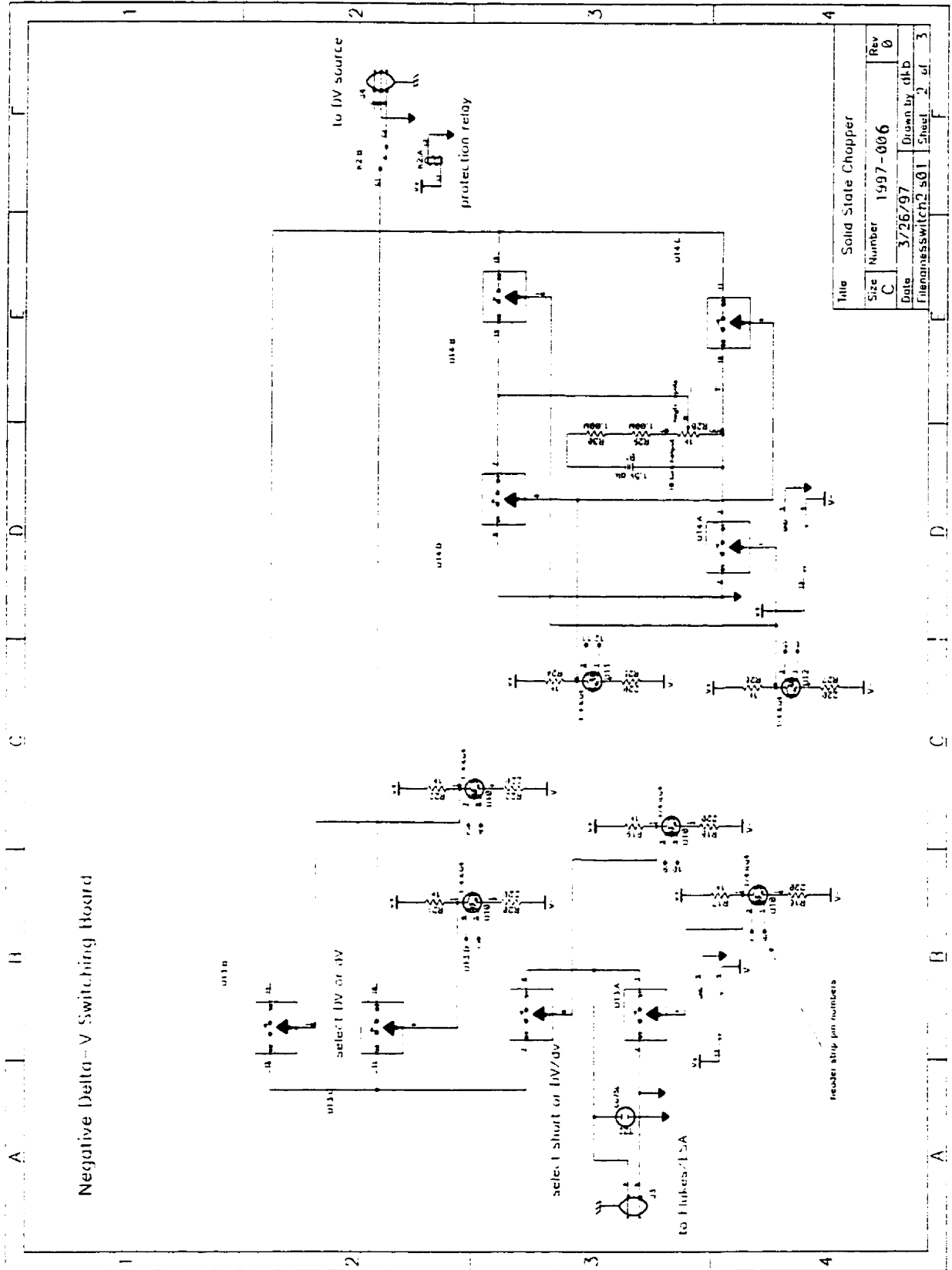
Title		Precision Voltage Multiplier	
Size	Number	Rev	
A	1996-051	0	
Date	19/6/96	Drawn by	DKB
Filename	stabref.s01	Sheet	1 of 1



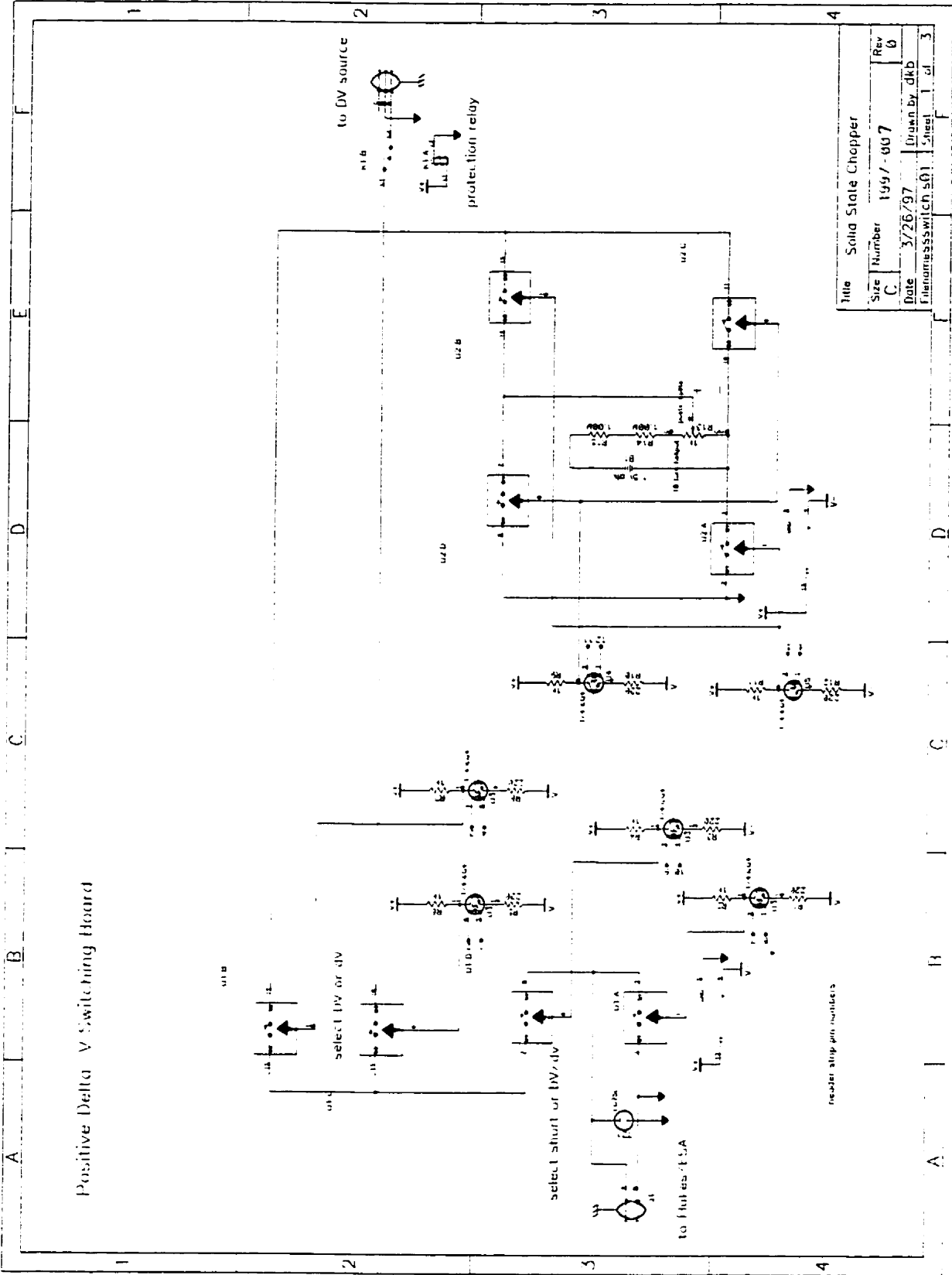
Digital Switching Drivers

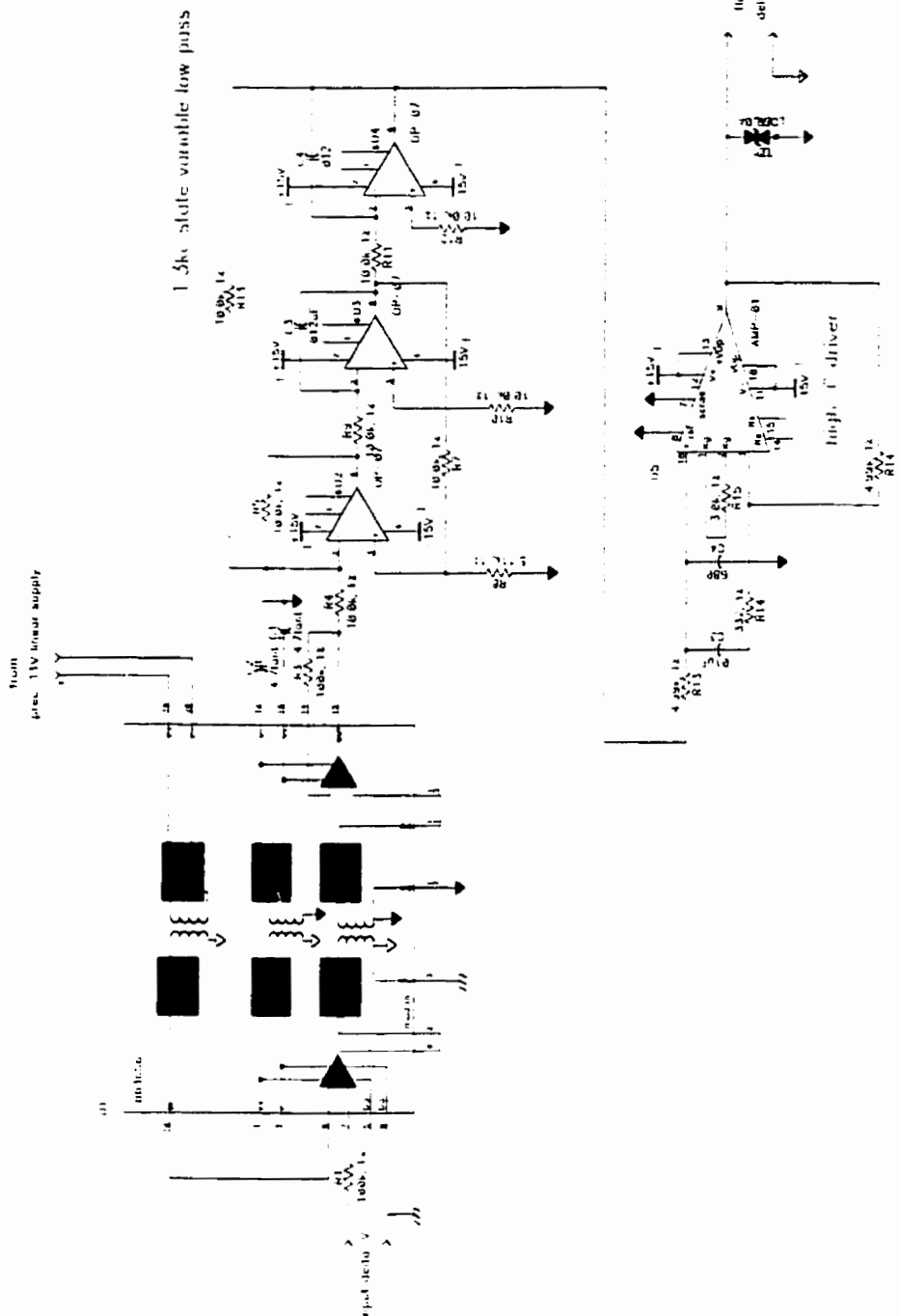
Title		Digital Switching Drivers	
Size	Number	1997-005	Rev
C			0
Date	4/2/97		Drawn by
Filename		sswitch3.s01	Sheet
		3 of	3

Negative Delta-V Switching Board



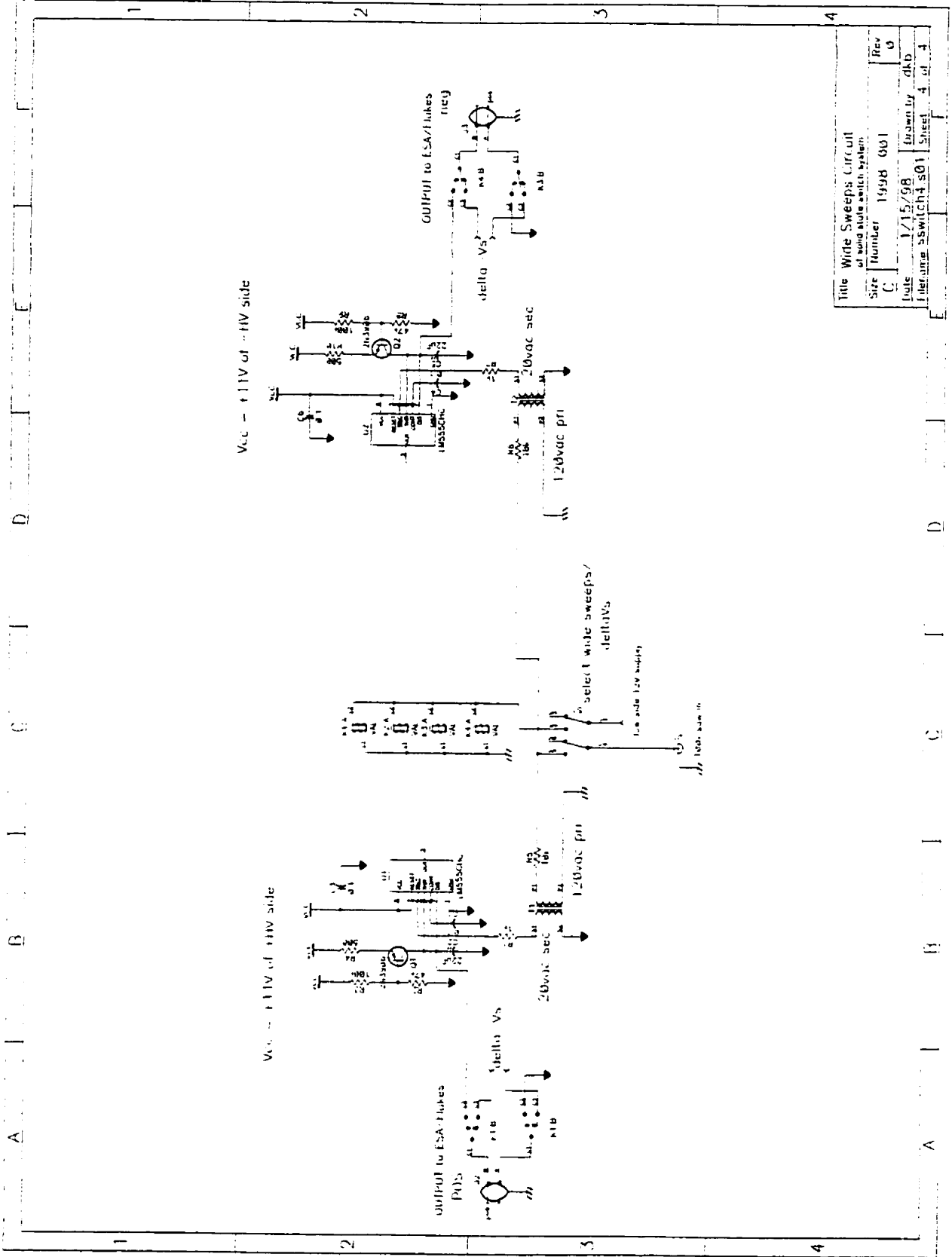
Info Solid State Chopper			
Size	Number	1997-006	Rev
C			0
Date	3/26/97	Drawn by	dkb
Filename	switch2.s01	Sheet	2 of 3



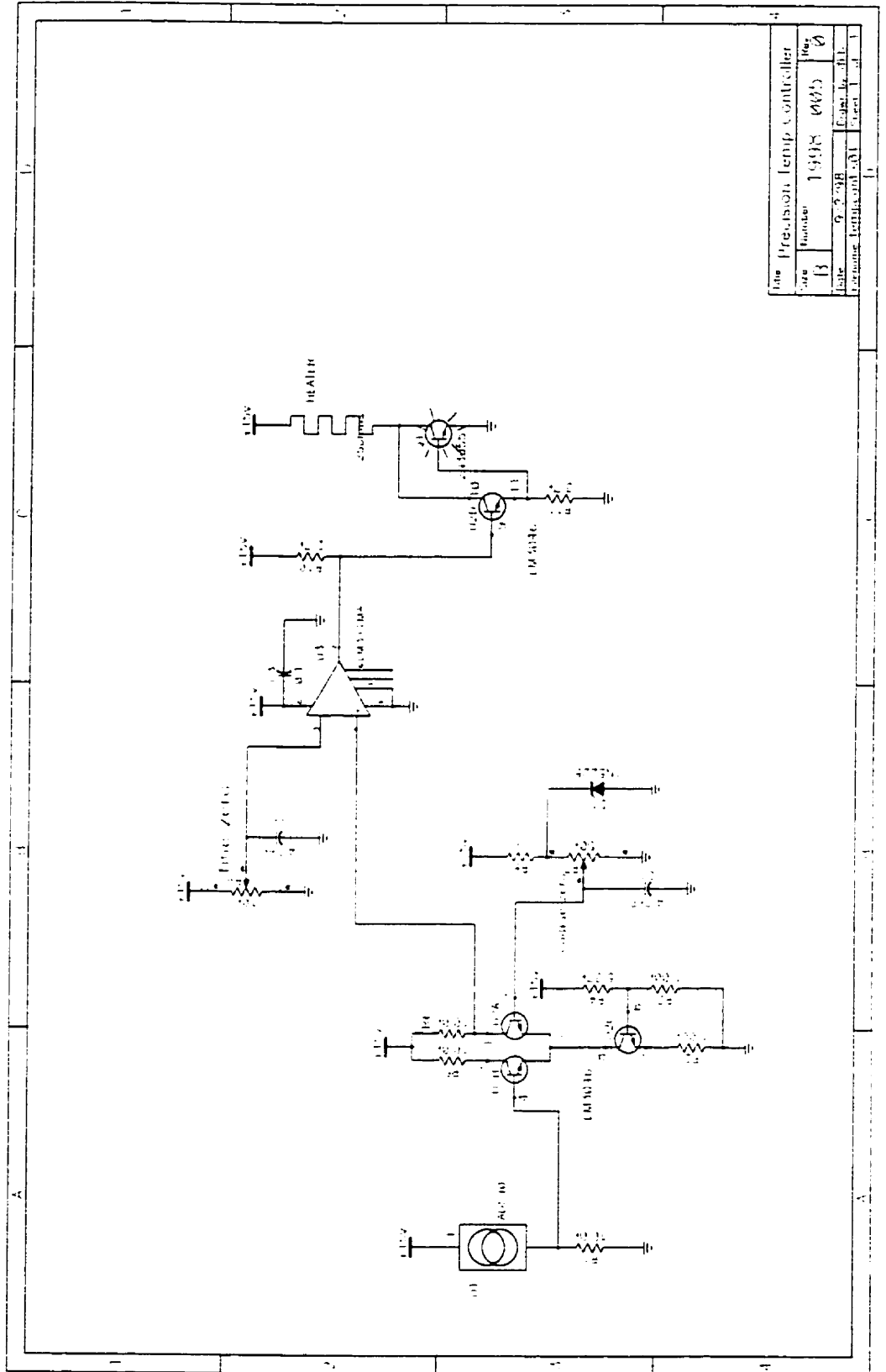


100 Hz audio amplifier

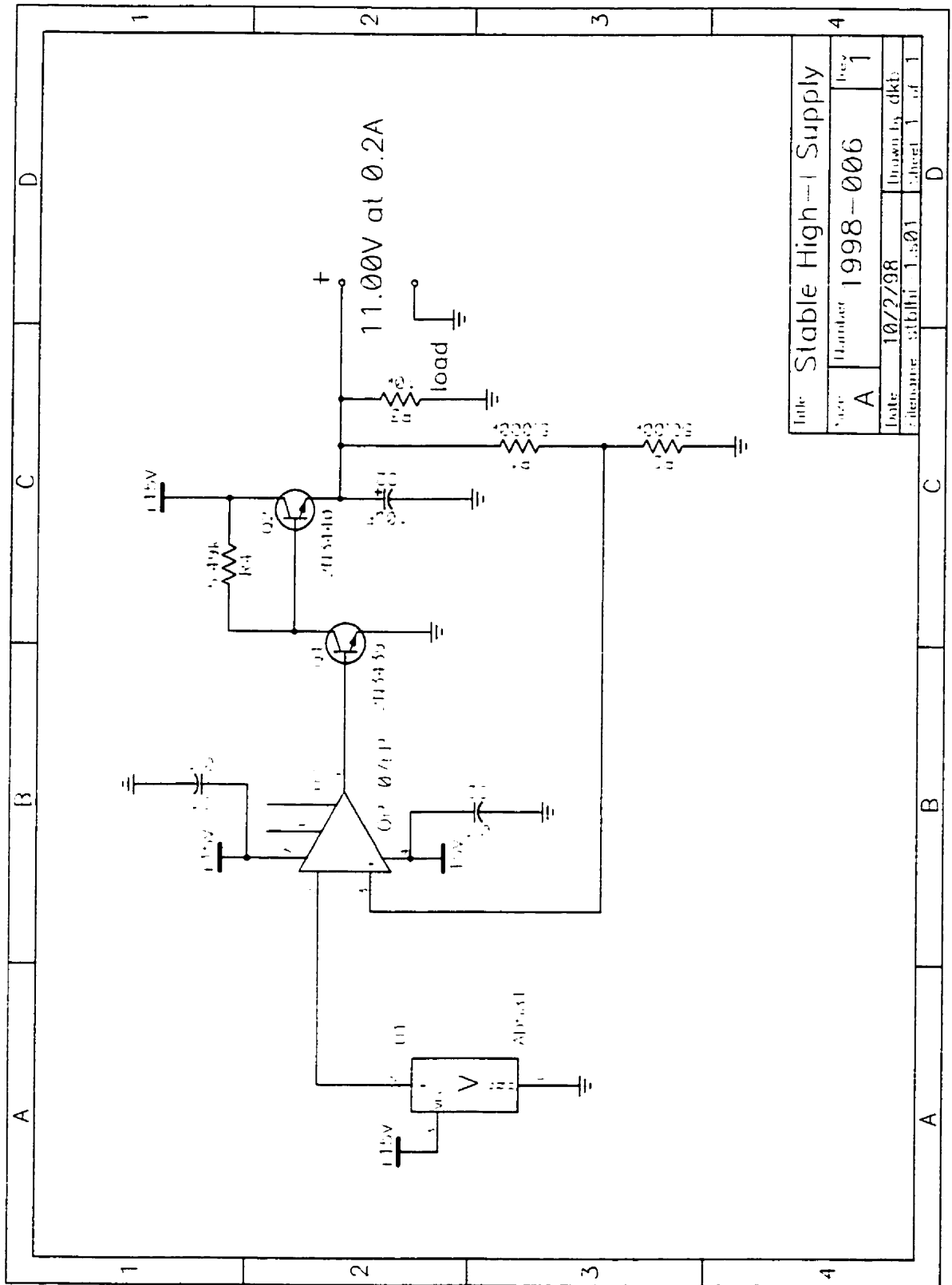
Title	100 Hz audio amplifier	Rev	0
Size	100 Hz audio amplifier	Drawn by	asb
File name	newsys.s01	Sheet	1 of 1



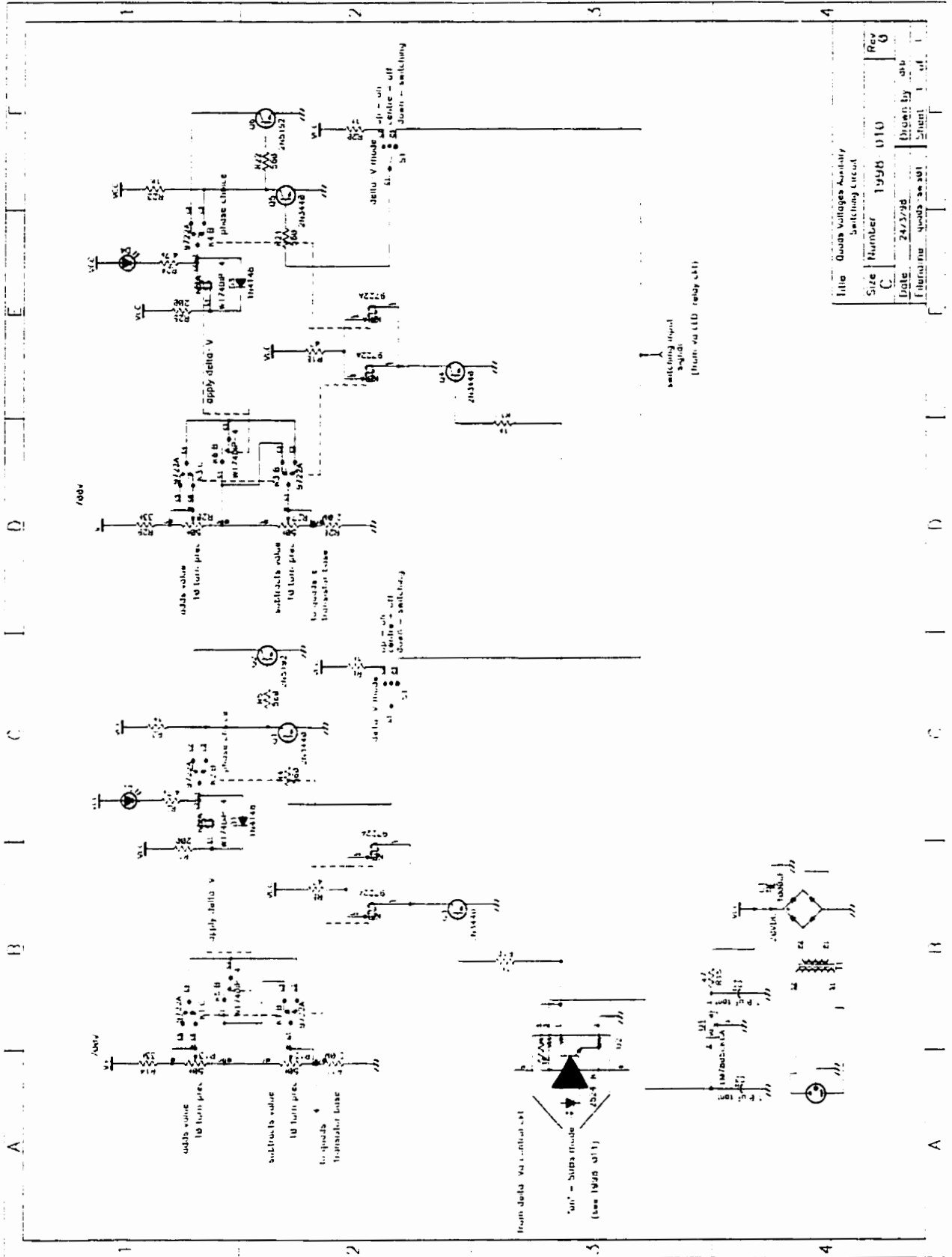
Title Wide Sweeps Circuit of wide sweeps system	
Size C	Rev 0
Date 1/15/98	Drawn by dkb
Iteration SW1CH4 501	Sheet 4 of 4

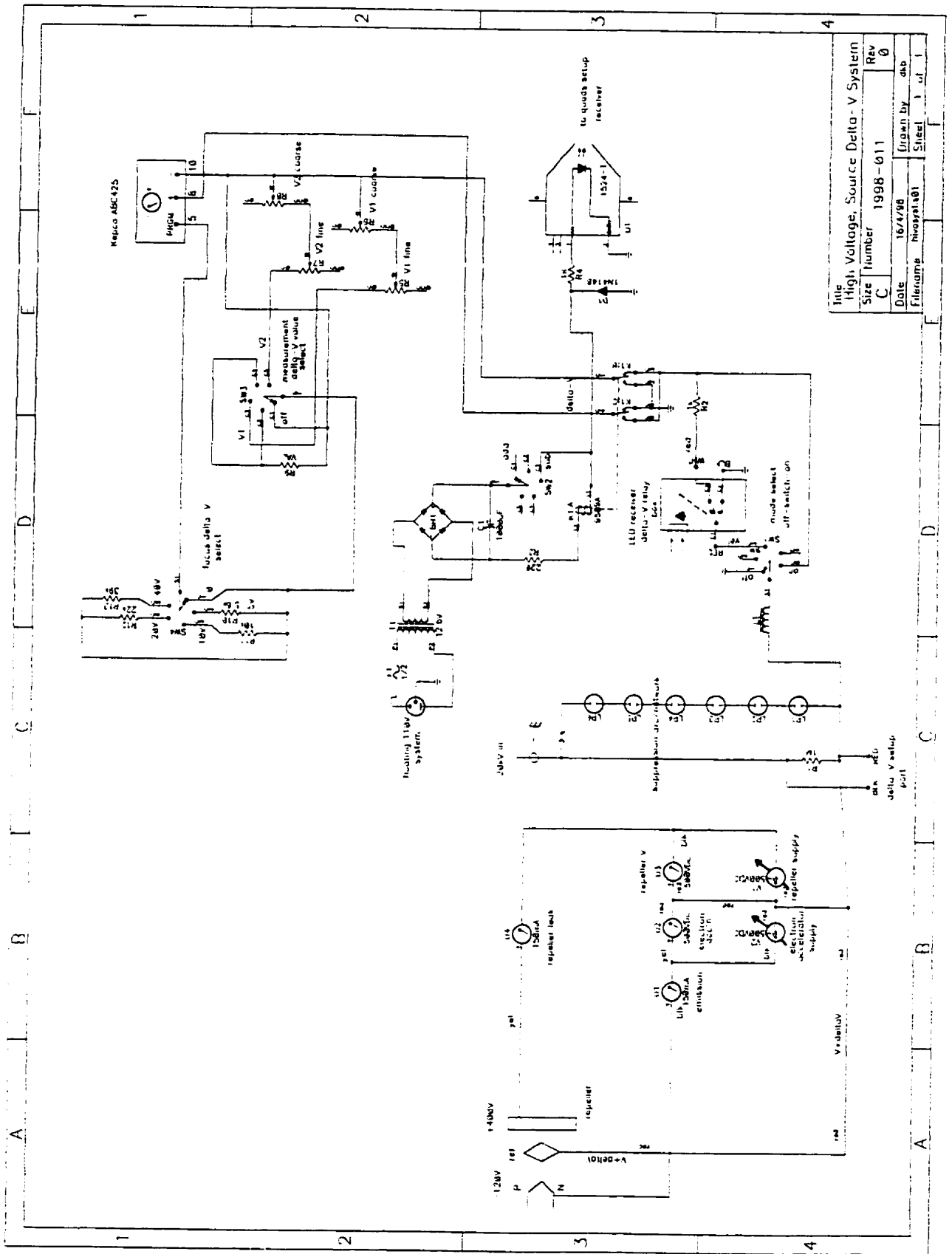


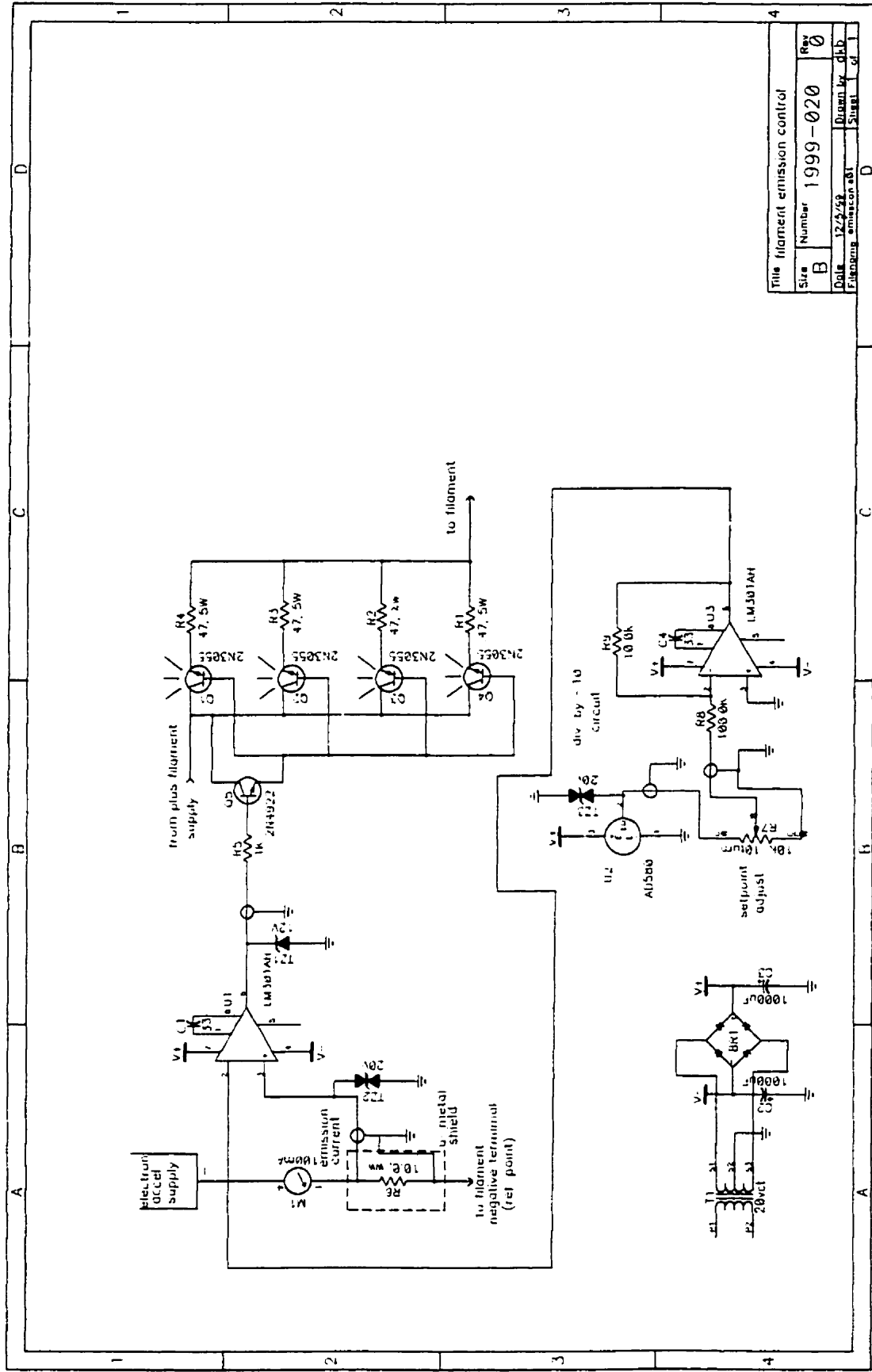
Title Precision Temp Controller			
Date	Revision	Quantity	Drawn
1/3	15998	0005	0
Date	Checked	Checked	Checked
1/3/58	10/11/58	10/11/58	10/11/58



Title: Stable High-Current Supply			
Sheet: A	Number: 1998-006	Rev: 1	
Date: 10/2/98	Drawn by: dkt	Checked by:	
Filename: s1b1h1_1.s01	Sheet: 1	of: 1	







Title filament emission control			
Size	Number	1999-020	Rev
B			0
Date	12/2/99	Drawn by	dlb
Engineering	emission&f	Checked by	dlb
		Subst	dl

Appendix D: Example Linkage Calculations

Table D.1

Chain Φ 1 of §VIII.4:

($E \equiv$ the energy to mass conversion $1.073\,544\,38 \pm 0.08 \mu\text{u} / \text{keV}$ [Au(1993)])

connection	type	Δm calculation, result in μu
$^{185}\text{Re}-^{183}\text{W}$	$^{185}\text{Re}^{37}\text{Cl}-^{183}\text{W}^{37}\text{Cl}$ chloride m.s.doublet	$\Delta m_{\text{doublet}} + \Delta m \text{ for } (^{37}\text{Cl}-^{35}\text{Cl}) =$ $2\,002\,728.59 \pm 1.0$
$^{185}\text{Re}-^{187}\text{Re}$	$^{185}\text{Re}^{37}\text{Cl}-^{187}\text{Re}^{35}\text{Cl}$ chloride m.s.doublet	$\Delta m_{\text{doublet}} + \Delta m \text{ for } (^{37}\text{Cl}-^{35}\text{Cl}) =$ $2\,002\,728.59 \pm 1.2$
$^{187}\text{Re}-^{189}\text{Os}$	$^{187}\text{Re}^{37}\text{Cl}-^{189}\text{Os}^{35}\text{Cl}$ chloride m.s.doublet	$\Delta m_{\text{doublet}} + \Delta m \text{ for } (^{37}\text{Cl}-^{35}\text{Cl}) =$ $2\,002\,390.89 \pm 3.0$
$^{189}\text{Os}-^{192}\text{Os}$	$^{189}\text{Os}^{35}\text{Cl}-^{192}\text{OsO}_2$ mixed m.s. doublet	$\Delta m_{\text{doublet}} + \Delta m \text{ for } (^{16}\text{O}_2-^{35}\text{Cl}) =$ $3\,003\,324.47 \pm 3.5$
$^{192}\text{Os}-^{193}\text{Os}$	(n, γ) reaction	$m_n - E \times Q\text{-value} =$ $1\,002\,669.28 \pm 5$
$^{193}\text{Os}-^{193}\text{Ir}$	β -decay	$-E \times Q\text{-value} =$ $-1\,215.25 \pm 5$
$^{193}\text{Ir}-^{193}\text{Pt}$	K-capture	$E \times Q\text{-value} =$ 60.76 ± 0.3
$^{193}\text{Pt}-^{194}\text{Pt}$	(p,d) reaction	$E \times Q\text{-value} + \Delta m \text{ for } (\text{d-p}) =$ $999\,683.04 \pm 3.0$
$^{194}\text{Pt}-^{195}\text{Pt}$	(n, γ) reaction	$m_n - E \times Q\text{-value} =$ $1\,002\,110.87 \pm 0.12$
$^{195}\text{Pt}-^{196}\text{Pt}$	(n, γ) reaction	$m_n - E \times Q\text{-value} =$ $1\,000\,160.42 \pm 0.15$
$^{196}\text{Pt}-^{197}\text{Pt}$	(n, γ) reaction	$m_n - E \times Q\text{-value} =$ $1\,002\,388.44 \pm 0.3$
$^{197}\text{Pt}-^{197}\text{Au}$	β -decay	$-E \times Q\text{-value} =$ -771.89 ± 0.6
$^{197}\text{Au}-^{198}\text{Au}$	(n, γ) reaction	$m_n - E \times Q\text{-value} =$ $1\,001\,673.78 \pm 0.22$
$^{198}\text{Au}-^{198}\text{Hg}$	β -decay	$-E \times Q\text{-value} =$ $-1\,215.25 \pm 5$
$^{198}\text{Hg}-^{199}\text{Hg}$	(n, γ) reaction	$m_n - E \times Q\text{-value} =$ $1\,001\,509.42 \pm 0.9$
$\Delta m (^{199}\text{Hg}-^{183}\text{W})$		$16\,018\,033.58 \pm 9.13$
equiv. ($^{199}\text{Hg}-^{183}\text{W}^{16}\text{O}$)		$- m(^{16}\text{O}) =$ $23\,118.96 \pm 9.13$

Table D.2

Loop Γ of §II.2:($E \equiv$ the energy to mass conversion $1.073\,544\,38 \pm 0.08 \mu\text{u} / \text{keV}$ [Au(1993)])

connection, given according to path direction	link type	Δm calculation, result in μu
$^{188}\text{Pt}-^{188}\text{Ir}$	K-capture	$-E \times \text{Q-value} =$ -563.61 ± 10
$^{188}\text{Ir}-^{188}\text{Os}$	β^+ decay	$-E \times \text{Q-value} =$ $-3\,030.61 \pm 9$
$^{188}\text{Os}-^{189}\text{Os}$	(n, γ) reaction	$m_n - E \times \text{Q-value} =$ $1\,002\,308.89 \pm 0.5$
$^{189}\text{Os}-^{190}\text{Os}$	(n, γ) reaction	$m_n - E \times \text{Q-value} =$ $1\,000\,300.40 \pm 1.0$
$^{190}\text{Os}-^{192}\text{Os}$	(p,t) reaction	$E \times \text{Q-value} + \Delta m$ for (t-p) = $2.003\,032.58 \pm 0.3$
$^{192}\text{Os}-^{193}\text{Os}$	(n, γ) reaction	$m_n - E \times \text{Q-value} =$ $1\,002\,669.28 \pm 0.9$
$^{193}\text{Os}-^{193}\text{Ir}$	β^- decay	$-E \times \text{Q-value} =$ $-1\,215.25 \pm 5.0$
$^{193}\text{Ir}-^{194}\text{Ir}$	(n, γ) reaction	$m_n - E \times \text{Q-value} =$ $1\,002\,151.73 \pm 0.4$
$^{194}\text{Ir}-^{194}\text{Pt}$	β^- decay	$-E \times \text{Q-value} =$ $-2\,416.54 \pm 2.0$
$^{194}\text{Pt}-^{193}\text{Pt}$	(p,d) reaction	$-\{E \times \text{Q-value} + \Delta m$ for (d-p) $\} =$ $-999\,683.04 \pm 3.0$
$^{193}\text{Pt}-^{192}\text{Pt}$	(n, γ) reaction	$-\{m_n - E \times \text{Q-value}\} =$ $-1\,001\,958.49 \pm 3.0$
$^{192}\text{Pt}-^{190}\text{Pt}$	(p,t) reaction	$-\{E \times \text{Q-value} + \Delta m$ for (t-p) $\} =$ $-2.001\,107.71 \pm 7.0$
$^{190}\text{Pt}-^{188}\text{Pt}$	(p,t) reaction	$-\{E \times \text{Q-value} + \Delta m$ for (t-p) $\} =$ $-2.000\,548.40 \pm 10$
loop residual as Δm , μu		60.77 ± 9.13

References

Ion Optics and Deflection Mass Spectrometry

- Ba K.T. Bainbridge, (1953), *Charged Particle Dynamics and Optics, Relative Isotopic Abundances of the Elements, Atomic Masses*, in *Experimental Nuclear Physics*, **vI**, p.559, E. Segré, ed., Wiley.
- Bl W. Bleakney, (1936), *The Mass-Spectrograph and Its Uses*, *American Physics Teacher*, **4**, 12.
- Ca L. Cartan, (1937), *Sur la focalisation des faisceaux de particules chargées par déviation circulaire en champ magnétique transversal*, *Journal de Physique et le Radium*, **8**, 453.
- Du H.E. Duckworth, R.C. Barber and V.S. Venkatasubramanian, (1986), *Mass Spectroscopy*, 2nd edn., (Cambridge).
- Ew H. Ewald and H. Hintenberger, (1952), *Methoden und Anwendungen der Massenspektroskopie*, Verlag Chemie, GmbH Weinheim.
- Hi H. Hintenberger and L.A. König, (1959), *Mass Spectrometers and Mass Spectrographs Corrected for Image Defects*, *Advances in Mass Spectrometry*, p.16, J.D. Waldron, ed., (Pergamon Press, London).
- Hi H. Hintenberger, H. Wende and L.A. König, (1955), *Massenspektrographen mit Doppelfokussierung zweiter Ordnung*, *Zeit.fNatur.*, **10a**, 605.
- Hi H. Hintenberger and L.A.König, (1957), *Massenspektrographen mit Doppelfokussierung zweiter Ordnung*, *Zeit.fNatur.*, **12a**, 773.
- Ke L. Kerwin, (1949), *Improved Magnetic Focusing of Charged Particles*, *Rev.Sci.Instr.*, **20**, 36.
- Ma H. Matsuda and H. Wollnik, (1970a), *The Influence of an Inhomogeneous Magnetic Fringing Field on the Trajectories of Charged Particles in a Third Order Approximation*, *Nuc.Instr.Meth.*, **77**, 40.
- Ma H. Matsuda and H. Wollnik, (1970b), *Third Order Transfer Matrices of the Fringing Field of an Inhomogeneous Magnet*, *Nuc.Instr.Meth.*, **77**, 283.
- Ma H. Matsuda and H. Wollnik,(1972), *Third Order Transfer Matirces for the Fringing Field Magnetic and Electrostatic Quadrupole Lenses*, *Nuc.Instr.Meth.*, **103**, 117.
- Ma H. Matsuda, S. Fukumoto, Y. Kuroda and M. Nojiri, (1966), *Zeit.f Natur.*, **21a**, 25.
- MaM T. Matsuo, H. Matsuda, Y. Fujita and H. Wollnik, (1976), *Mass.Spec.(Japan)*, **24**, 19.

- Ma H. Matsuda ,(1976), *Double Focusing Mass Spectrometers of Second Order*, in *Atomic Masses and Fundamental Constants 5*, Paris, June 1975, p.185, J.H. Sanders and A.H. Wapstra, eds., Plenum.

Measurement Technique

- Bi R.L. Bishop, (1969). *Atomic Mass Differences for Some Rare Earth Isotopes Near N=90*, PhD Thesis, Department of Physics, University of Manitoba.
- Bi R.L. Bishop and R.C Barber, (1970). *A High Precision Ratio Potentiometer*, *Rev.Sci.Instr.*, **41**, 327.
- Ko K.S. Kozier, (1977). *Atomic Mass Determinations for Some Isotopes of Ti, W and Hg*, PhD Thesis, Department of Physics, University of Manitoba.
- Pe Y. Petiti-Clerc and J.D. Carette, (1968), *The Surface Potential of Metal Surfaces Under Electron Bombardment at High Vacuum*, *Vacuum*, **18**, 7.
- Sh K.S. Sharma, (1997). private communication.
- Sm L.G. Smith, (1967), *First Results with the Princeton RF Spectrometer*, p.811, in *Proceedings of the Third Conference on Atomic Masses*, Aug.28-Sept.1, 1967, Winnipeg, University of Manitoba Press.

Traps

- Ba R.C. Barber *et al.*, (1994), *A Canadian Penning Trap Mass Spectrometer*, (A proposal to the Natural Sciences and Engineering Research Council).
- Bo G. Bollen *et al.*, (1998), *Mass Measurements with a Penning Trap Mass Spectrometer at ISOLDE*, p.3, in *Proceedings of ENAM '98*, International Conference on Exotic Nuclei and Atomic Masses, Bellaire, MI, 1998, B.M. Sherill, D.J. Morrissey and C.N. Davids, eds.
- Kl H.-J. Kluge and G. Bollen, (1992), *Ion traps - recent applications and developments*, *Nuc.Instr.Meth.Phys.Res.*, **B70**, p.473.
- Kl H.-J. Kluge and G. Bollen, (1993), *ISOLTRAP: A tandem Penning trap mass spectrometer for radioactive isotopes*, in *Traps for Antimatter and Radioactive Nuclei*, TRIUMF, Vancouver, 1993, J.M. D'Auria, D.R. Gill and A.I. Yavin eds; J.C. Baltzer AG, pub.
- Sc P.F. Schewe, (1993), *Physics New Update #125*, April 22, 1993.

- Sh K.S. Sharma *et al.*, (1995), *The Canadian Penning Trap Mass Spectrometer*, p.811, in Proceedings of ENAM'95, International Conference on Exotic Nuclei and Atomic Masses, Arles, France, 1995, M. de Saint Simon and O. Sorlin, eds.
- Sh K.S. Sharma *et al.*, (1998), *Status of the Canadian Penning Trap Mass Spectrometer at the Argonne National Laboratories*, p.130, in Proceedings of ENAM'98 (see above).
- VnD R.S. Van Dyck, Jr., P. B. Schwinberg and S.H. Bailey, (1980), *High Resolution Penning Trap as a Precision Mass-Ratio Spectrometer*, p.173 in Atomic Masses and Fundamental Constants 6 (AMCO-6), Proceedings of the Sixth International Conference on Atomic Masses and Fundamental Constants, East Lansing, Michigan, 1979, J.A. Nolen Jr. and W. Benenson, eds., Plenum .

Least-Squares Mass Adjustments

- Au G. Audi, W.G. Davies and G.E. Lee-Whiting, (1986), *A Method of Determining the Relative Importance of Particular Data on Selected Parameters in the Least-Squares Analysis of Experimental Data*, Nucl.Instr.Meth.Phys.Res., **A249**, 443.
- Au G. Audi, A.H. Wapstra and M. Dedicu, (1993), *The 1993 Atomic Mass Evaluation (IV) Nuc.Phys. A565*, pp.193-397.
- Ibid. pp. 206-207
- Co E.R. Cohen, (1960), *The Validity of Least Squares for the Adjustment of Experimental Data*, Proc, International Conf. on Nuclidic Masses, McMaster University, H.E. Duckworth, ed., (University of Toronto Press).
- Fa R.W. Farebrother, (1988), *Linear Least Squares Computations*, New York, (Marcel Dekker Inc.).
- Kö L.A. König, (1960), *Mathematical Details of the Mass Computation*, Proceeding of the International Conference on Nuclidic Masses, McMaster University, H.E. Duckworth, ed., (University of Toronto Press).
- So F.C.G. Southon, (1973), *Measurement of Wide and Narrow Mass Differences on the Manitoba II Mass Spectrometer*, PhD Thesis, Department of Physics, University of Manitoba.
- Wa A.H. Wapstra and G. Audi, (1985), *The 1983 Atomic Mass Evaluation, (I). Atomic Mass Table*, Nuc.Phys. **A432**, pp.1-11.
- Wa A.H. Wapstra, (1960), *Treatment of Input Data for a Least Square Nuclidic Mass Adjustment*, Proc. International Conf. on Nuclidic Masses, McMaster University, Sept. 1960, H.E. Duckworth, ed., (University of Toronto Press).

Nuclear Physics and Mass Measurements

- As F.W. Aston, (1942), *Mass Spectra and Isotopes*, 2nd edn., London, (Edward Arnold and Company).
- Ba R.C. Barber *et al.*, (1971), *A High Resolution Mass Spectrometer for Atomic Mass Determinations*, *Rev.Sci.Inst.*, **42**, 1.
- Ba R.C. Barber and K.S. Sharma, (1999), private communication.
- Ba M. Bauer, (1975), *The Liquid Drop Mass Formula as a Shell Model Average*, pp.286-292, in *Proceedings of the Fifth International Conference on Atomic Masses and Fundamental Constants, (AMCO-5)*, Paris, June 1975, J.H. Sanders and A.H. Wapstra, eds., Plenum.
- BeB H.A. Bethe and R.F. Bacher, (1936), *Nuclear Physics, A. Stationary States of Nuclei*, *Rev.Mod.Phys.* **8**, 82.
- BeJ H. A. Bethe and R.W. Jackiw, (1968), *Intermediate Quantum Mechanics*, 2nd Ed., W.A. Benjamin, Inc.
- Br R.A. Britten and W.H. Johnson, Jr., (1973), *Atomic Masses of ^{232}Th , ^{235}U , and ^{238}U and a Mass Table for the Heavy Isotopes*, *Phys.Rev.* **C7**, 1545.
- Br R. Brockmann, (1978), *Relativistic Hartree-Fock Description of Nuclei*, *Phys.Rev.* **C18**, 1510.
- De A.J. Dempster, (1938a), *The Atomic Masses of the Heavy Elements*, *Phys.Rev.*, **53**, 64.
- De A.J. Dempster, (1938b), *The Energy Content of the Heavy Nuclei*, *Phys.Rev.*, **53**, 869.
- Fe E. Feenberg and K.C. Hammack, (1949), *Nuclear Shell Structure*, *Phys.Rev.*, **75**, 1877.
- Gr W. Greiner and J.A. Maruhn, (1996), *Nuclear Models*, Springer-Verlag.
- Ki D.A. Kirzhnits, (1967), *Field Theoretical Methods in Many-Body Systems*, (trans. from the Russian by A. J. Meadows), Pergamon Press.
- Ko K.S. Koziar, K.S. Sharma, R.C. Barber, J.W. Barnard, R.J. Ellis and V.P. Derenchuk, (1980), *Precise Atomic Masses and Mass Differences for Mercury*, *Can.J.Phys.*, **58**, 1311.
- Ma R.D. Mattuck, (1976), *A Guide to Feynman Diagrams in the Many Body Problem*, Dover.
- Ma M.G. Mayer, (1948), *On Closed Shells in Nuclei*, *Phys.Rev.*, **74**, 235.
(1949), *On Closed Shells in Nuclei II*, *Phys.Rev.*, **75**, 1969.

- Me J.O. Meredith et al., (1972), *Precise Atomic Mass Differences Using Peak Matching by Computer*, Int.J.Mass Spec.and Ion Phys., **10**, 359.
- Ni J.R. Nix and P. Möller, (1995), *Macroscopic-Microscopic Mass Models*, pp. 23-32, **ENAM 95**: International Conference on Exotic Nuclei and Atomic Masses, Editions Frontieres.
- Pe J.M. Pearson, Y. Aboussir, A.K. Dutta, R.C. Nayak and M. Farine , (1991), *Thomas-Fermi Approach to Nuclear Mass Formula*, (III) Force fitting and construction of the mass table, Nuc.Phys. **A528**, 1.
- Qu P. Quentin and H. Flocard, (1978), *Self-Consistent Calculations of Nuclear Properties with Phenomenological Effective Forces*, Ann.Rev.Nuc.Part.Sci., **28**, 523.
- St V.M. Strutinsky. (1967), *Shell Effects in Nuclear Masses and Deformation Energies*, Nuc.Phys. **A95**, p.420.
- Th D.J. Thouless, (1972). *The Quantum Mechanics of Many Body Systems*, 2nd ed., Academic Press.
- Ze N. Zeldes. (1972), *Shell Model Masses and Nuclear Structure*, pp.245-254, in Proceedings of the Fourth International Conference on Atomic Masses and Fundamental Constants, (AMCO-4), Teddington, Sept. 1971, J.H. Sanders and A.H. Wapstra, eds., Plenum.

Reaction Methods

- Bc K.E. Bergkvist. (1972), *Improvements in the Determination of β -spectra End-point Energies*, p.77 in Atomic Masses and Fundamental Constants 4 (AMCO-4), Proceedings of the Fourth International Conference on Atomic Masses and Fundamental Constants, Teddington England, 1971, J.H. Saunders and A.H. Wapstra, eds., Plenum.
- De R.D. Deslattes and E.G. Kessler, Jr., (1980), *Precision Gamma- and X-Ray Energies*, p.203 in Atomic Masses and Fundamental Constants 6 (AMCO-6), Proceedings of the Sixth International Conference on Atomic Masses and Fundamental Constants, East Lansing, Michigan, 1979, J.A. Nolen Jr. and W. Benenson, eds., Plenum.
- Ko V.T. Koslowsky et al., (1985), *Precise Determination of Q_{EC} Differences Between Four Pairs of Superallowed β Emitters*, p.60, in Proceedings of the 7th International Conference on Atomic Masses and Fundamental Constants, (AMCO-7), 3-7 Sept., 1984, Darmstadt-Seeheim, O. Klepper ed.
- Ry A. Rytz, B. Grennberg and D.J. Gorman, (1972), *New Alpha Energy Standards*, p.1 in **AMCO-4** (see above).
- Ry A. Rytz, (1980), *Absolute Measurement of the Energy of Alpha Particles Emitted by ^{239}Pu* , p.249 in **AMCO-6** (see above).

- Sc O.W.B. Schult, H.R. Koch, H.A. Baader and D. Breitig, (1972), *Measurement of (n, γ) -lines with a High-resolution Dumond-type Diffractometer*, p.123 in **AMCO-4** (see above).

Programming and Analysis

- Be P.R. Bevington, (1969), *Data Reduction and Error Analysis for the Physical Sciences*, McGraw-Hill.
- Bi R.T. Birge, (1932), *The Calculation of Errors by the Method of Least Squares*, *Phys.Rev.*, **40**, 207.
- Hy J.G. Hykawy , (1991), *Precise Determination of the ^{76}Ge - ^{76}Se Atomic Mass Difference and the Majorana Mass of the Electron Neutrino*, PhD Thesis, Department of Physics, University of Manitoba.
- KaJ D.C. Kayser and W.H. Johnson, Jr., (1975), *New Mass Measurements of Samarium and Gadolinium and a Mass Table for the Light Rare Earths*, *Phys. Rev. C* **12**, 1054.
- Ko J. Konger, (1992), *Windows Programming Primer Plus*, Waitc Group Press.
- Pc C. Petzold. (1992), *Programming Windows 3.1*, MicroSoft Press.
- Pr W.H. Press, B.P. Flannery, S.A. Teukolsky and W.T. Vetterling, (1988), *Numerical Recipes in C, The Art of Scientific Computing*, Cambridge.
- Si M.H. Sidky, (1990), *Precision Atomic Mass Difference Determinations for Tl and Pb*, PhD Thesis, Department of Physics, University of Manitoba.

Neutrinoology

- Ci O. Civitarese, A. Faesler and T. Tomoda, (1987), *Suppression of Two-Neutrino Double β Decay*, *Phys.Let.* **B194**,11.
- Do M. Doi, T. Kotani and E. Takasugi, (1985), *Double Beta Decay and Majorana Neutrino*, *Prog.Th.Phys.Suppl.*, **83**, 1.
- El S.R. Elliot, A.A. Hahn and M.K. Moe, (1987), *Direct Evidence for Two-Neutrino Double-Beta Decay in ^{32}Se* , *Phys.Rev.Let.*, **59**, 2020.
- El R.J. Ellis, R.C. Barber, G.R. Dyck, B.J. Hall, K.S. Sharma, C.L. Lander and H.E. Duckworth, (1985), *Nuc.Phys.*, **A435**.
- Gr K. Grotz and H.V. Klapdor, (1990), *The Weak Interaction in Nuclear, Particle and Astrophysics*, (trans. S.S. Wilson), Adam Hilger.

- Ha W.C. Haxton and G.J. Stephenson, Jr., (1984), *Double Beta Decay*, Prog.Part.Nucl.Phys., **12**, 409.
- Ka B. Kayser, (1986), *Neutrino Mass and Related Problems*, Proceedings of the Oregon Meeting (Annual Meeting of the Division of Particles and Fields of the American Physical Society), p.387, R. Hwa, ed., World Scientific.
- Si J.J. Simpson, (1981), *Measurement of the β -Energy Spectrum of ^3H to Determine the Anti-Neutrino Mass*, Phys.Rev.D, **23**, 649.

Miscellaneous

- Ca J. Caesar, (1917), H.J.Edwards. trans, *Bellum Gallicum*, Loeb Classics, Harvard University Press.
- Ch J.H. Christenson, J.W.Cronin, V.L.Fitch and R.Turlay, (1964), *Evidence for the 2π Decay of the K_2^0 Meson*, Phys.Rev., **13**, 138.
- Ka B. Kayser, F. Gibrat-Debu and F. Perrier, (1989), *The Physics of Massive Neutrinos*, World Scientific.
- Ku P.Kusch and H.M. Foley, (1948), *On the Intrinsic Moment of the Electron*, Phys.Rev. **73L**, 412;
(1948), *The Magnetic Moment of the Electron*, Phys.Rev., **74**, 250.
- La Lamb Jr., W.E. and Retherford, R.C. (1947), *Fine Structure of the Hydrogen Atom by Microwave Method*, Phys.Rev.. **72**, 241;
(1950), *Fine Structure of the Hydrogen Atom I*, Phys.Rev.. **79**, 549;
(1950), *Fine Structure of the Hydrogen Atom II*, Phys.Rev., **81**, 222;
(1952), *Fine Structure of the Hydrogen Atom IV*, Phys.Rev., **86**, 1114.